Global Ocean Salinity: A Climate Change Diagnostic?

Paul James Durack

BSc (Honours 1A), Murdoch University

Submitted in fulfilment of the requirements for the degree of

Doctor of Philosophy in Quantitative Marine Science
(A Joint CSIRO and University of Tasmania PhD Program)

University of Tasmania

June 2011

Supervisors:
Dr Susan E. Wijffels
Dr Helen E. Phillips
Prof. Nathaniel L. Bindoff

Statement of Originality

To the best of my knowledge, this thesis contains no material that has been accepted for a degree, diploma or award by the University of Tasmania or any other educational institution, or has been previously published or written by another person except by way of background information that has been duly acknowledged in the text of this thesis, nor does this thesis contain any material that infringes copyright.

Paul James Durack
16th June 2011

Statement of Authority of Access

I, the undersigned, the author of this thesis, understand that the University of Tasmania will make it available for use within the university library and by microfilm, digital or other photographic means, allow access to users in other approved libraries.

This thesis may be made available for loan and limited copying in accordance with the Copyright Act 1968.

Beyond this, I do not wish to place any restrictions on access to this thesis.

Paul James Durack
16th June 2011

Statement of Co-authorship

Thesis title: Global Ocean Salinity: A Climate Change Diagnostic?
Submitted for review: 3rd December 2010
Candidate: Paul J. Durack

Publications produced as part of this thesis include:

Chapter 2 (Paper 1):
Durack, P.J. and S.E. Wijffels (2010) Fifty-Year Trends in Global Ocean Salinities and Their Relationship to Broad-Scale Warming. *Journal of Climate*, **23**, pp 4342-4362. doi: 10.1175/2010JCLI3377.1

To be submitted:

Chapter 3 (Paper 2):
Durack, P.J. and S.E. Wijffels (in prep) Ocean Salinities Confirm a Strengthening Global Water Cycle

Chapter 4 (Paper 3):
Durack, P.J. and S.E. Wijffels (in prep) Revisiting Halosteric and Thermosteric Sea-level Rise 1950-2000

The following people and institutions contributed to the publication of the work undertaken as part of this thesis:

Chapter 2 (Paper 1): Paul J. Durack (50%), Susan E. Wijffels (50%)

Details of the Authors roles:

Paul Durack and Susan Wijffels contributed to the idea, its development and formalisation. Paul Durack undertook the analysis and both shared responsibility for writing the paper.

Susan Wijffels provided guidance and supervision in all aspects of this PhD, and provided assistance in the interpretation and writing of Chapters 2, 3 and 4.

We the undersigned agree with the above stated “proportion of work undertaken” for each of the above published peer-reviewed manuscripts contributing to this thesis:

Signed:

Dr Susan E. Wijffels
Candidate Supervisor
CSIRO CMAR, Hobart, Tasmania
3rd December 2010

Signed:

Prof. Michael Coffin
Director
Institute for Marine and Antarctic Studies
University of Tasmania
3rd December 2010

Abstract

This thesis aims to use historical and recent global ocean observations to ascertain changes to the water cycle, expressed by ocean salinity changes. The analysis is dependent on over 1.6 million profiles of salinity, potential temperature and neutral density from historical archives and the international Argo Program. The period of analysis extends from 1950-2008, and takes care to minimise the aliasing associated with the seasonal and major global El Nino-Southern Oscillation modes.

The thesis is structured in 5 chapters. Chapter 1 introduces the reader to ocean observations and observed changes over the 20th and early 21st century. It provides an introduction to the global water cycle and the ocean's role in its operation and the anticipated future, as well as observed changes in response to climate change. Chapter 2 presents new estimates of global ocean salinity changes in dual pressure and density analyses and attempts to tease out primary processes driving these changes. Chapter 3 focuses on the pattern of sea surface salinity changes, and compares these to current state-of-the-art climate models which comprise the Coupled Model Intercomparison Project phase 3 (CMIP3) database. A comparison of the spatial patterns of change and the explicit rates of salinity pattern amplification in the 20th century realisations (20C3M) is made against the new observational estimates of change (Chapter 2). Chapter 4 concentrates on the three dimensional changes expressed by these new estimates; by combining the concurrent temperature analysis, it provides new coherent estimates of regional (and global) sea level rise as expressed by halosteric (salinity-) and thermosteric (temperature-driven) changes. Chapter 5 summarises these results, reviews key new findings and suggests areas for future research.

This research has uncovered large, robust and spatially coherent multi-decadal linear trends in salinity to 1800 dbar depth. Salinity increases at the surface are found in evaporation-dominated regions and freshening in precipitation-dominated regions. This spatial pattern of change strongly resembles the climatological mean sea surface salinity field, consistent with an amplification of the global water cycle. Recorded changes in the ocean subsurface suggest that subduction and circulation by the ocean's mean flow of surface salinity and temperature anomalies are driving regional changes on the 50-year timescales.

A robust amplification of the mean surface salinity pattern of 8% is found globally, with 5-9% apparent in each of the 3 key independently analysed ocean basins. 20th century realisations (20C3M) from the CMIP3 model suite support the broad-zonal relationship between amplified patterns of surface freshwater flux driving an amplified pattern of ocean surface salinity. The warming response represented in realistic (when compared to observed estimates) 20th century realisations appear similar in their patterns to those of 21st century projected future realisations (these projections are strongly forced by greenhouse gases).

New observed surface salinity change estimates suggest a pattern amplification of 8% (16±7% K^{-1}; associated with a 0.5K global surface temperature increase) has been experienced for 1950-2000. Using modelled relationships this equates to an inferred change of 4% (8±5% K^{-1}) for evaporation minus precipitation (E-P) replicating the theoretical response described by the Clausius-Clapeyron relation. While there is a large spread in the CMIP3 20th century

comparison results, the ensemble best-estimate tends to underestimate observed salinity changes by 50%, with $\%K^{-1}$ rates also found to be similar in projected 21st century realisations.

Considering the full three dimensional salinity and temperature changes yields new quantitative estimates of steric sea level rise for 1950-2000. Thermosteric linear trend estimates for 0-700m replicate the rates expressed by well documented time series, however, provide new insights into the spatial pattern of these counteracting steric contributions. Halosteric estimates indicate large contractions (enhanced salinity) in the Atlantic, with corresponding expansions (freshening) occurring in the Pacific and a near neutral globally integrated response. When considering the total steric changes, the Atlantic (the most dynamically changing basin over the analysis period) undergoes strong warming (expansion) and strong enhanced salinity (contraction) with these signals cancelling to provide a muted total steric response.

These new estimates of ocean changes for 1950-2000 provide a globally coherent and stringent target for coupled modelling systems when undertaking 20th century hindcast simulations. A better understanding of observed changes will aid in the evaluation of the upcoming CMIP5 (phase 5) database, providing a benchmark by which to assess the poorly known water cycle intensification and ocean changes expressed in the 20th century and beyond.

Acknowledgements

I'd like to thank many people who assisted me during this project – providing both a great deal of background assistance with research, encouragement to kick me along during slower periods and light-hearted discussions to make things seem a little less serious.

I would firstly like to thank Dr Susan Wijffels for many hours of often tedious conversations about the oceans and the Earth's climate system, data sources (woes, benefits, and tripwires), interpretation of new results and for putting up with constant queries, triple-checks and endless revisions. She has provided me with a solid grounding into the world of rigorous scientific practise and achieving research outcomes – thanks so much for your continued support, encouragement and for providing me with the opportunity to get my scientific hands dirty with a real world problem that needs our collective attention.

Many thanks go to Dr Helen Phillips, who laboured through early revisions and early results. You've really helped me elucidate key points, focus on key findings and trim off excess waffle. Many thanks for your early, late and very late efforts!

Many thanks also to Prof. Nathan Bindoff, for enlightening discussions about early results, and providing an alternative interpretation from which new scientific insights and research directions developed.

For her many years assisting with administration through the Quantitative Marine Science (QMS) Graduate Program, dealing with all aspects of University administration… And for helping me greatly with the final production of the printed, bound thesis, I would very much like to thank Dr Denbeigh Armstrong. Denbeigh, you're the QMS pillar on which we've all come to depend.

There are many folks who have provided scientific insights, fruitful discussions, assistance with administration, graphics and presentations, communication, computing support, data acquisition, light-hearted lunches and many other aspects too numerous to mention in no particular order: Catia Domingues, John Church, Richard Matear, Richard Coleman, Tom Trull, Bernadette Sloyan, Steve Rintoul, Trevor McDougall, Andreas Schiller, Janet Sprintall, Steve Griffies, Jay McCreary, Gary Meyers, Peter Campbell, Sean McInnes, Jerry Coppleman, Jeff Dunn, Ann Thresher, Neil White, Jim Mansbridge, Terry O'Kane, Jan Zika, Andreas Klocker, Anne-Elise Nieblas, Jane Alpine, Laura Herraiz-Borreguero, Katy Hill, Kyla Drushka, Les Muir, Didier Monselesan, Lidia Pigot, Paul Barker, Louise Bell, Craig Macauley, Jeff Dunn, Amelie Meyer, Kieran Helm, Stephanie Downes, Andrew Meijers, Ben Galton-Fenzi, Bec Cowley, Jillian Enraght-Moony, Denise McMullen and Russ Fiedler.

To actually achieve any quantitative results within a PhD timeframe is a difficult task, and would be made even harder if many folks hadn't spent their blood, sweat and tears locating, acquiring, tirelessly validating, tidying and providing data to the climate research community for use in studies such as this. Many thanks must go to Taiyo Kobayashi, Shinya Minato and Toshio Suga (JAMSTEC-IORGC; for the SeHyD & IOHB databases), Ruth Curry and Alison MacDonald (WHOI; for the Hydrobase2 database), Alejandro Orsi and Thomas Whitworth (Texas A&M University; for the SODB database) and the global community of 27 countries

which comprise the Argo Program. Many thanks also to the NODC, Sydney Levitus and colleagues for their continued work to locate, obtain and digitise high quality historic ocean data – without the contributions from such data sources, this study would simply not be possible. I'd also like thank the global climate modelling community for constructing, running and contributing all the model output which comprises the Coupled Model Intercomparison Project Phase 3 (CMIP3) database. Without this very large and significant resource, studies such as the result presented in Chapter 3 would simply not be possible.

Some personal words of thanks must be extended to my family. First of all to Moyz, many thanks for your love and support, constant check-ups and relentless ability to prize early drafts out of my hands. To Packa, Weeza and Hels, I've been very lucky to have the love and support of my close family for 31 years, and although I take it all for granted, really do appreciate all your efforts either big or small over the last 4 years to kick me along. To brother Thomas, for the enlightened words "good enough", sharing with me many new aspects of procrastination that I'd never known before, and for making my early time in Tasmania much more fun than it would have been otherwise..

Finally to my wife, Dr Julia Durack, for your on-going love and support, ability to bounce around scientific ideas and provide feedback (no matter how many, many times I bring them up..), countless efforts (in the kitchen, garden and many domestic chores) over the last 4 years, I thank you. Without having you to prompt me along on the journey, scribble with red/blue/black pen on early (late, and very late..) copies of chapters, and debate the vagaries of the English language in front of a computer screen into the late hours, or very early mornings, I'm quite sure I would not have made it.. I am and will be eternally indebted – and I'm sure I'll enjoy every last minute of my indebted-ness ☺.

Yay, I'm finally done.. Now on to the papers..

Table of Contents

Acronyms and Abbreviations

20C3M	CMIP3 20th century realisations
A1B	SRES A1B (rapid economic & technology growth, population peaks mid-21st century)
A2	SRES A2 (slower economic & technology growth, continuous population growth)
AABW	Antarctic Bottom Water
AAIW	Antarctic Intermediate Water
ACC	Antarctic Circumpolar Current
AR4	Fourth Assessment Report of the IPCC
B1	SRES B1 (rapid economic & green technology growth, population peaks mid-21st century)
CC	Clausius-Clapeyron (7% K^{-1})
CFC-11	Chlorofluorocarbon (Trichlorofluoromethane)
CMIP2	Coupled Model Intercomparison Project Phase 2 (1997-2001)
CMIP3	Coupled Model Intercomparison Project Phase 3 (2005-2007)
CMIP5	Coupled Model Intercomparison Project Phase 5 (2010-2013)
dbar	Decibar (pressure)
E-P	Evaporation minus precipitation (also freshwater flux)
EAC	East Australian Current
ENACT3	ENhanced ocean data Assimilation and ClimaTe prediction (2002-2004)
ENSO	El-Nino Southern Oscillation (also SOI)
ERA40	ECMWF 40 Year Re-analysis
EUC	Equatorial Undercurrent
F_w	Total surface freshwater flux (E-P) and terrestrial runoff
GHG	Greenhouse Gas
GIN	Greenland Iceland and Norwegian Seas
ICOADS	International Comprehensive Ocean-Atmosphere Data Set
ITCZ	Intertropical Convergence Zone
IOHB	Indian Ocean Hydrobase
IPCC	Intergovernmental Panel on Climate Change
ITF	Indonesian Throughflow
LHS	Left hand side
MOW	Mediterranean Outflow Water
NAO	North Atlantic Oscillation
NCEP	National Centers for Environmental Prediction
NPIW	North Pacific Intermediate Water
NPSTMW	North Pacific Subtropical Mode Water
PA	Pattern Amplification
PC	Pattern Correlation
PDO	Pacific Decadal Oscillation
PGW	Persian Gulf Water
PPMV	Parts per million by volume
PSS-78	Practical Salinity Scale of 1978 (also pss)
PW	Precipitable water (column integrated water vapour)
RHS	Right hand side
RSW	Red Sea Water
SAM	Southern Annular Mode
SAMW	Subantarctic Mode Water
SeHyD	Selected Hydrographic Dataset
SMOS	Soil Moisture and Ocean Salinity
SODB	Southern Ocean Database
SOI	Southern Oscillation Index (also ENSO)
SRES	Special Report on Emissions Scenarios
SST	Sea Surface Temperature
STMW	Subtropical Mode Water
Sv	Sverdrup (10^6 m^3 s^{-1})
T-S	Temperature-salinity relationship
UCDW	Upper Circumpolar Deep Water
UDW	Upper Deep Water

Chapter 1

Introduction

Overview

Climate change is arguably the biggest challenge facing humankind today. It encapsulates a complex mix of issues which extend from international politics to personal power usage. The key message is that changing climate patterns pose a real challenge. Global water cycle changes in response to climate change in particular, will provide the greatest potential impacts on society, and a significant intensification of droughts and floods will pose the most severe test.

Changes to global water distribution are anticipated in the 21st century, as anthropogenic climate change signatures become more apparent over natural global climate system variability. Future projections of water distribution indicate that regions dominated by evaporation (over rainfall), and prone to drought, will become drier, and regions dominated by rainfall (over evaporation) will become wetter (Held & Soden, 2006; Meehl *et al*., 2007; Seager *et al*., 2010). This will enhance the already apparent separation between the "haves" and "have nots". In water-stressed areas the human population and surrounding ecosystems are particularly vulnerable to decreasing and more variable rainfall due to climate change. It is important that probable future changes to the global water cycle are well understood, and prepared for, as the considerable uncertainties associated with global climate change are likely to impact on many billions of people around the world.

Present-day civilisation thrives in a wide range of temperatures at different latitudes across the Earth, but cannot cope without available freshwater. Most modern day food production depends, directly or indirectly, on freshwater sources. In the absence of importation of food commodities, population growth is constrained by the availability of local resources, including water, along with cultural and health-related factors. Globalisation and the evolution of international trade of large quantities of food make local societies less reliant on local water resources, and consequently have enabled some large populations to greatly exceed the limits imposed by their local geography and water budget. Globalisation and international connectedness ensures the virtual (or embodied water within food stores) transfer of water resources from areas of food production to regions of import. While in the short term this import of water may prevent malnourishment, famine and conflicts over regional water resources, the long term implications to changing water resources is not well understood (D'Odorico *et al*., 2010).

This thesis explores observed changes in the global water cycle, as expressed by its largest single component by storage, the global oceans. In the following sections of this Introduction, the reader will be introduced to some key concepts relating to: climate change diagnosis, the history of ocean observation, the role of the ocean in the global water cycle, observed climate change in the ocean, anticipated global water cycle changes due to climate change, observed 20th and early 21st century estimates of water cycle change and finally some key questions which will be discussed in the following chapters.

Understanding Observed Global Climate Change

Attempts to ascertain observed changes to the Earth's climate system have been the focus of scientific research since the 1950s. The prospect of humankind changing the Earth's climate by modifying atmospheric chemical composition was first discussed by Arrhenius (1896). This research has historically been atmospheric focused. However, climate change influences the coupled climate system which includes the ocean, atmosphere, terrestrial and cryospheric subsystems, and interactions between these.

Continuous observations of atmospheric carbon dioxide (CO_2) have been made since 1957 at the Mauna Loa observatory, Hawaii in the centre of the Pacific Ocean. These have shown a steady and increasing rate of atmospheric CO_2 concentrations, primarily sourced from the burning of fossil fuels in industrialised society. Similar measurements at other locations around the world in more recent times have confirmed this increasing trend, with Friedlingstein *et al*. (2010) suggesting the continuing increase is currently being driven largely by the emerging economies of China and India.

Detecting the CO_2 signal and evidence of change in other variables are the primary objectives in climate change research. These are confounded by poor long-term historical observational records of the global climate system. Attempting to ascertain the CO_2 signal from geophysical noise associated with sparse temporal and spatial data coverage is extremely difficult, and is also confounded by other factors. Some of these include: the effects of natural (volcanic) and anthropogenic aerosols suppressing the CO_2 warming signal; inhomogeneities and biases due to changes to observational platforms, their locations and interactions with the immediate physical environment; Contamination by geodetic biases (land rising and sinking for sea-level data for example). Von Storch & Zwiers (1999), provide a comprehensive overview of geophysical data problems. Even though there are significant challenges, detection and attribution of the CO_2 signal is a key focus of climate change research. The key intention is to best inform and prepare humankind for likely Earth system changes now and into the future.

In addition to the lack of comprehensive observational records, climate variability is another effect which confounds detection and attribution of CO_2-forced anthropogenic climate change. This manifests in largely cyclical climate modes on global and regional-scales. Such climate modes include the: El Nino Southern Oscillation (ENSO), Pacific Decadal Oscillation (PDO), North Atlantic Oscillation (NAO), and the Southern Annular Mode (SAM), amongst others. These modes have regional, and in some cases, broad-scale influence over many coupled ocean-atmosphere climate variables. Their influence can range from 3-7 years in the case of ENSO, to 20-30 years in the case of the PDO. The phenomena manifest in oscillations to broad-scale surface ocean temperature and rainfall patterns. The climate variability "envelope", determined by observed secular magnitudes and amplitudes, needs to be considered explicitly when attempting to ascertain long-term changes for any given climate variable. The International Meteorological Organisation defines mean climate over a 30-year averaging interval, an attempt to average out variability, providing a "baseline" over which changes can be computed. Changes determined from timeseries <30-years therefore can be problematic, as biases due to the effects of variability may skew the resolved changes. This long-term trends versus climate variability "envelope" is a key concept, and provides a framework through which to consider new estimates of change presented in the following chapters.

History of Global Ocean Observation

Modern oceanography began with the Challenger Expedition. The HMS *Challenger* was the first true oceanographic research vessel specifically designed to investigate physical, biological, geological and chemical properties of the Atlantic Ocean and seafloor. A 4-year long research cruise was undertaken on this vessel from 1872-1876. Since this time, oceanography has undergone many observational, platform and data-precision revolutions.

Hydrographic (salinity, temperature and select chemical tracers) sampling first came to prominence in an early Atlantic Ocean survey undertaken in 1925-27 on the FS *Meteor*. This expedition used discrete bottle measurements, obtained at depth and then analysed for salinity and chemical properties, along with reversing thermometers. Since this early 20th century expedition, there have been a number of major efforts to explore the full-depth properties of the global and regional oceans. The sequence of key expeditions includes: the International Geophysical Year (IGY; 1956-1960) which provided Atlantic Ocean coverage with a systematic, high quality, top-to-bottom, continent-to-continent grid of hydrographic stations; the Geochemical Ocean Sections Study (GEOSECS; 1972-1978) which provided a global survey of chemical, isotopic and radiochemical tracers in the ocean for the Atlantic (1972-1973), Pacific (1973-1974) and Indian Oceans (1977-1978); and the Transient Tracers in the Ocean (TTO; 1981-1983) which considered the North Atlantic (1981) and tropical Atlantic (1983) hydrography.

In parallel to observational expeditions, new and evolving platforms ensured that data quality was increasingly more accurate, and easier to obtain. Nansen bottles (or metal cylinders) were designed in 1910, and allowed deep seawater samples to be retrieved and for the first time provided an efficient method to record in-situ salinity alongside temperature measurements from reversing thermometers. Mechanical BathyThermographs (MBTs) were developed in the 1940s and became a standard temperature observation platform, providing measurements to 200m. Salinity-Temperature-Depth (STD) and Conductivity-Temperature-Depth (CTD) platforms were developed in the mid-1950's and for the first time provided an efficient method to record in-situ salinity alongside temperature measurements from thermistors (semiconductors used in oceanography). This breakthrough, largely due to technical improvements in the measurement of conductivity of seawater, provided a dramatic increase in global ocean observations being recorded to full depth. Previously, ocean observations of salinity were undertaken by various chemical titration techniques for a given seawater sample. The use of CTD's provided an increase in data accuracy, with the precision of the titration method of salinity measurement commonly in practise during this time noted as 0.02 (PSS-78), whereas CTD's provided improved accuracies to 0.002 (PSS-78). Alongside the development of CTD's, eXpendable BathyThermographs (XBTs) were under development. XBTs came into service in the late 1960s, providing observational coverage to either 460m or 750m depending on their design (Wijffels *et al*., 2008). The temporal and zonal coverage from these various platform types is presented in Figure 1.1.

The dominance of Northern Hemisphere observations is clear in Figure 1.1, with particularly good spatial and temporal coverage found in the Atlantic basin (Figure 1.2).

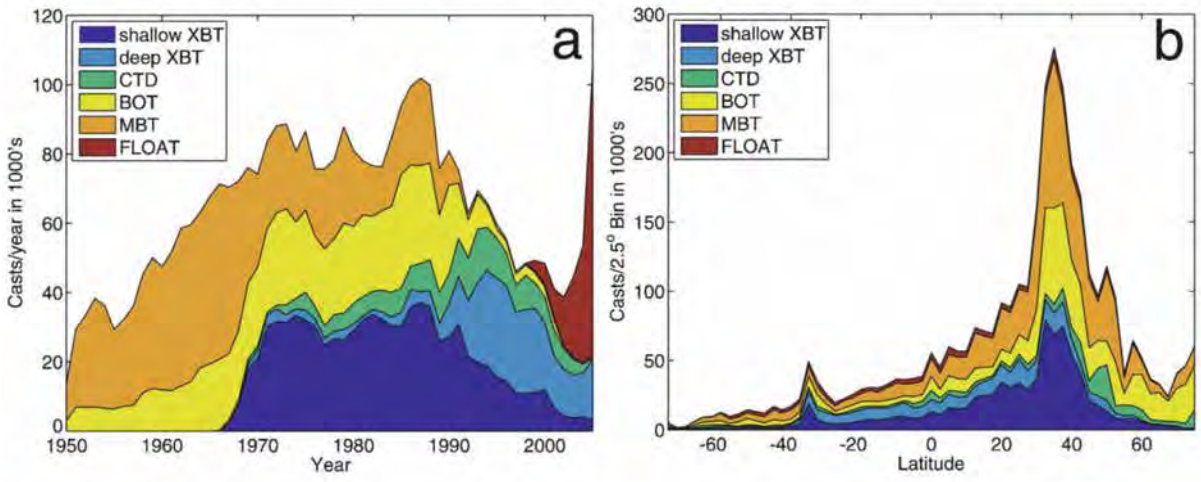

Figure 1.1. Ocean profile data from the ENACT3 data archive and platform type for (a) per year and (b) in 2.5° zonal (latitude) bins. Reproduced from Wijffels et al. (2008).

The significant variability associated with the ocean mesoscale had been recognised by previous expeditions, and in the 1990's resulted in the World Ocean Circulation Experiment (WOCE) Hydrographic Programme (WHP). The WOCE program (1990-1998) undertook global ocean sampling, for all of the 3 major ocean basins. These observed sections were continuously sampled during the experiment in an attempt to capture the interannual variability of the ocean. The precision of the WOCE measurements was truly unique, with hydrographic observations providing very high quality in situ temperature (0.002°C) and salinity (0.002 PSS-78) measurements with these accuracies dependent on the frequency and technique of calibration. This collective historical database totalled approximately 7.9 million temperature profiles and 2.3 million salinity profiles from the various platforms up to 2005 (Bindoff *et al*., 2007).

A new era of ocean observation began in 1999, with the development and implementation of the Argo Program (Gould *et al*., 2004). The program was specifically designed in an attempt to address the issues associated with discontinuous global hydrographic observations. The clear improvement in the observational spatial and temporal coverage is expressed in Figure 1.2, with near complete global coverage achieved around 2005.

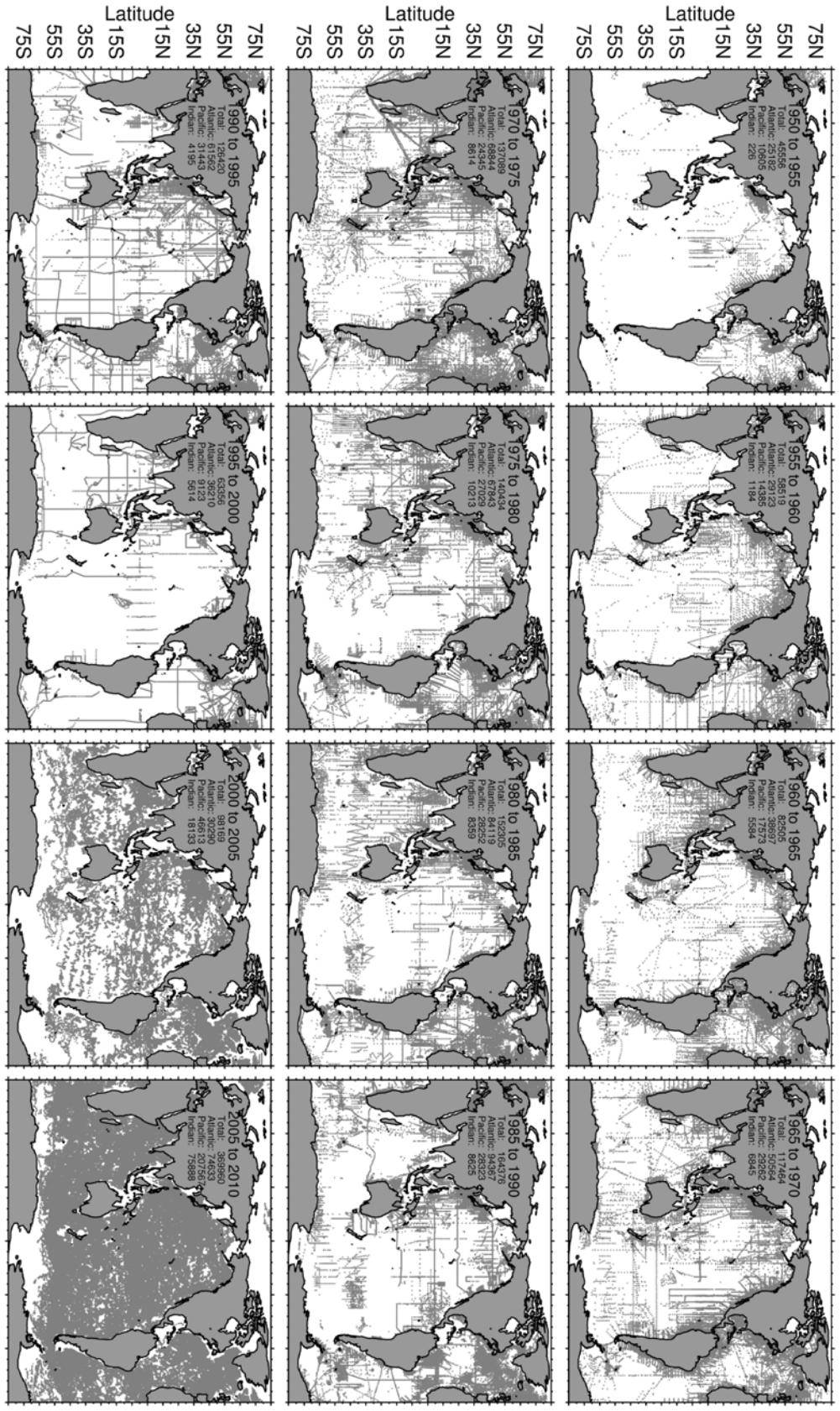

Figure 1.2. Hydrographic profile data used in this study. Global coverage for 5-year temporal bins, from 1950-1955 (top left) to 2005-2010 (bottom right). The dominance of the Argo floats and the improved spatial and temporal observational coverage is clear over 2000-2010 when compared to the earlier period.

Argo floats provide unprecedented observational data coverage from the near surface to 2000m, with temperature and salinity measurements that approach ship-based data accuracy. For the first time, near-global ocean observation was achieved, providing complete seasonal data coverage. In particular the Argo Program is providing much higher temporal and spatial coverage which is enabling a better understanding of ocean variability. With its continued operation, the Argo Program will provide a much-needed baseline from which a quantitative assessment of long-term ocean climate change can be made.

Active Argo floats now number over 3200 as of November 2010, the current database including profiles from over 6800 floats since the project began. Well over 700,000 individual profiles from 1999 to the present have been obtained. This new data stream accounts for almost half the entire 1.6 million profiles stored in the high-quality historical hydrographic database. Regionally, Argo provides well over half the austral winter profile coverage south of 30°S, with just 10 years of data, compared to the historical database which spans 130 years (Figure 1.2; Chapter 2 contains more information).

Observed Changes to the Global Ocean

Large temperature and associated heat content changes, along with subsurface salinity changes for the global ocean were reported by Bindoff *et al.* (2007) as part of the IPCC Fourth Assessment Report (AR4). They concluded that ocean salinity changes were consistent with changes to the water cycle, with near-surface waters in evaporation regions becoming saltier, and high latitude regions freshening, consistent with enhanced rainfall.

Ocean salinity has been the focus of few global studies, primarily due to the paucity of historical data coverage for the global oceans (Figure 1.1 & 1.2). Previous studies have reported long-term changes to ocean surface and subsurface salinity. Using 2.3 million salinity profiles available from 1955-1998, Boyer *et al*. (2005) described a freshening global ocean, however large uncertainties for this global estimate were considered, due to poor data coverage. They suggested that the Atlantic was experiencing a subtropical enhanced salinity contained in the upper 500m, a result supported by Curry *et al*. (2003) however with larger magnitudes. An Atlantic freshening north of 42°N was reported by Curry & Mauritzen (2005) and also supported by Boyer *et al*. (2007). Enhanced surface salinities were also found in the subtropical regions of the South Pacific and near-surface Indian Ocean. Freshening was found in the Mode Waters of the South Indian Ocean (5°-42°S) and freshening in the remainder of the Pacific outside the gyre zone. Their results suggested regions of high salinity were experiencing increases, and conversely regions of low salinity were freshening, with a general broad-scale amplification of the mean pattern. These results have more recently been confirmed in regional or global studies by Cravatte *et al.* (2009), Delcroix *et al*. (2007), Helm *et al.* (2010), Hosoda *et al*. (2009) and Roemmich & Gilson (2009). More details are provided in Chapter 2.

Coherent and broad-scale warming was also described for the upper 700m. Domingues *et al.* (2008) provided new estimates of globally-integrated ocean heat content and thermosteric sea-level rise, with their analysis for the first time considering bias corrections to XBT profiles (e.g. Wijffels *et al.*, 2008). This analysis provided trends around 50% larger than past estimates, for the period 1961-2003. Ongoing work is continuing to most accurately diagnose and correct problems with the XBT platform, which comprises around 70% of the historical temperature profile database for the global oceans. In comparison, ship-based CTD profiles and data from Argo floats are largely free from systematic platform biases. More details are provided in Chapter 4.

More recent estimates of ocean variability and seasonal cycle operation were made possible from Argo data, with Roemmich & Gilson (2009) quantifying the attributes of the modern ocean using 5-years of data from 2004-2008. In particular, Southern Hemisphere coverage was for the first time “global” with large increases, particularly in the ocean interior, a region of historical data paucity. This data provided a unique regional perspective of the oceans, and with unprecedented spatial and temporal coverage, largely validated climatologies generated from previous historical databases. Their analysis suggested regional patterns of change were occurring, by comparing the Argo modern climatology to historical climatology, a phase change from the previous estimates of integrated global total changes, particularly for ocean heat content (e.g. Domingues *et al*., 2008).

The Ocean's Role in the Global Water Cycle

The global water cycle comprises flux interactions between the ocean, atmosphere, land surface (and subsurface) and cryospheric subsystems. Covering 71% of the globe, capturing ~80% of global surface freshwater fluxes and containing 96% of its free water; the global ocean plays a large role in the Earth's water cycle (Figure 1.3).

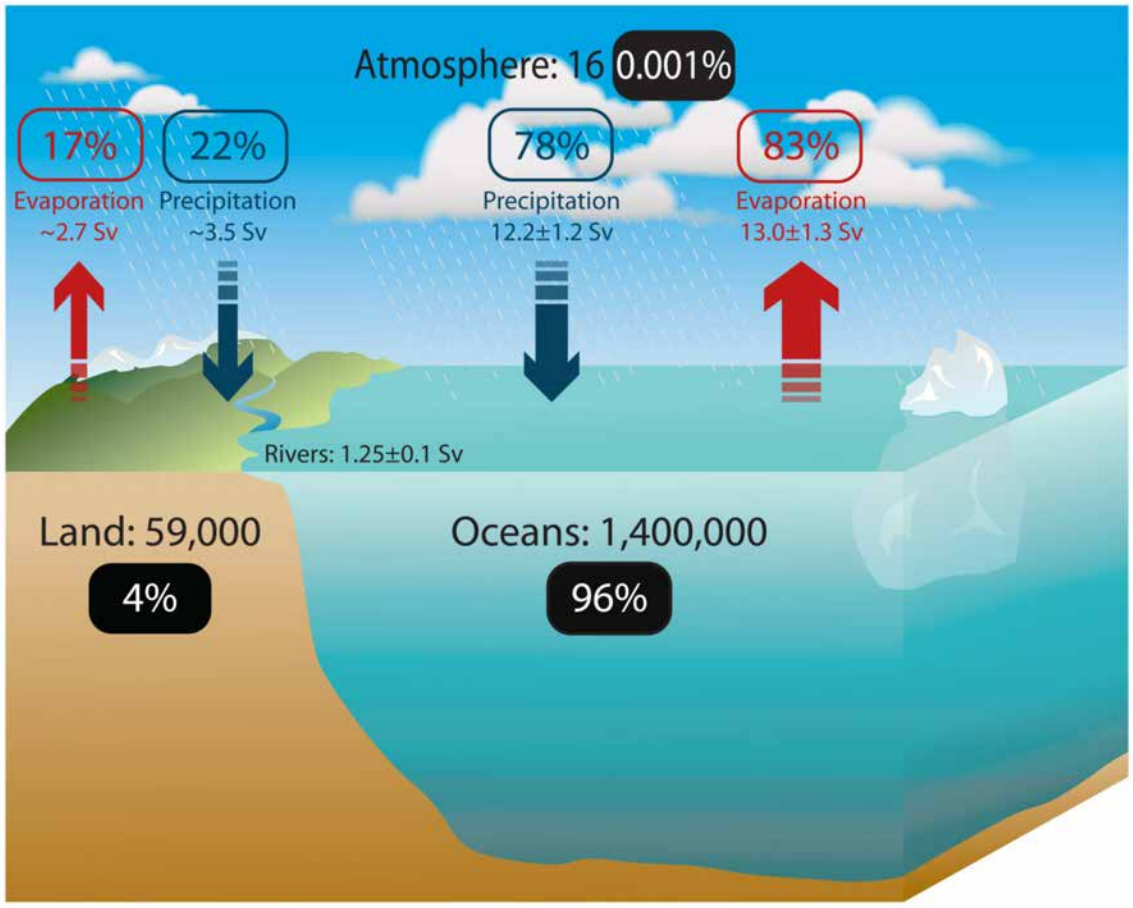

Figure 1.3. Adapted schematic (after Schmitt, 1995 and Schanze *et al.*, 2010) represents the key role of the ocean in the global water cycle. Reservoir estimates represent storages in 10^3 km^3, flux estimates represent transports in Sverdrups (10^6 m^3 s^{-1}) and values within boxes represent the approximate percentage of total storages (black boxes) or flux estimates (rainfall = blue; evaporation = red) for the global surface.

The ocean's water cycle is reflected in the surface and subsurface salinity field. There is a strong spatial pattern correlation between climatological mean sea surface salinity and the evaporation minus precipitation (E-P) field, which drives it at the ocean surface (Chapter 3). The distribution of regional ocean salinity reflects changes to E-P and the associated atmospheric transports of freshwater from one part of the ocean to another. In a long-term, steady-state sense, systematic freshwater transports by the atmosphere, for example from the ocean subtropics to the subpolar regions, between oceans as well as from the oceans to land, are counteracted by equally large freshwater transports in the oceans. These act to restore freshwater and salt balances (Wijffels *et al.*, 1992). The sum of meridional oceanic and atmospheric freshwater transport must equal the terrestrial meridional flow (both land surface

and groundwater). The large portion of this global transport (95%) occurs through the ocean and atmosphere (Schanze *et al*., 2010).

Due to the general zonal character of atmospheric circulation, the presence of high meridional topography on land leads to net moisture fluxes between ocean basins. Moisture is transported both poleward and equatorward from the subtropics which have positive E-P. The equatorward freshwater transport, mainly through the Hadley circulation, causes a net equatorward transfer of heat, with the convergence of moisture near the equator causing large negative E-P (Stigebrandt, 2000). Both the Atlantic and Indian Oceans have positive basin-average E-P, with the excess moisture transported to the Pacific, which has a negative basin-average E-P (Chen *et al*., 1994).

This imbalance then drives equivalent magnitude restoring freshwater transports in the oceans, with the transports having to be such that salinity distribution is preserved in steady state. Net atmospheric freshwater fluxes lead to anomalous freshening and higher sea-level in the Pacific compared to the Atlantic. This causes a restoring flow through the Bering Strait into the Arctic and a net circulation of salt in the global ocean. Baumgartner & Reichel (1975) indicate the following freshwater fluxes are necessary to maintain balance in the global system: North Pacific +0.75 Sv, South Pacific +0.13 Sv, North Atlantic -0.12 Sv, South Atlantic -0.33 Sv and the Indian Ocean -0.44 Sv. As shown in Wijffels *et al*. (1992), and updated in Stigebrandt (2000) the ocean and atmosphere work in concert to transport global freshwater when considered zonally. These transports also appear to have a clear seasonal cycle, with meridional transports represented by hemispheric means directly offsetting over a year (Chen *et al*., 1995).

Ocean salinity is affected by E-P, mixing, formation and sublimation of sea-ice and terrestrial cryospheric components. Atmospheric freshwater transports tend to change the distribution of ocean salinity. A complex system of oceanic freshwater transports restore this, including: 1) barotropic transports due to unbalanced precipitation minus evaporation plus runoff (P-E+R); 2) baroclinic transports due to horizontal salinity (freshwater) gradients; 3) baroclinic transports due to temperature (heat) gradients; 4) Ekman transports forced by steady winds in the upper layers; and 5) dispersive transports by eddies and wind anomalies. Oceanic transport of types 1 & 2 are directly forced by E-P at the ocean surface, while 3, 4 & 5 are due to thermal and wind-forcings which are essentially independent of E-P. The long-term oceanic response to E-P forcing is complex, as it includes density and wind-forced circulation as well as tidal diapycnal mixing and turbulent mixing associated with topography (Stigebrandt, 2000). More details are provided in Chapter 3 and 4.

Anticipated Changes to the Global Water Cycle

Future changes to the global water cycle, in response to anthropogenic climate change, are a key focus of ongoing research. Climate model realisations for the 21st century consistently project rainfall increases in high latitudes and parts of the tropics, with corresponding decreases in subtropical and lower latitude regions (Bates *et al.*, 2008). Models agree more consistently in their broad-scale patterns over terrestrial regions, with large uncertainties apparent over the global oceans (Meehl *et al*., 2007). As the climate warms, thermodynamic changes described by the Clausius-Clapeyron (CC) relation, suggest saturation vapour pressure in the lower troposphere will increase at a rate of 7% K^{-1}. This increase in the ability of the atmosphere to "hold" and transport more water will drive an increase in water cycling, through the ocean-atmosphere freshwater fluxes which comprise 80% of globally integrated totals.

A number of recent model-based studies have suggested the response of global mean rainfall will not follow the idealised rate suggested by CC. Energetic constraints on future water cycle changes, have been discussed by Schneider *et al*. (2010), Held & Soden (2006) and Allen & Ingram (2002). They suggest the reason for the muted response of global mean rainfall (1-3% K^{-1}) compared to CC, is the inability of the lower troposphere to radiate the latent heat of condensation, constrained by the relatively small changes in radiative fluxes. E-P changes, which represent atmospheric water cycling through water vapour transport, are expected to change at the CC rate, with this feature more relevant for regional changes to rainfall in contrast to the global mean. These results strongly support the concept that climatological wet regions will get wetter and arid regions drier in response to warming.

Anticipated global ocean water cycle changes have not been extensively considered in previous analyses. Stott *et al.* (2008), one of the first studies to consider model salinity fields, attributed salinity changes in the North Atlantic to climate change. They used a detection and attribution technique for a single climate model and the available observational estimates of Boyer *et al*. (2005) and Smith & Murphy (2007). They concluded that North Atlantic salinity increases (20°-50°N) are attributable to anthropogenic climate change, suggesting changes have already occurred to the water cycle over the ocean, and are expected to continue into the future. Changes to the ocean water cycle as captured in integrated sea-level rise (SLR) halosteric (salinity) estimates were presented by Pardaens *et al*. (2011). They considered 21st century projections from the CMIP3 suite, and suggested that the spatial patterns of change described in observations were likely to continue to amplify, with strong enhanced salinities for the Atlantic basin, and freshening for the Pacific basin in response to warming. More details are provided in Chapter 4.

Observed Change to the Global Water Cycle

Changes to the global water cycle have been observed over the 20th and early 21st century. Many previous studies have determined changes to the water cycle, most considering changes to water cycle properties over the global oceans. Changes to properties such as precipitable water (PW; column integrated water vapour), global and regional rainfall and evaporation, and changes to ocean salinity (discussed above) have all suggested an enhanced water cycle has occurred. Paucity of observed data however, ensures that complete confidence in these estimates is not currently achievable.

When considering global surface changes, sparse observational networks have ensured global data coverage is not available. However, Trenberth *et al*. (2007) suggest that rainfall has generally increased over land north of 30°N in the 20th century, but drying trends have dominated the tropics since the 1970s. They also suggest that extreme rainfall events have increased in their intensity over land regions, even in locations where a downward trend in overall average rainfall has been observed. However, this data is only statistically significant for a few locations where sufficient data coverage is available.

The prevalence of drought conditions has also increased, as summarised by Trenberth *et al*. (2007). These changes have been driven by decreases in terrestrial precipitation and concurrent warming, which have enhanced evapotranspiration. Enhanced drought conditions appear to have a strong relationship with sea surface temperature (SST) changes, especially in tropical regions, and the associated atmospheric circulation and rainfall changes (Trenberth *et al*., 2007).

In the more recent period (1980-) the prevalence of satellite observations has enabled more accurate global analyses to be undertaken. These records suggest that tropospheric water vapour (precipitable water) is increasing in response to warming, with a consistent increasing trend over the global oceans since 1988. Trenberth *et al.* (2007) suggest that a 4% increase in column water vapour has occurred since 1970. More details on observed global water cycle changes will be presented in Chapter 3.

Key Questions Addressed in this Thesis

It is clear that observed changes to the coupled ocean-atmosphere-terrestrial water cycle have been expressed in the 20th and early 21st century. As the global ocean comprises a very large portion of water cycle operation (~80% of global surface fluxes), it is expected that ocean changes will strongly reflect coherent water cycle changes, integrated over the long-term in ocean salinity.

Some key questions to be addressed in the following chapters include:

1. How has global ocean salinity changed over the 20th century?
2. Can the patterns of salinity change be used as a climate diagnostic? If yes, does this provide a quantitative estimate of past water cycle changes?
3. Do CMIP3 models capture the observed spatial salinity patterns?
4. Do CMIP3 models replicate the reported rates of observed water cycle changes?
5. Considering the full-depth global ocean, are observed changes coherent in their structure, and are the spatial patterns of ocean change represented in CMIP3 future projections?

Further questions and suggested areas for continued research, prompted by new results presented in the following chapters are summarised in Chapter 5.

References

Allen, M.R. and W.J. Ingram (2002) Constraints on future changes in climate and the hydrologic cycle. *Nature*, **419**, pp 224-232. doi: 10.1038/nature01092

Arrhenius, S.A. (1896) On the Influence of Carbonic Acid in the Air upon the Temperature of the Ground. *Philosophical Magazine and Journal of Science*, **41**, pp 237-276

Bates, B.C., Z.W. Kundzewicz, S. Wu and J.P. Palutikof, Eds (2008) Climate Change and Water. Technical Paper of the Intergovernmental Panel on Climate Change, IPCC Secretariat, Geneva, 210 pp. Available online: http://www.ipcc.ch/publications_and_data/publications_and_data_technical_papers_climate_change_and_water.htm

Baumgartner, A. and E. Reichel (1975) *The World Water Balance: Mean Annual Global, Continental and Maritime Precipitation, Evaporation and Runoff*. Elsevier Science Ltd. Amsterdam. 179 pp

Bindoff, N.L., J. Willebrand, V. Artale, A. Cazenave, J. Gregory, S. Gulev, K. Hanawa, C. Le Quere, S. Levitus, Y. Nojiri, C.K. Shum, L.D. Talley and A. Unnikrishnan (2007) Observations: Oceanic Climate Change and Sea Level. In: *Climate Change 2007: The Physical Science Basis. Contribution of Working Group I to the Fourth Assessment Report of the Intergovernmental Panel on Climate Change*. Solomon, S., D. Qin, M. Manning, Z. Chen, M.C. Marquis, K. Averyt, M. Tignor and H.L. Miller (Eds). Cambridge University Press, Cambridge, United Kingdom and New York, NY, U.S.A. pp 385-432

Boyer, T.P., S.Levitus, J.I. Antonov, R.A. Locarnini and H.E. Garcia (2005) Linear trends in salinity for the World Ocean, 1955-1998. *Geophysical Research Letters*, **32**, L01604. doi: 10.1029/2004GL021791

Boyer, T., S. Levitus, J. Antonov, R. Locarnini, A. Mishonov, H. Garcia and S.A. Josey (2007) Changes in freshwater content in the North Atlantic Ocean 1955-2006. *Geophysical Research Letters*, **34**, L16603. doi: 10.1029/2007GL030126

Chen, T-C., J. Pfaendtner, S-P. Weng (1994) Aspects of the Hydrological Cycle of the Ocean-Atmosphere System. *Journal of Physical Oceanography*, **24**, pp 1827-1833. doi: 10.1175/1520-0485(1994)024<1827:AOTHCO>2.0.CO;2

Chen,T-C., J-M. Chen and J. Pfaendtner (1995) Low-Frequency Variations in the Atmospheric Branch of the Global Hydrological Cycle. *Journal of Climate*, **8**, pp 92-107. doi: 10.1175/1520-0442(1995)008<0092:LFVITA>2.0.CO;2

Cravatte, S., T. Delcoix, D. Zhang, M. McPhaden and J. LeLoup (2009) Observed freshening and warming of the western Pacific Warm Pool. *Climate Dynamics*, **33**, pp 565-589. doi: 10.1007/s00382-009-0526-7

Curry, R., B. Dickson and I. Yashayaev (2003) A change in the freshwater balance of the Atlantic Ocean over the past four decades. *Nature*, **426**, pp 826-829. doi: 10.1038/nature02206

Curry, R. and C. Mauritzen (2005) Dilution of the Northern North Atlantic Ocean in Recent Decades. *Science*, **308**, pp 1772-1774. doi: 10.1126/science.1109477

D'Odorico, P., F. Laio and L. Ridolfi (2010) Does globalization of water reduce societal resilience to drought? *Geophysical Research Letters*, **37**, L13403. doi: 10.1029/2010GL043167

Delcroix, T., S. Cravatte and M.J. McPhaden (2007) Decadal variations and trends in tropical Pacific sea surface salinity since 1970. *Journal of Geophysical Research*, **112**, C03012. doi: 10.1029/2006JC003801

Domingues, C.M., J.A. Church, N.J. White, P.J. Gleckler, S.E. Wijffels, P.M. Barker and J.R. Dunn (2008) Improved estimates of upper-ocean warming and multi-decadal sea-level rise. *Nature*, **453**, pp 1090-1093. doi: 10.1038/nature07080

Friedlingstein, P., R.A. Houghton, G. Marland, J. Hackler, T.A. Boden, T.J. Conway, J.G. Canadell, M.R. Raupach, P. Ciais and C. Le Quéré (2010) Update on CO_2 emissions. *Nature Geoscience*, **3**, pp 811-812. doi: 10.1038/ngeo1022

Gould, J., D. Roemmich, S. Wijffels, H. Freeland, M. Ignaszewsky, X. Jianping, S. Pouliquen, Y. Desaubies, U. Send, K. Radhakrishnan, K. Takeuchi, K. Kim, M. Danchenkov, P. Sutton, B. King, B. Owens and S. Riser (2004) Argo Profiling Floats Bring New Era of In Situ Ocean Observations. *Eos, Transactions of the American Geophysical Union*, **85**, pp 190-191. doi: 10.1029/2004EO190002

Held, I.M. and B.J. Soden (2006) Robust Responses of the Hydrological Cycle to Global Warming. *Journal of Climate*, **19**, pp 5686-5699. doi: 10.1175/JCLI3990.1

Helm, K.P., N.L. Bindoff and J.A. Church (2010) Changes in the global hydrological-cycle inferred from ocean salinity. *Geophysical Research Letters*, **37**, L18701. doi: 10.1029/2010GL044222

Hosoda, S., T. Sugo, N. Shikama and K. Mizuno (2009) Global Surface Layer Salinity Change Detected by Argo and Its Implication for Hydrological Cycle Intensification. *Journal of Oceanography*, **65**, pp 579-586

Meehl, G.A., T.F. Stocker, W.D. Collins, P. Friedlingstein, A.T. Gaye, J.M. Gregory, A. Kitoh, R. Knutti, J.M. Murphy, A. Noda, S.C.B. Raper, I.G. Watterson, A.J. Weaver and Z.-C. Zhao (2007) Global Climate Projections. In: *Climate Change 2007: The Physical Science Basis. Contribution of the Working Group I to the Fourth Assessment Report of the Intergovernmental Panel on Climate Change*. Solomon, S., D. Qin, M. Manning, Z. Chen, M. Marquis, K.B. Averyt, M. Tignor and H.L. Miller (Eds). Cambridge University Press, Cambridge, United Kingdom and New York, NY, U.S.A. pp 747-845

Pardaens, A.K., J.M. Gregory and J.A. Lowe (2011) A model study of factors influencing projected changes in regional sea level over the twenty-first century. *Climate Dynamics*, **36**, pp 2015-2033. doi: 10.1007/s00382-009-0738-x

Roemmich, D. and J. Gilson (2009) The 2004-2008 mean and annual cycle of temperature, salinity, and steric height in the global ocean from the Argo Program. *Progress in Oceanography*, **82**, pp 81-100. doi: 10.1016/j.pocean.2009.03.004

Schanze, J.J., R.W. Schmitt and L.L. Yu (2010) The Global Oceanic Freshwater Cycle: A Best-Estimate Quantification. *Journal of Marine Research*, **68**, pp 569-595. doi: 10.1357/002224010794657164

Schmitt, R.W. (1995) The ocean component of the global water cycle. U.S. National Report to the International Union of Geodesy and Geophysics, 1991-1994. *Reviews of Geophysics*, **33** (Supplement), pp 1395-1409

Schneider, T., P.A. O'Gorman and X.J. Levine (2010) Water Vapor and Dynamics of Climate Changes. *Reviews of Geophysics*, **48**, RG3001. doi: 10.1029/2009RG000302

Seager, R., N. Naik and G.A. Vecchi (2010) Thermodynamic and Dynamic Mechanisms for Large-Scale Changes in the Hydrological Cycle in Response to Global Warming. *Journal of Climate*, **23**, pp 4651-4668. doi: 10.1175/2010JCLI3655.1

Smith, D.M. and J.M. Murphy (2007) An objective ocean temperature and salinity analysis using covariances from a global climate model. *Journal of Geophysical Research*, **112**, C02022. doi: 10.1029/2005JC003172

Stigebrandt, A. (2000) Oceanic Freshwater Fluxes in the Climate System. In: *Freshwater Budget of the Arctic Ocean*. Lewis, E.L. (Ed). Kluwer Academic Publishers, Boston, MA, U.S.A. pp 1-20

Von Storch, H.V. and F.W. Zwiers (1999) Statistical Analysis in Climate Research. Cambridge University Press, Cambridge, United Kingdom and New York, NY, U.S.A. 484 pp

Stott, P.A., R.T. Sutton and D.M. Smith (2008) Detection and Attribution of Atlantic salinity changes. *Geophysical Research Letters*, **35**, L21702. doi: 10.1029/2008GL035874

Trenberth, K.E., P.D. Jones, P. Ambenje, R. Bojariu, D. Easterling, A. Klein Tank, D. Parker, F. Rahimzadeh, J.A. Renwick, M. Rusticucci, B. Soden and P. Zhai (2007) Observations: Surface and Atmospheric Climate Change. In: *Climate Change 2007: The Physical Science Basis. Contribution of Working Group I to the Fourth Assessment Report of the Intergovernmental Panel on Climate Change*. Solomon, S., D. Qin, M. Manning, Z. Chen, M. Marquis, K.B. Averyt, M. Tignor and H.L. Miller (Eds). Cambridge University Press, Cambridge, United Kingdom and New York, NY, U.S.A. pp 235-336

Wijffels, S.E., R.W. Schmitt, H.L. Bryden and A. Stigebrandt (1992) Transport of Freshwater by the Oceans. *Journal of Physical Oceanography*, **22**, pp 155-162. doi: 10.1175/1520-0485(1992)022<0155:TOFBTO>2.0.CO;2

Wijffels, S.E., J. Willis, C.M. Domingues, P. Barker, N.J. White, A. Gronell, K. Ridgway and J.A. Church (2008) Changing Expendable Bathythermograph Fall Rates and Their Impact on Estimates of Thermosteric Sea Level Rise. *Journal of Climate*, **21**, pp 5657-5672. doi: 10.1175/2008JCLI2290.1

Bibliography

Brewer, P.G., J.L. Sarmiento, W.M. Smethie Jr (1985) The Transient Tracers in the Ocean (TTO) Program: The North Atlantic Study, 1981; The Tropical Atlantic Study, 1983. *Journal of Geophysical Research*, **90**, C4. pp 6903-6905. doi: 10.1029/JC090iC04p06903

Craig, H. and K.K. Turekian (1980) The GEOSECS program: 1976-1979. *Earth and Planetary Science Letters*, **49**, pp 263-265. doi: 10.1016/0012-821X(80)90071-0

Emery, W.J. and R.E. Thomson (1998) *Data Analysis Methods in Physical Oceanography*. Elsevier Science Ltd. Oxford, U.K. 634 pp

Gould, W.J., J.M. O'Toole, J. Church, S. Rintoul, S. Wijffels, L. Talley, P. Robbins, G.C. Johnson, S. Imawaki, N. Suginohara, K. Hanawa, P. Koltermann, S. Osterhus, H. Freeland, A. Clarke and H. Mercier (2001) Hydrographic Section Observations. In: *Observing the Oceans in the 21st Century: A Strategy for Global Ocean Observations*. Koblinsky, C.J., N.R. Smith and Global Ocean Data Assimilation Experiment (Eds.). Godae Project Office and Bureau of Meteorology, Melbourne. CSIRO Publishing, Collingwood, Victoria, Australia. pp 351-360

King, B.A., E. Firing and T.M. Joyce (2001) Shipboard Observations during WOCE. In: *Ocean Circulation and Climate: Observing and Modelling the Global Ocean*. Siedler, G., J. Church and J. Gould (Eds.). Academic Press, London, U.K. pp 99-122

Pickard, G.L. and W.J. Emery (1990) *Descriptive Physical Oceanography: An Introduction (5th Edition)*. Pergamon Press PLC, Headington Hill Hall, Oxford OX3 OBW, U.K. 320 pp

Chapter 2

Ocean Salinity Changes 1950-2000

Abstract

Using over 1.6 million profiles of salinity, potential temperature and neutral density from historical archives and the international Argo Program, this study develops the three dimensional field of multi-decadal linear change for ocean state properties.

The period of analysis extends from 1950-2008, taking care to minimise the aliasing associated with the seasonal and major global El Nino Southern Oscillation modes. Large, robust and spatially coherent multi-decadal linear trends in salinity to 2000 dbar depth are found. Salinity increases at the sea surface are found in evaporation-dominated regions and freshening in precipitation-dominated regions with the spatial pattern of change strongly resembling that of the mean salinity field, consistent with an amplification of the global water cycle.

Subsurface salinity changes on pressure surfaces are attributable to both isopycnal heave and real water mass modification of the temperature-salinity relationship. Subduction and circulation by the ocean's mean flow of surface salinity and temperature anomalies appear to account for most regional subsurface salinity changes on isopycnals.

Broad-scale surface warming and the associated poleward migration of isopycnal outcrops drive a clear and repeating pattern of subsurface isopycnal salinity change in each independent ocean basin. Qualitatively, the observed global multi-decadal salinity changes are thus consonant with both broad-scale surface warming and the amplification of the global water cycle.

This chapter has been published and has the following citation:

Durack, P.J. and S.E. Wijffels (2010) Fifty-Year Trends in Global Ocean Salinities and Their Relationship to Broad-Scale Warming. *Journal of Climate*, **23**, pp 4342-4362. doi: 10.1175/2010JCLI3377.1

Chapter 3

Water Cycle Change expressed by Ocean Salinity

Abstract

New observed estimates of ocean surface salinity changes from 1950-2000 are compared to the latest results from the Coupled Model Intercomparison Project 3 (CMIP3) to diagnose explicit rates of water cycle change expressed by this model suite. Examining 20C3M realisations (which most closely resemble the observed 20th century climate system); explicitly dealing with model drift; and using a technique to extract the broad-scale, zonal change patterns – a strong relationship is found between changes in the global freshwater flux (E-P) over the oceans (where 80% of water exchange occurs between the ocean and atmosphere) and changes to ocean surface salinity.

The model ensemble mean, a frequently-used metric to express projected changes into the future, greatly underestimates the observed rate of 20th century ocean salinity change. Global average rainfall is confirmed to change weakly with surface warming (2-4% K^{-1}), agreeing with past results, however the pattern amplification of both E-P and ocean salinity fields indicate larger responses. New observed surface salinity estimates suggest a change of 16±7% K^{-1} has occurred since 1950, a marker of change to the ocean water cycle. Using the CMIP3 relationship between E-P and ocean salinity change which suggests salinity responds at twice the rate of E-P, allows a new estimate of observed E-P changes to be ascertained, yielding 4% (8±5% K^{-1}) for 1950-2000, closely following Clausius-Clapeyron.

The rate of observed 20th century change is also underestimated in future projections under the IPCC SRES scenarios for 2050-2099, expressing similar rates (% K^{-1}) to corresponding 20C3M realisations.

This chapter is to be submitted:

Durack, P.J. and S.E. Wijffels (in prep) Ocean Salinities Confirm a Strengthening Global Water Cycle

Introduction

Anthropogenic global climate changes in the latter half of the 20th and beginning of the 21st century are a well-accepted fact in the climate science community (IPCC, 2007; Stott *et al.*, 2010). A series of extreme climatic events occurring around the globe in the last decade have been experienced (continuing in 2010) and have already caused significant fatalities (Patz et al, 2005). The likelihood that these extrema will continue to rise in the future is very high indeed (Palmer & Räisänen, 2002; Stott *et al.*, 2004).

Anthropogenic climate change poses a significant threat to the global community, and will affect many aspects of the global and regional climate system. Warming of the global surface will drive a robust response in the global water cycle. This will result in an amplification of existing patterns of global mean rainfall and evaporation (Allen & Ingram, 2002; Held & Soden, 2006; Wentz *et al.*, 2007; Seager *et al.*, 2010). These water cycle changes will likely have adverse effects on the human built environment, with enhanced extreme events (droughts and floods; Allen & Ingram, 2002; Emori & Brown, 2005), and changes to regional water availability which will test our societal resilience to change (World Water Assessment Programme, 2009; Bates *et al.*, 2010). Therefore, a clear understanding of how the global water cycle operates and how this has changed over the observed climate of the past 20th century is required. Obtaining a better understanding of past changes will then facilitate more accurate projections of future changes in regions of habitation in the 21st century.

Current 21st century projections of future climate, from the Coupled Model Intercomparison Project Phase 3 (CMIP3; Meehl *et al.*, 2007a) suggest regions of high rainfall will become wetter, and arid regions become drier, attributable to climate change. There is however, little consistency in the seasonal changes provided by model projections. More importantly, regions of the greatest uncertainty in CMIP3 projections are found over the global oceans, which comprise 71% of the Earth's surface (Figure 3.1).

These models do not simulate the observed mean global water cycle perfectly, with biases present in the highly active equatorial zones in particular (e.g. Lin, 2007; de Szoeke & Xie, 2008; Bellucci *et al.*, 2010). Issues with the strength of modelled water cycles have also been reported, with Pardaens *et al*. (2003) considering HadCM3, suggesting it is over active when compared to observed estimates, particularly over the global ocean. Hagemann *et al*. (2006) drew a similar conclusion for ECHAM5. However, constant improvements are being made with the latest modelling systems more closely resembling observed patterns and magnitudes when compared to previous versions, a result reported by Hack *et al*. (2006) for the NCAR CCSM3.0 model. Currently these modelling systems however, are the best tools to investigate and understand past and future global water cycle changes. The observed rate of global water cycle change in the 20th century (and CMIP3 replication) is the key question being addressed by this analysis. A number of previous studies have indicated other metrics of 20th century water cycle changes have been underestimated by these models (Wentz *et al.*, 2007; Zhang *et al.*, 2007; Allan & Soden, 2008).

Water cycle changes are expected to follow the Clausius-Clapeyron relation, which suggests atmospheric water vapour saturation pressure varies with temperature. At temperatures normally expressed in the lower troposphere, this leads to an increase of ~7% K^{-1}, and assumes

relative humidity remains fixed. Consequently, as global temperatures increase, so too will water cycle activity, as the atmosphere "holds" and transports more water following this relationship.

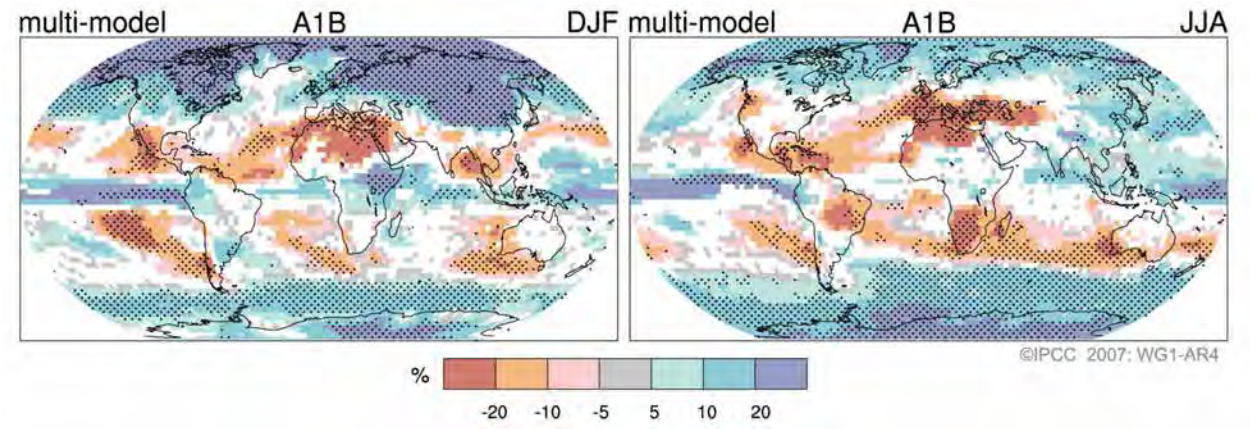

Figure 3.1. Projected patterns of rainfall changes (percent) for the period 2090-2099, relative to 1980-1999. Values are based on a model ensemble average from the SRES A1B scenario for December-February (left) and June-August (right). White areas indicate regions where less than 66% of models agree in the sign of changes, with stippling expressing regions where more than 90% of models agree in the sign of change. Reproduced from IPCC (2007).

Projections suggest regional changes are expected in response to climate change. However, global mean changes have been the focus of most previous studies, rather than regional estimates (e.g. Allen & Ingram, 2002; Held & Soden, 2006). These studies suggest water cycle changes expressed by global mean rainfall are constrained by atmospheric energy balances to increase at only 1-3% K^{-1} rather than the expected increase of 7% K^{-1} (Clausius-Clapeyron; CC). The inability of the troposphere to radiate latent heat released during phase changes from vapour to precipitation is thought to control the global rainfall change (e.g. Allen & Ingram, 2002; Held & Soden, 2006; Stephens & Ellis, 2008; Schneider *et al.*, 2010; Andrews & Forster, 2010). In contrast, recent observational estimates (Wentz *et al.*, 2007) have suggested tropical changes to rainfall and evaporation actually show a larger rate of increase (6% K^{-1}; 1987-2006) than model global average rainfall projections. These observed values are near those predicted by CC, and Wentz *et al.* (2007) questioned whether the weaker response in mean rainfall changes is a modelling artefact, rather than a real physical constraint of the observed global water cycle.

Global average rainfall is a useful metric of model performance. However, it is the regional changes of water fluxes which are most sought after by policy makers and the global community. While global average change may be constrained by the energy budget, regional changes may not. Large increases in high rainfall regions may be balanced by large decreases in low rainfall regions, and small net perturbations will be recorded in the global average. This *rate of regional and global water cycling* is the key climate attribute that we are interested in, and recent studies have suggested that large rates of observed regional change (in wet and dry zones over the tropical ocean), exceeding CC, are occurring (Allan *et al.*, 2010). This redistribution of evaporation and precipitation (E-P) has been investigated in the CMIP3 model suite by Seager *et al.* (2010). They suggest an amplification of the global E-P pattern follows CC with an expansion of the subtropical gyres poleward, the latter due to dynamic (circulation)

changes in response to warming. Concurrent thermodynamic changes, following the 7% K^{-1} response suggested by CC are also reported. This result suggests redistribution and enhancement to water cycling occurs with a weaker change in the global mean rainfall (Figure 3.2).

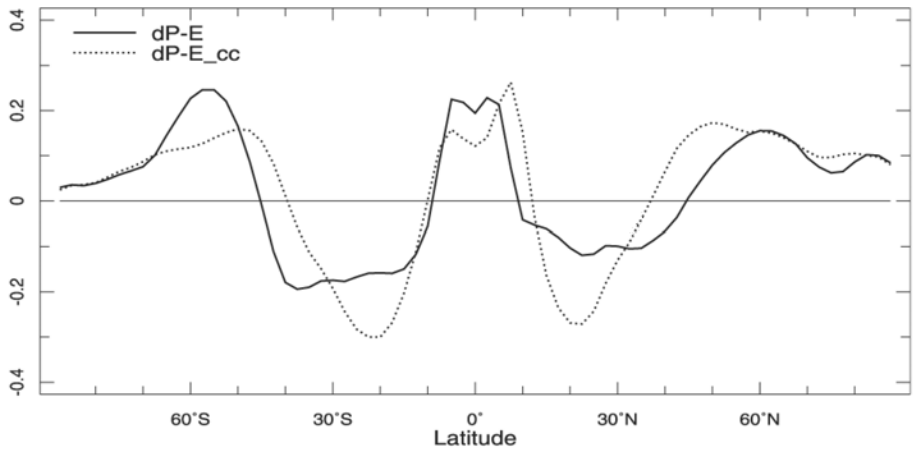

Figure 3.2. Annual zonal mean precipitation minus evaporation changes (P-E – solid line; P is positive) together with the changes in these terms estimated by the Clausius-Clapeyron (CC) relation (dashed line) in response to a lower troposphere warming. Units are mm day^{-1}. Reproduced from Seager *et al.* (2010).

The world oceans contain 97% of total global water stores and 80% of surface water fluxes across the globe occur over the ocean (Figure 1.3, Chapter 1). As the engine room of the global water cycle, can ocean salinity changes provide an estimate of past water cycle changes and their regional patterns?

Global ocean salinity patterns potentially provide a novel way to monitor changes to the water cycle. Climatologically, the surface open ocean regions (which are not influenced by terrestrial runoff) which receive excess rainfall over evaporation are fresher, with the converse true for regions which are dominated by evaporation (Figure 3.3). Annual mean climatologies of surface water flux (Josey *et al.*, 1998) and salinity (Chapter 2) have a spatial pattern correlation over the global oceans of 0.55. This suggests that the E-P annual mean climatology drives the surface salinity pattern beneath, a relationship reported for the tropical oceans by Johnson *et al.* (2002). The separate components of the climatological surface ocean freshwater budget have recently been quantified by Schanze *et al*. (2010) who concluded E-P fluxes dominate (95%) and nearly cancel with a smaller term for terrestrial runoff (5%). The influence of ice-melt was found to be negligible in global-integrals over their period of analysis (Table 3.1).

Table 3.1. Best-estimates of the global oceanic annual mean freshwater cycle for 1987-2006. Reproduced from Schanze *et al.* (2010)

Freshwater Source	Volume (Sv)	Percentage of total
Annual Mean Evaporation	-13.04±1.3	49.3
Annual Mean Precipitation	+12.18±1.2	46.0
Annual Mean Terrestrial runoff	+1.25±0.1	4.7
Annual Mean Budget imbalance	*0.39±1.8*	*1.5*
Cryospheric contributions (1993-2006)	0.01±0.01	~0

The relationship between surface salinity and E-P is understood to be one-way, as there is no known strong feedback from salinity to E-P for normal ocean salinities (salinity feedbacks on evaporation have only been recorded for highly saline brine waters; e.g. Panin & Brezgunov, 2007). A strong spatial correlation between multi-decadal changes to ocean surface salinity (Chapter 2 and Figure3.3A) and surface mean freshwater flux (E-P) patterns (Figure 3.3B) is also apparent, with pattern correlations of 0.45 for the global ocean surface (Figure 3.3).

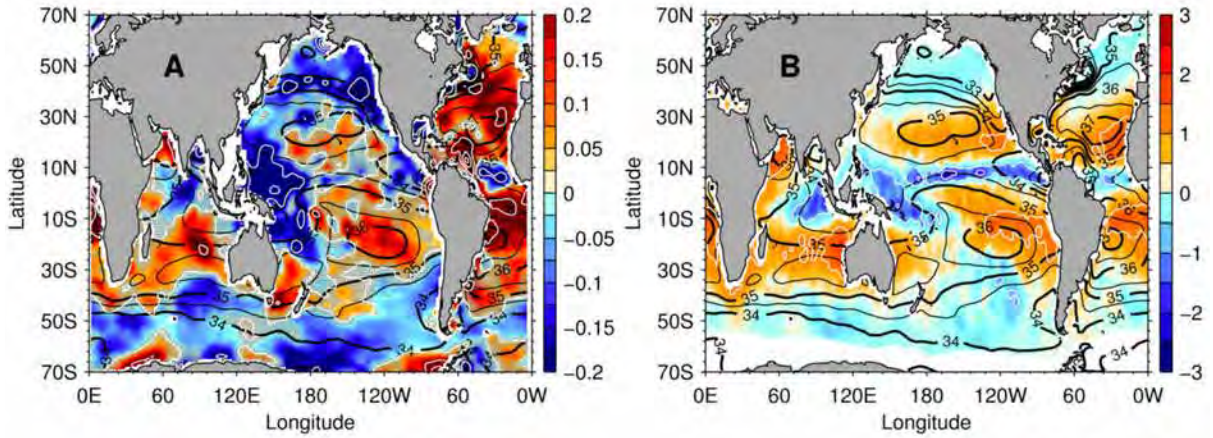

Figure 3.3. A) The 50-year linear surface salinity trend (pss 50yr^{-1}). Contours every 0.25 pss are plotted in white. B) Ocean-atmosphere freshwater flux (E-P; m^3 yr^{-1}) averaged over 1980-1993 (Josey *et al.*, 1998). Contours every 1 m^3 yr^{-1} are in white. On both panels, the 1975 surface mean salinity is contoured black (contour interval 0.5 pss for thin lines, 1 for thick lines).

Ocean Salinity as a Climate Diagnostic

The relationship between surface salinity and surface E-P changes might provide an insight into global water cycle changes. Changes to E-P over this 1950-2000 period are poorly known. These are reliant on sparse meteorological observations. The regionally variable nature of rainfall, a lack of long-term records over the oceans, and a poor understanding of highly regional surface fluxes confounds accurate estimates of change. The relationship between salinity and E-P provides a novel method to better approximate water cycle changes.

Chapter 2 documented clear and coherent ocean salinity changes from 1950-2000. Can these new estimates provide a better understanding of the changing water cycle? From these results it is clear that regions dominated by rainfall, such as the western equatorial Pacific Ocean and

Southern Ocean, are getting fresher, and the dry centre of the subtropical gyres of each ocean basin, are becoming saltier (dominated by evaporation) particularly in the Southern Hemisphere (Figure 3.3). These 50-year changes essentially represent an amplification of the mean spatial pattern of surface salinity (and imply changes to E-P have occurred), consistent with expectations of an enhanced water cycle.

The spatial correlation of multi-decadal linear surface salinity changes and climatological mean surface salinity is 0.5 (Figure 3.4) and implies an amplification of the mean ocean surface salinity pattern of 7.7%. This suggests fresh regions get fresher and salty regions saltier, following the expected response of an amplified water cycle – wet gets wetter and dry gets drier (Allen & Ingram, 2002; Held & Soden, 2006; Wentz *et al.*, 2007; Seager *et al.*, 2010).

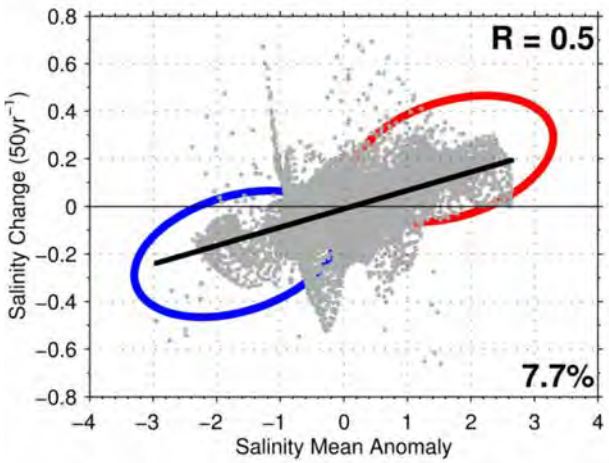

Figure 3.4. Observed surface salinity changes versus mean salinity spatial anomalies. The x-axis is the point-wise anomaly from the spatially average mean surface salinity (34.8 pss), and the Y-axis the associated point-wise multi-decadal linear salinity change trend (pss 50yr^{-1}). The blue and red ellipse represent regions where fresh regions (compared to the global surface mean salinity) are getting fresher and salty regions getting saltier, respectively. Using the full global surface salinity analysis, yields a pattern amplification of 7.7%.

Is the observed amplification of the surface salinity patterns (Figure 3.4) simulated in CMIP3 20th century (20C3M) realisations? And if so, what do salinity changes suggest about the global water cycle response to warming?

Diagnosing Salinity and Water Cycle Changes in CMIP3

Model data analysed in this study was sourced from available 20C3M realisations from CMIP3, obtained from the Program for Coupled Model Intercomparison and Diagnosis (PCMDI) data portal for the 5 variables presented in Table 3.2. These variables were selected as they provide an insight into water cycle representation. More detailed information for each model is found in Table 3.S1.

Table 3.2. Available models and variables for 20C3M experiments from the CMIP3

Model Variable	Available models	Available realisations	De-drifted realisations
Ocean Salinity	23	58	50
Ocean Freshwater Flux (E-P)	17	47	44
Ocean Temperature	24	63	41
Global Surface Temperature	25	78	70
Global Precipitation	25	73	68

Monthly fields were used to form annual averages which were then analysed point-wise for linear multi-decadal trends. Model grids were interpolated onto the 1° latitude and 2° longitude observed grid (Chapter 2), and the marginal sea exclusion grid was applied to all model ocean fields (Figure 2.1).

In addition, corrections to CMIP3 data were required before proceeding with the analysis. Consideration of individual realisations allowed for the diagnosis and correction of; incorrectly signed model fields, wrongly labelled scenarios, time axes, missing values and other problems which would not be noticed in model ensemble-average analyses. Such data issues would lead to spurious diagnostics, and may have been overlooked in previous analyses.

In order to quantitatively determine rates of change due to external climate forcing, there is a need to explicitly account for the spurious climate drift which is inherent in model realisations (more detail is available in Appendix 1). Model drift confounds climate change rate assessments, and can mask the true forced transient response. Drift removal is therefore required before accurate rates of global and regional estimates of changes can be made. While globally averaged surface drift is generally small (e.g. Figure 3.S3), drift can have a noticeable effect when considering regional patterns. This is particularly true for the 20C3M realisations, where anthropogenic greenhouse gas (GHG) forcing is relatively small compared to strongly forced model projections of 21st century climate following the Special Report on Emissions Scenarios (SRES) GHG trajectories. A comprehensive assessment of de-drifted 1950-2000 surface change magnitudes for model variables assessed in this study is summarised in Table 3.S3 for reference.

The analysis presented in this chapter accounts for model drift by explicitly resolving the 1900-2050 (or closely equivalent period) linear point-wise spatial trend from the corresponding pre-industrial control (PICNTRL) model run, and removes this point-wise from the 20C3M 1950-2000 trend field. While prudent to undertake these corrections, spatial pattern correlations are not consistently improved between mean and change fields when the full PICNTRL model drift is accounted for – if anything this diminishes the magnitudes of amplification reported in

20C3M realisations. Accounting for drift however, provides more certainty in the resolved rates of change, distinguishing a clearer forced signal from modelled climate variability. Undertaking drift removal leads to a lower number of available analysed realisations, as corresponding PICNTRL data is not available for all variables and all time periods for each 20C3M realisation (Table 3.2).

Linear trends provide a more conservative representation of change (than snapshot analyses; Chapter 2), and are less affected by natural and modelled variability over the 50-year period of analysis. Individual model realisations show spatially noisy salinity trend fields (Figure 3.5E, F). To further enhance signal-to-noise, it was necessary to exclude regions poleward of 60°. In observations this is due to poor spatial and temporal data coverage, high synoptic variance related to surface E-P, and the presence of sea ice which strongly affects available observational samples. The highest spatial pattern correlation of 0.68 between observed surface mean salinity and salinity change was obtained when excluding data poleward of 60°, and this result then guided the analysis of model fields, similarly excluding poleward data.

Analysing individual model realisations rather than model ensemble averages (e.g. Meehl *et al*., 2007b) allows evaluation of the relationships between salinity, E-P and warming rates within a single realisation. It also allows separation between models and realisations with different 20C3M forcing configurations (e.g. pure GHG, or GHG in combination with aerosols). When multiple realisations from the same model configuration are available this also provides an estimate of how model internal climate variability impacts on change analysis.

Besides having different approaches to the various aerosol forcings (volcanic, anthropogenic direct and indirect effects, e.g. Forster *et al*., 2007) used in 20C3M realisations, some CMIP3 models apply freshwater flux adjustments which play a large role in constraining the spatial pattern of surface salinity. There was a strong move away from these unphysical adjustments between CMIP2 and CMIP3, while also providing large improvements in observed climate replication (Reichler & Kim, 2008), an impressive achievement by the model development teams. By construction the few remaining freshwater flux-adjusted models more closely reproduce the climatological mean from observational salinity products (compare Figure 3.5B vs C; Figure 3.S3; Table 3.S1).

Model fields of surface salinity and E-P are analysed for the strength of their mean pattern amplification (PA) to determine the rate of change for each variable. In order to focus on broad-scale changes and enhance signal-to-noise, zonal averages were formed for each basin, for both observations and individual model realisations. In this analysis PA is defined as the linear slope of the basin zonal average 50-year change versus the basin zonal average anomaly from the 50-year global surface mean. This slope provides an estimate of the changing intensity of spatial salinity gradients. The corresponding coefficient of correlation of these quantities is defined as the pattern correlation (PC) and provides an estimate of the spatial coherence of the change pattern with the mean pattern.

Rates of Change and Pattern Amplification in CMIP3

The full 20C3M CMIP3 model suite was analysed, and for illustration two representative model results are presented in Figure 3.5, compared to the new surface salinity observational result (Chapter 2).

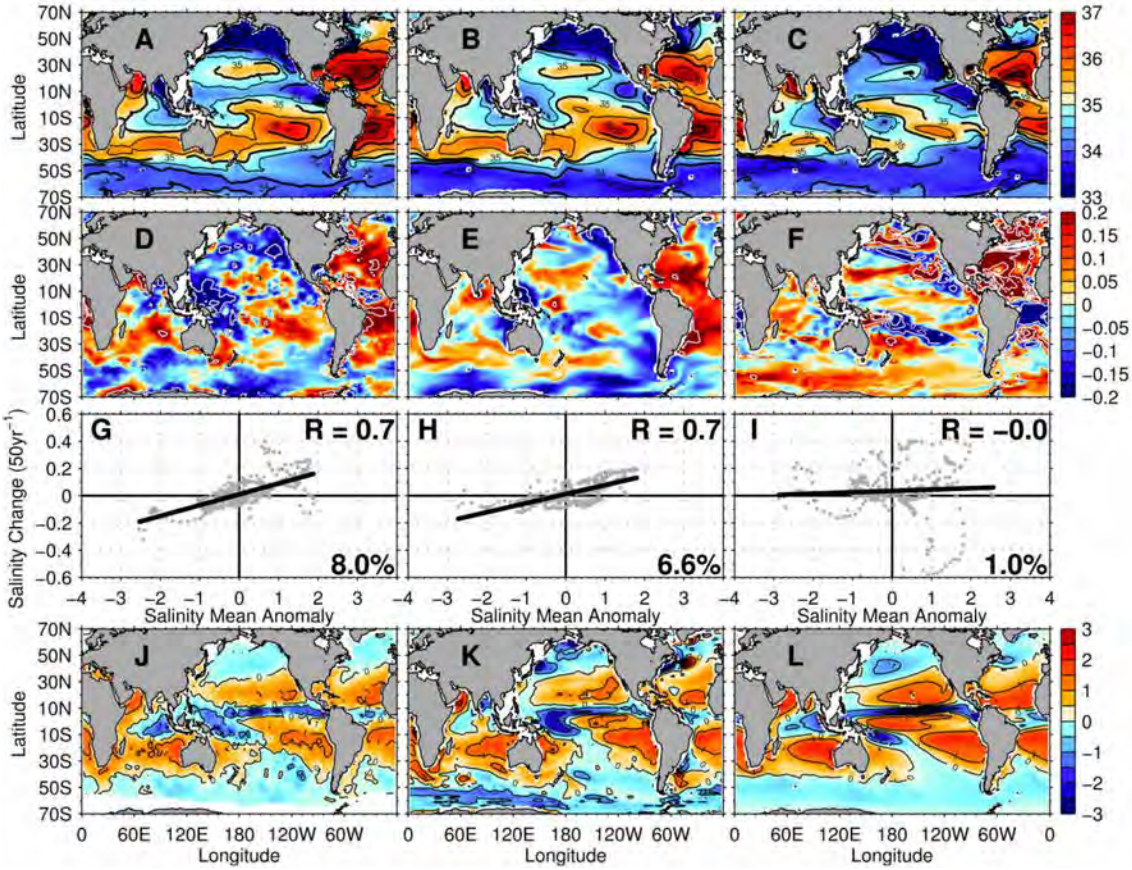

Figure 3.5. Examples of 1950-2000: surface mean salinity (A, B, C); surface salinity change (D, E, F); basin zonal-mean pattern amplification (PA; G, H, I) and surface water flux (E-P; J, K, L) for the global ocean for (A, D, G) the observed result presented in Chapter 2 and (J) the observed result of Josey *et al.* (1998) for 1980-1993; (B, E, H, K) the Canadian Centre for Climate Modelling & Analysis: CGCM3.1 (T63); and (C, F, I, L) the United Kingdom MetOffice: HadGEM1. For A, B, C, contours every 1 pss for bold line and 0.5 pss for thin. For D, E, F, contours every 0.25 pss are plotted in white. For J, K, L contours every 1 m^3 yr^{-1}.

Clearly the CMIP3 models do not provide a perfect simulation of observed surface mean salinity patterns or its change over 1950-2000 (Figure 3.5, Figure 3.S3). The models shown in (Figure 3.5B, E and C, F) represent the “best” and “worst” simulations of observed 1950-2000 surface mean salinity and illustrate the range of behaviour in the CMIP3 suite. A high spatial correlation (full analysis grid) is found with observed surface mean salinity for both models (Figure 3.5B: 0.95 and Figure 3.5C: 0.85). Simulated E-P patterns also compare well to observations (Figure 3.5J-K) - the models capture the Intertropical Convergence Zone (ITCZ), South Pacific Convergence Zone (SPCZ) in the Pacific basin, and broad-scale gyre structure elsewhere, with this conclusion supported by high spatial correlations with observed estimates (Figure 3.5K: 0.66 and Figure 3.5L: 0.78; full analysis grid).

A weak correspondence is found between the observed (Figure 3.5D) and "best" model (Figure 3.5E) estimates of salinity change with a spatial correlation of 0.28 (full analysis grid). While basin-scale changes such as a freshening Pacific and Southern Ocean, and increased Atlantic salinity are as observed, the more regional features such as the strongly and broadly freshening Pacific Warm Pool are not clearly evident in this model. The "worst" model (Figure 3.5F) however, provides an almost inverse spatial pattern of salinity changes to observations (correlation: -0.06), the opposite of what would be expected if the model's own E-P pattern had amplified. In general, the 50-year perturbation fields in CMIP3 20C3M realisations provide a weaker replication of observed salinity change patterns (compare Figure 3.5D, E & F).

The PA and PC for models and observations can be compared. For surface salinity, observations yield a PA of 8.0% (Figure 3.5G) with a corresponding PC of 0.7 (spatial correlation of the basin zonal pattern in Figure 3.5A & D). For the "best" model (Figure 3.5B, E, H) the PA yields 6.6% with a PC of 0.7, similar to observed. The "worst" model (Figure 3.5C, F, I) has a PA of 1.0% with a PC of 0, sharing little broad-scale resemblance to the observed changes. This suggests there is utility in investigating salinity changes in some of the CMIP3 model realisations, however not all realisations resemble the observed changes. A range of responses are found for 50-year salinity PA in CMIP3. All available CMIP3 fields are presented in Figure 3.S3 for comparison. The reasons for these varying responses in the CMIP3 realisations is explored below.

To test whether model internal variability over the selected 50-year (1950-2000) period strongly impacts salinity PA and PC (Figure 3.5), a comparison analysis was undertaken using the full model grid (no basin zonal mean) for the full length of the 20C3M realisation (~1850-2000) for both models used above. The results suggest that the 1950-2000 analysis was representative of changes occurring over the full 20C3M realisation (~150-years; Figure 3.S1,). Therefore a 1950-2000 analysis window will be used for the full CMIP3 suite, directly comparable to observations.

PA and PC for both surface salinity and E-P are calculated for each of the available 20C3M CMIP3 realisations, and an exploration of its relationship to the global mean surface warming rate, as well as their relationship to one another is undertaken. For the observed salinity PA, this is paired to the corresponding global surface average warming (ΔT_a; 0.5°C) obtained from the HadCRUT3 gridded surface temperature data product for 1950-2000 (Brohan *et al.*, 2006). A complete summary from this comprehensive model analysis and selected observational products are presented in Table 3.S3.

Additional external forcings (to GHG) used in the 20C3M realisations were considered to further explore reasons for variability between results. Individual model realisations were labelled either volcanic or non-volcanic (aerosol forcing) following Santer *et al.* (2007). Volcanic aerosol forcing has been shown to inhibit ocean warming and slow sea-level rise in models and observations (Church *et al.*, 2005), along with a rapid global atmospheric cooling (Robock, 2000) and reduction in rainfall (Gillett *et al.*, 2004). It should be noted that realisations that incorporate volcanic aerosol forcing also generally include more comprehensive anthropogenic aerosol effects (Table 3.S1). Therefore, in the following analysis the differences between "volcanic" and "non-volcanic" realisations also incorporate effects from these pollutants.

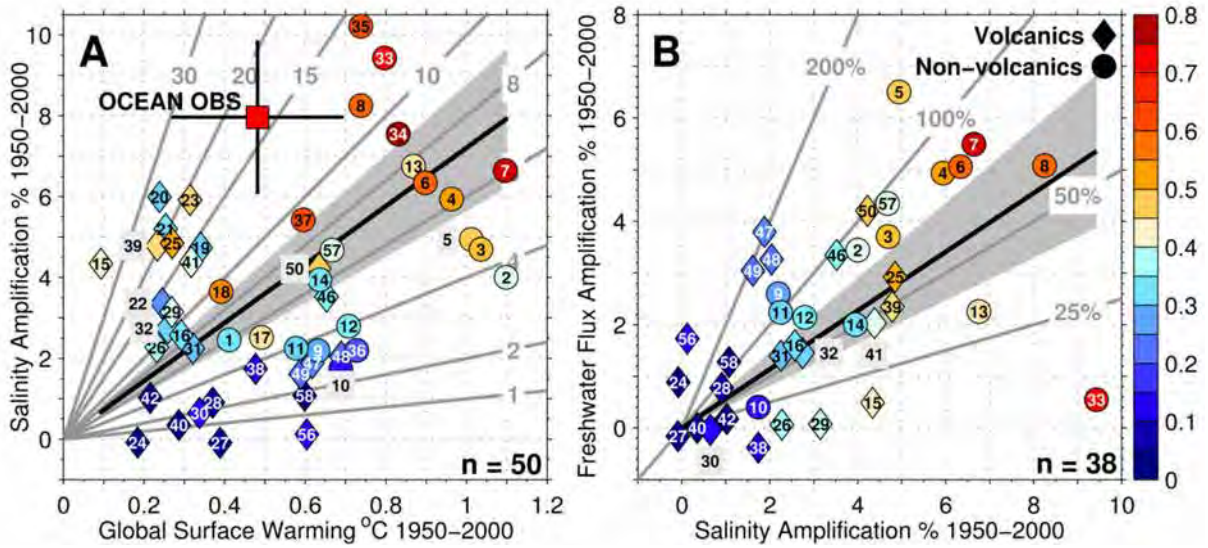

Figure 3.6. Pattern amplification (PA) rates for 1950-2000 in individual de-drifted CMIP3 (20C3M realisations) for A) surface salinity (y-axis) versus the corresponding global average surface temperature change (ΔT_a; x-axis) B) freshwater flux (E-P; y-axis) versus surface salinity (x-axis). Colours are the salinity pattern correlation (PC) for both panels A & B. Grey lines express constant proportional change. Grey shading (99% C.I.) bounds the correlation-weighted linear best fit to the model ensemble for a line intersecting 0 in black.

Although there is a large scatter, the 20C3M salinity PA results show that more strongly warming models (>0.7°C) respond with a higher salinity PA (4-12% K^{-1}) and PC values (Figure 3.6). Most models with a salinity PA above 4% along with a ΔT_a above 0.4°C do not include volcanic forcing (Figure 3.6A, upper right yellow to red circles) – a response close to that observed. In general, when compared to the observed result (16% K^{-1}), models tend to underestimate the strength of salinity PA, with a PC-weighted line of best fit for all 50 realisations expressing a model response of around half the observed rate (7% K^{-1}). The low PA and PC in weakly warming realisations (including most with volcanic forcing, diamonds) suggest a signal to noise problem, and that other factors mask the GHG response. Conversely, the strongly warming models show more coherent spatial changes (with larger PA and PC values), closer to that observed.

A strong relationship is evident between salinity and E-P PA (Figure 3.6B). While scatter remains, realisations expressing high salinity PA and PC values also appear to have a high E-P PA. The inverse is also true (bottom left, blue colours PC <0.4). Realisations with PA values closest to observed salinity PA (~8%) appear to have high PC values (>0.5), again suggesting a signal to noise process at work in 20C3M model suite. A PC-weighted line of best fit for all 38 realisations indicates that surface salinity PA increases at roughly twice the magnitude of E-P PA (57%), a result for which the authors currently do not have a clear explanation, and deserves further investigation. This result suggests that within this model suite, salinity PA is a representative measure of global water cycle changes, and is particularly sensitive when compared to E-P.

To further investigate water cycle responses reproduced by this suite, E-P PA against ΔT_a and average global rainfall changes against ΔT_a are presented in Figure 3.7.

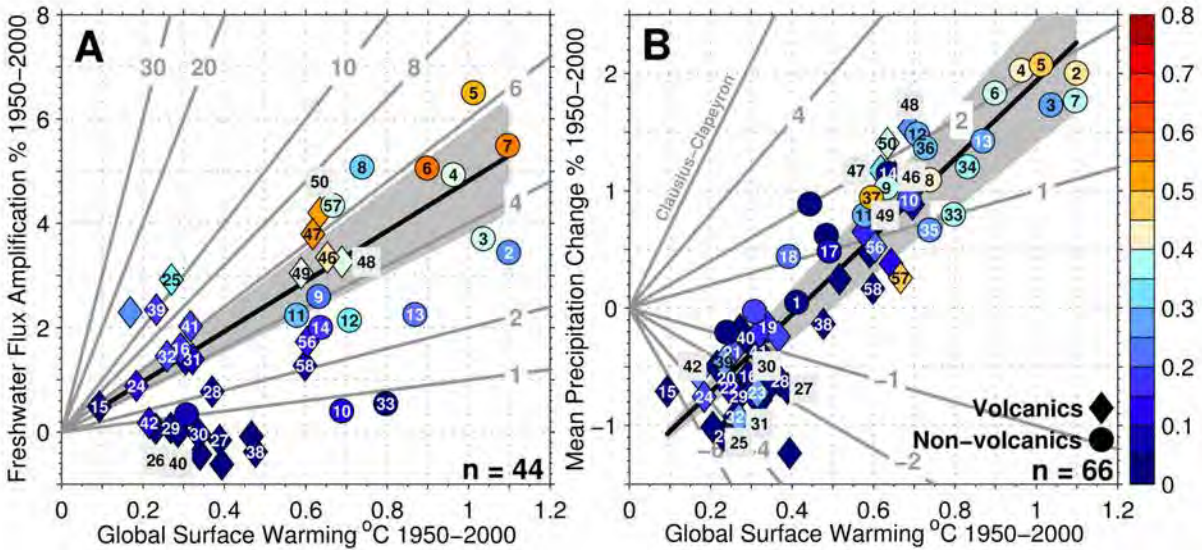

Figure 3.7. Pattern amplification (PA) rates for 1950-2000 in individual de-drifted CMIP3 (20C3M realisations) for A) freshwater flux (E-P) B) mean global rainfall change (ΔP) versus their corresponding global average surface temperature change (ΔT_a; x-axis). Colours indicate the pattern correlation (PC) for both panels A & B - Freshwater flux (E-P) and rainfall PC respectively. Grey lines express constant proportional change; line representing Clausius-Clapeyron (CC) is 7% K^{-1}. Grey shading (99% C.I.) bounds the correlation-weighted linear best fit to the model ensemble for a line intersecting 0 (A), and -1.4 (B) in black.

Similar to salinity PA, there is a large scatter in E-P PA. However a relationship with ΔT_a also appears (Figure 3.7A). There are generally lower PC values expressed for E-P compared with salinity (likely due to the integrating and smoothing role of ocean advection). As for salinity PA, strongly warming (non-volcanic) models show the strongest signal to noise (higher PA and PC values). A PC-weighted line of best fit for all 44 realisations expresses a model amplification of the E-P pattern of around 5% K^{-1}.

Average global rainfall change (ΔP) is a commonly analysed and discussed metric of water cycle change, as it is believed to be strongly controlled by both the surface (through evaporation) and upper troposphere energy budgets (Schneider *et al*., 2010). A strong positive relationship between ΔP and ΔT_a is found, with a slope of 3.4% K^{-1} (Figure 3.7B; note change in y-axis scale). This robust result has been found by many previous studies, which considered multiple model suites and forcing scenarios (CMIP2 and CMIP3; e.g. Allen & Ingram, 2002; Held & Soden, 2006; Stephens and Ellis, 2008; Andrews *et al.*, 2010). A clear offset from zero is apparent in the vertical axis, intercepting at -1.4% (Figure 3.7B), also noted by Allen & Ingram (2002; 4.8%, their Figure 2) in the CMIP2 experiments. The negative offset may be attributable to aerosols, suppressing the water cycle as suggested by Shiogama *et al.* (2010) for a single CMIP3 model. Non-volcanic, strongly warming models also appear to show more coherent PC (colours in Figure 3.7A).

Modelled salinity (Figure 3.6A) and E-P PA (Figure 3.7A) responses to warming, while noisy, appear to more closely follow the theoretical CC (for fixed relative humidity) scaling with rates of 7% and 5% K^{-1} respectively compared to global mean rainfall 3-4% K^{-1} (Figure 3.7B). The reasons for differences been the ΔP versus E-P PA responses are discussed in detail by Schneider *et al*. (2010).

It appears the 20C3M realisations in CMIP3 suggest a strong relationship exists between salinity and E-P PA, with the strength of the PA and PC in salinity and E-P approximately scaling with warming rates, however with large scatter. Thus the signal may be contaminated with noise due to the weak GHG forcing, or confounding aerosol effects in these realisations. To investigate further and attempt to improve the signal to noise found in the 20C3M realisations, the response from a select number of realisations expressing future SRES scenarios for the period 2050-2099 were analysed. As with the 20C3M results, these realisations have been de-drifted using the technique described above. Figure 3.8 replicates the results presented in Figure 3.6, with the addition of SRES results.

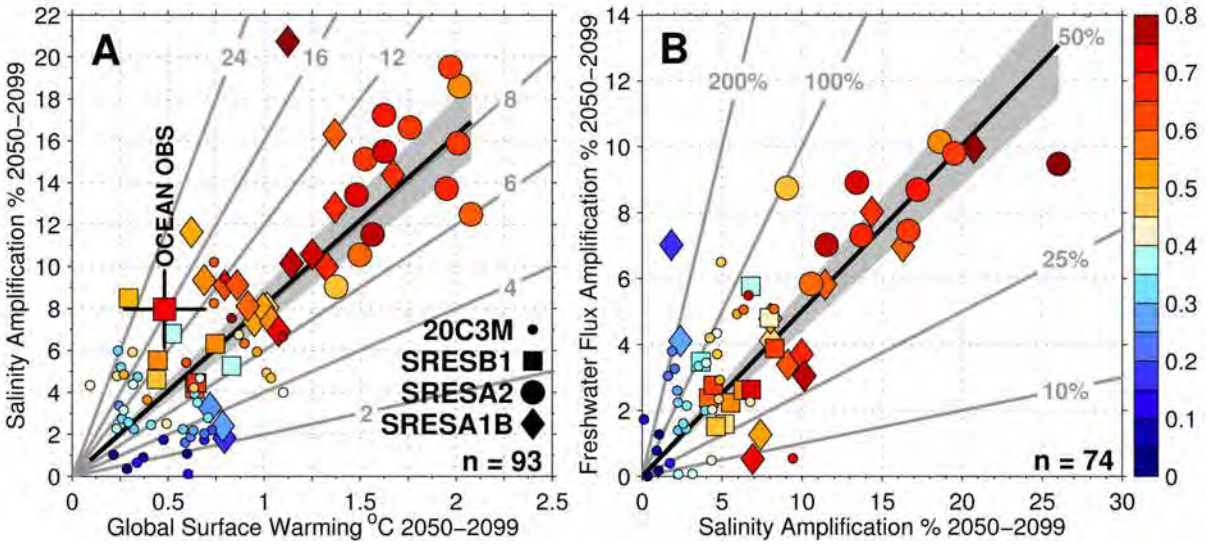

Figure 3.8. As in Figure 3.6 for 2050-2099 SRES realisations (1950-2000 for 20C3M data). Pattern amplification (PA) rates for both A) surface salinity (y-axis) versus the corresponding global average surface temperature change (ΔT_a; x-axis) B) freshwater flux (E-P; y-axis) versus surface salinity (x-axis). Colours are the salinity pattern correlation (PC) for both panels A & B. Grey lines express constant proportional change. Grey shading (99% C.I.) bounds the correlation-weighted linear best fit to the model ensemble for a line intersecting 0 in black.

In the SRES realisations a clear enhancement to salinity PC in concert with warming is evident (Figure 3.8A), and a strong relationship is revealed between surface warming and salinity PA. A PC-weighted line of best fit through the available 93 realisations suggests salinity patterns intensify with warming, near the CC rate, with 8% K^{-1} clearly expressed by this model suite. Individual realisations, which express high PC values, capture lower rates compared to observed change. The line of best fit indicates models capture half of the observed rate (8% vs 16% K^{-1}), with many of the strongest GHG-forced SRES A2 realisations expressing relationships between 6-11% K^{-1} (Figure 3.8A)

A clear linear correspondence between E-P PA and salinity PA is also apparent (Figure 3.8B). The relationship of salinity PA twice that of E-P (suggested in Figure 3.6) is represented even more clearly with the larger number of realisations. In particular, the strongest GHG-forced SRESA2 realisations show this relationship in Figure 3.8B above.

The results presented in Figure 3.7 are replicated in Figure 3.9, with the addition of SRES realisations for the period 2050-2099. 20C3M realisations are plotted for their 1950-2000 values.

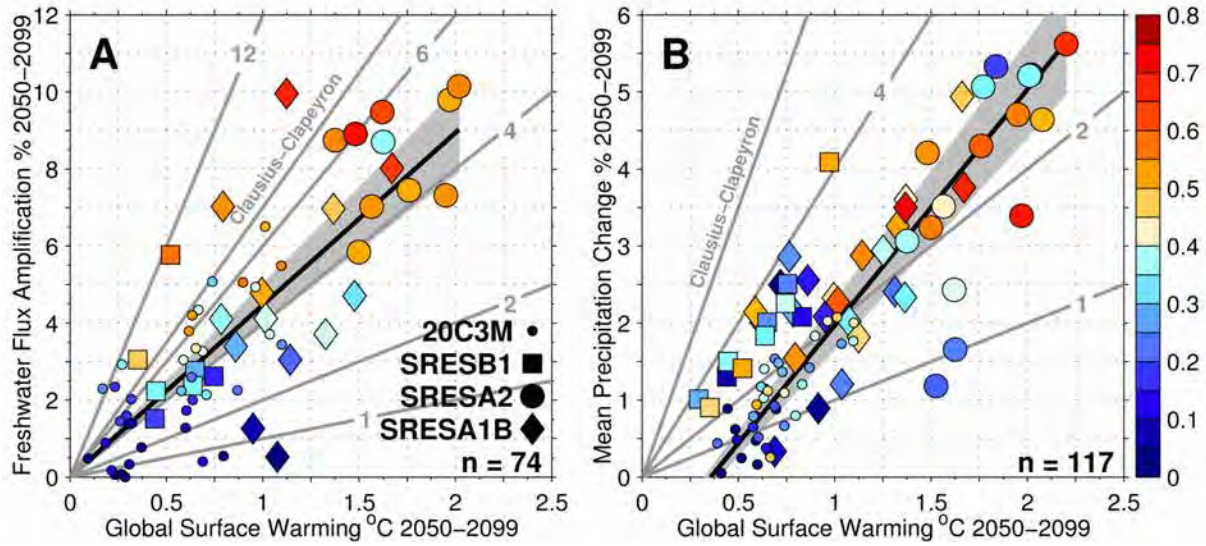

Figure 3.9. As in Figure 3.7 for 2050-2099 SRES scenarios (1950-2000 for 20C3M data). Pattern amplification (PA) rates for A) freshwater flux (E-P) and B) mean global rainfall change (ΔP) versus their corresponding global average surface temperature change (ΔT_a; x-axis). Colours indicate the pattern correlation (PC) for both panels A & B - Freshwater flux (E-P) and rainfall PC respectively. Grey lines express constant proportional change; line representing Clausius-Clapeyron (CC) is 7% K^{-1}. Grey shading (99% C.I.) bounds the correlation-weighted linear best fit to the model ensemble for a line intersecting 0 (A), and -1.4 (B) in black.

Similar to salinity PA, there is a large scatter in E-P PA, though in the SRES realisations a clearer relationship with ΔT_a is revealed (Figure 3.9A). There are generally lower PC values expressed for E-P when compared to salinity, however the same linear relationship emerges. Strongly warming models show the strongest change signal represented with higher PA and PC values. A PC-weighted line of best fit for all 74 realisations expresses a model response of around 5% K^{-1} for the amplification of the E-P pattern. The SRES realisations show that average global rainfall change (ΔP) against ΔT_a (Figure 3.9B) closely replicate the 20C3M result with the line of best fit expressing a relationship of 3-4% K^{-1} for ΔP even when twice the number of realisations is considered.

Discussion

The CMIP3 model suite analysed in this study reproduces salinity PA and PC responses to warming, resembling observations, particularly in the strongly warming SRES realisations. However, the model ensemble average PA rate is half that of observed. The clear signal, represented by strong PA and PC values for future projections is not clearly simulated in 20C3M realisations which appear too cool on average.

Realisations that include comprehensive (volcanic) aerosol forcing show consistently lower warming and salinity PA than those without, clearly apparent in Figure 3.6A (compare lower left, mostly diamonds, with upper right, all circles). The GHG-only realisations respond more closely to observations in their rates and patterns. The cooling effect of aerosols may be a source of the weak signal to noise presented in 20C3M realisations; however their role is not well quantified. Realisations which incorporate volcanic and other aerosols may therefore systematically underestimate change magnitudes as they appear to have done in CMIP3 realisations for the second half of the 20th century.

The effects of different forcing agents are impossible to isolate in the CMIP3 suite. Carbon aerosol effects are present in most 20C3M realisations that include the volcanic effect (Table 3.S1). Volcanic aerosol forcing is not included in SRES realisations for 21st century climate, primarily because there are no reliable ways to predict future volcanic eruptions, and are therefore excluded as a source of uncertainty. The effects of additional anthropogenic aerosols are included in SRES scenarios however, with the role of black and organic carbon the focus of a study by Shiogama *et al.* (2010). They suggested a process for weakened GHG response in the water cycle using some sensitivity experiments with the MIROC3.2 model. They found suppressed rainfall and E-P changes could be attributed to carbon aerosols (black carbon (BC) and organic carbon (OC)) suppressing the GHG forced warming. This is supported by Ming *et al.* (2010) who using a different model, suggested BC has a dampening effect on global mean rainfall, primarily through damped atmospheric heating in the low-GHG forced 20C3M simulations. This dampening of global rainfall may explain the offset and negative ΔP presented in some models (Figure 3.7B and 3.9B).

Hansen *et al.* (2005) quantified the BC effect on temperature only, suggesting this agent has a climate efficacy of ~58-~78% (a reduction in warming per unit forcing of ~22-42%, compared to CO_2 which is 100%) depending on its source. Additional to the effects of BC and OC, scattering sulfate aerosols have been shown to affect the global water cycle intensity, reducing rainfall (Roeckner *et al.*, 1999). In a very regional observation-based study, Adachi *et al.* (2010) quantified the effect of radiative forcing from soot particles over Mexico City, and they suggest current CMIP3 models overestimate the cooling efficacy of aerosols by ~20%. The effects of aerosols are regional, whereas GHG forcing is considered as a well-mixed globally uniform forcing agent. There is a dominance of anthropogenic aerosols in the northern (compared to the southern) hemisphere, apparent in the historical sulphate aerosol history (Boucher & Pham, 2002) and aerosol optical depth observations (Ramanathan *et al.*, 2001). The regional nature of aerosols on water cycle change has not been undertaken in the analysis presented here, with global changes considered only. However a strong regional response in rainfall, linked to aerosol forcing will likely reduce the overall PC.

To evaluate the significance of aerosols on salinity PA, CMIP3 suite comparison results to Shiogama *et al.* (2010) are presented in Figure 3.8 & 3.9. There is no clear indication of aerosols playing a significant role in global water cycle changes (contrast B1 and A2 scenario results, which have time histories of much lower and higher carbon aerosols respectively, along with different GHG loadings; Figure 3.S2). It would appear that GHG is the strongest forcing agent, and not regional aerosols. A2 realisations generally provide larger PA and PC values compared to B1, with A2 having considerably higher GHG and carbon aerosol emissions. There is a possibility that low GHG forcing along with comparatively strong aerosol forcing (expressed in 20C3M realisations) may indeed be a source of negative water cycle responses, and a source of noise diminishing PA and PC in salinity and E-P from many of the 20C3M realisations. This is clear as just two negative E-P and salinity PA responses are apparent in all of the 141 sampled CMIP3 SRES realisations, compared to proportionally larger numbers for negative PA in the 20C3M realisations. A clear explanation of the processes driving this – unresolved variability due to weak GHG forcing or aerosols – will require further investigation outside the scope of this study and more work is needed to attribute the drivers of water cycle changes in CMIP3.

Comparison of model results to observations, yield some distinct patterns. The observed salinity PA of 8% in the 50-years analysed is equivalent to 16% K^{-1}, a response to the 0.5°C observed warming (PC: 0.68). This clear and strong response is underestimated by the CMIP3 20C3M realisations with equivalent warming. Even strongly GHG forced future scenarios suggest a salinity PA of 8% K^{-1}, which is half the observed rate (Figure 3.8A).

In CMIP3 a robust relationship is found between the PA of salinity and E-P (Figure 3.6B & 3.8B), with salinity PA twice that of the corresponding E-P PA, a result consistent across the full suite of CMIP3 20C3M and SRES realisations. This important result provides confidence surface salinity PA can be used as a quantitative marker of water cycle change, which is extremely difficult to measure directly. Using this modelled relationship between salinity and E-P PA, provides a scaling which can be applied to observed salinity change estimates. The observed salinity PA for 1950-2000 8% (16±7% K^{-1}), then yields an inferred observed water cycle amplification of 4% (8±5% K^{-1}), which corresponds very closely to the anticipated CC response. This estimate is also supported by Trenberth *et al*. (2007) who suggest a 4% increase to column water vapour has occurred from 1970-2005, suggested from a correlation with SST. The agreement with CC along with other estimates provides confidence in the use of salinity as a quantitative marker of water cycle change.

Using this inferred estimate of E-P change for 1950-2000, comparison to other observational estimates will now be undertaken to ascertain the range of rates reported for the 20th and early 21st century (Figure 3.10).

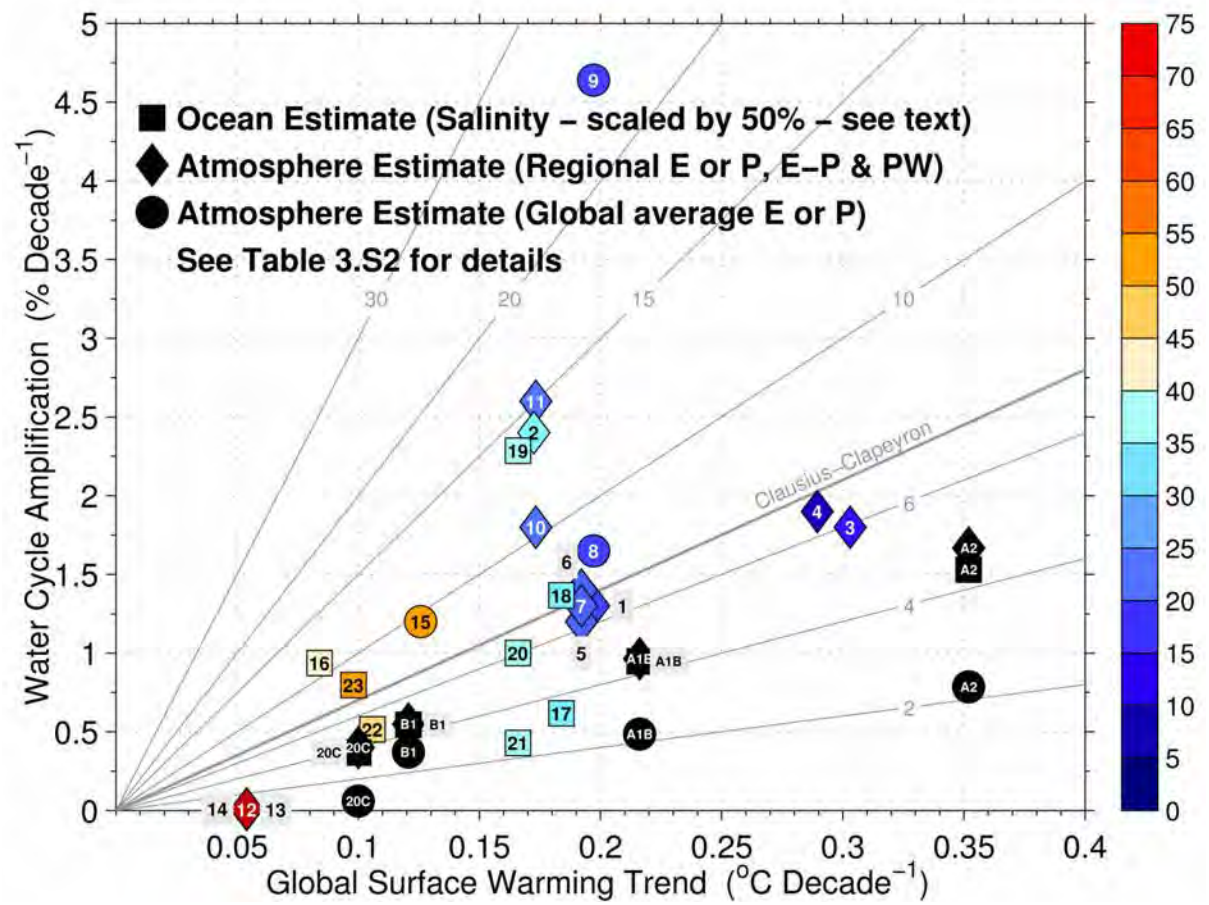

Figure 3.10. Reported observed water cycle changes (scaled in relative absolute change decade^{-1}). Colours indicate years over which reported changes are calculated (red is longer). As noted in the figure, ocean salinity estimates are presented as squares (scaled by 50% of their reported magnitudes to represent equivalent E-P change, see text), atmospheric water cycling estimates (non-average global rainfall/evaporation) are triangles and average global rainfall/evaporation are circles. All ΔT_a trends were obtained from HadCRUT3 (Brohan *et al.*, 2006) using a linear fit over the corresponding years (annual data) used to determine the water cycle change estimate. More detail, including error estimates for each of the noted studies is contained in Table 3.S2. The result suggested by this study is #23. For reference, equivalent scenario ensemble mean changes for the 20C3M (1950-2000; 20C) and SRES (2050-2099; B1, A1B, A2) realisations are included in black. Grey lines express constant proportional change; line representing Clausius-Clapeyron (CC) is 7% K^{-1}. A total of 14 independent studies and 23 estimates of global and regional changes which express different aspects of water cycle change are presented.

The trends presented here are obtained from various analyses which consider many different aspects of global and regional water cycle operation. Estimates range from surface terrestrial rainfall records extending over 75 years (1925-1999; Zhang *et al.*, 2007) through to shorter-term satellite record of precipitable water over 7 years (1996-2002; Mieruch, *et al.*, 2008). Numerous studies looking at global (and regional) ocean salinity changes (Curry *et al.*, 2003; Boyer *et al.*, 2005; Hosoda *et al.*, 2009; Helm *et al.*, 2010) were also considered. These were presented to provide independent clarification of water cycle changes across many observational platforms, global and regional assessments and temporal windows.

A wide range of observed changes to varying elements of the water cycle are reported for the 20th century. Reported rates of E-P change inferred from salinity (per degree of global surface warming) range from regional estimates; 14% K^{-1} for the Southern Ocean (Helm *et al.*, 2010; #19) and 11% K^{-1} for the Atlantic Ocean (Curry *et al.*, 2003; #16), to global estimates; 5% K^{-1} calculated from Boyer *et al*. (2005; #22) and 3.5% K^{-1} reported by Hosoda *et al*. (2009; #17). Water cycle change estimates from observed salinity change are inferred using the 50% scaling of salinity derived from the CMIP3 analysis above (more details are available in Table 3.S2). Other reported changes include 22% K^{-1} for global ocean evaporation estimates 1987-2004 (Liepert & Previdi, 2009; #9) to <1% K^{-1} for large zonal terrestrial rainfall changes 1925-1999 (Zhang *et al.*, 2007; #12-14). This suggests large variations are present due to various observational platforms, temporal windows of analysis, and the influences of climate variability reflected in the shorter change estimates, especially based on regional data.

Despite the scatter in observations, the model ensemble means show a weaker response compared with almost every observed estimate (Figure 3.10). The exceptions are changes in observed terrestrial precipitation of Zhang *et al.* (2007; #12, 13 & 14), the global surface salinity estimate (Hosoda *et al.*, 2009; #17) and subtropical surface salinity estimate (Helm *et al.*, 2010; #21) over which low (<4% K^{-1}) changes are reported.

The time period over which observed trends have been calculated must be taken into account when comparison to model results is made to consider biases due to natural climate variability. Trends calculated over a period less than 30-years will be more susceptible to noise due to climate variability at interannual and decadal timescales. Observed salinity and model estimates for this analysis were determined over a period of 50-years. Using models, extending the analysis period from 50-years to ~150-years yielded little differences in the resolved trends and spatial pattern correlation (Figure 3.S1). This suggests a 50-year temporal window is a sufficient time period to overcome noise due to climate variability. As observational coverage is sparse, it is not possible to obtain global ocean salinity trends longer than 50-years.

There are additional factors to consider when reviewing observational estimates of water cycle change. Many atmospheric estimates of water vapour and rainfall for instance, are dependent upon satellite data. The earliest satellite measurements began around 1980, providing less than 30-years of coverage. In addition, concerns regarding the reliability of satellite estimates of long-term trends have been expressed, with Trenberth *et al.* (2005) and Yin *et al.* (2004) detailing uncertainties with precipitable water and surface rainfall estimates (which are highly sensitive to data sources and satellite calibration techniques, in particular over the ocean). There are also problems with radiosonde upper atmosphere temperature measurements as reported by Sherwood *et al.* (2005). Atmospheric estimates of change must therefore be considered with these issues in mind, and rates diagnosed by such platforms should be considered with caution.

By comparison, ocean salinity changes are not currently subject to any known platform reliability issues and the signals are relatively large compared to the known accuracy of observational platforms (0.02 during the early 1950s and 0.002 in modern CTDs). However, when considering estimates of water cycle changes from ocean salinity, it is prudent to consider the assumptions which underlie these. For example Helm *et al.* (2010) use a technique which assumes static isopycnal circulation for their period of analysis 1970-2005,

and infer freshwater volume changes at the outcrop interface. This technique does not account for latitudinal shifts in outcropping isopycnals, with results in Chapter 2 (Figure 2.8) suggesting shifts of 50-100 km have occurred. These shifts are attributable to the observed broad-scale warming of the surface ocean and resulting regional subsurface salinity changes in response to migration are commonplace over 1950-2000 (Chapter 2, Figure 2.8). The surface Southern Ocean salinity change result of Hosoda *et al.* (2009) over the period 1974-2005 yields an inferred E-P change of 7.5% K^{-1} (Figure 3.10, #18), with Helm *et al.* (2010; 1970-2005) suggesting almost double that estimate, 14% K^{-1} (Figure 3.10, #19). Southern Ocean changes are more complex than just surface E-P change, with Chapter 2 (Figure 2.9) presenting isopycnally analysed changes for each ocean basin. These results suggest a large component of subsurface freshwater changes on outcropping isopycnals in the Southern Ocean (south of 40°S) can be attributed to isopycnal poleward migration. This leads to isopycnals being exposed to a "fresher" mean surface salinity in 2000 when compared to 1950, driving a freshening anomaly largely independent of surface E-P changes. A more thorough comparison of previous ocean salinity changes is provided in Chapter 2 (Table 2.2). Although ocean salinity observations are not subject to platform issues which confound atmospheric estimates, rates diagnosed by such analyses must be considered along with the assumptions from which they have been obtained.

Observed salinity PA suggests an increasing E-P trend of 8±5% K^{-1} (Figure 3.10, #23), agreeing well with many independent estimates which also indicate a global enhancement has occurred over the 20th century (Figure 3.10, Table 3.S2). For example two entries by Allan *et al*. (2010) indicate tropical regions, found in high-rainfall zones have seen more rainfall (+10% K^{-1}, #10) and equatorial regions which are found in low-rainfall zones have experienced rainfall decreases (-15% K^{-1}, #11). The result of Helm *et al.* (2010) also agrees with this pattern, with enhanced high latitude rainfall for both hemispheres (Figure 3.10, #19 & 20) and a decrease in subtropical regions (Figure 3.10, #21), with this result also confirmed by Cravatte *et al*. (2009), Hosoda *et al*. (2009) and Roemmich and Gilson (2009). An additional, though not directly comparable terrestrial result from four decades of subpolar glacier records also supports the conclusion of enhanced water cycling in the latter half of the 20th century (Dyurgerov, 2003). Regional water cycle changes have also been attributed in some cases to anthropogenic causes (e.g. Zhang *et al.*, 2007; Barnett *et al.*, 2008; Petrone *et al.*, 2010).

Using a simple linear box model, and enhancing climatological surface E-P by 4% over a two dimensional (no advection/subduction) mixed-layer ocean yields much larger surface salinity changes than reported in Chapter 2. This implies ocean circulation and mixing is responsible for removing more than 80% of the inferred 1950-2000 E-P changes from its surface source region. Dedicated model attribution studies are underway to ascertain how a dynamic ocean model responds to idealised E-P forcing. In particular, the dynamics driving the doubled sensitivity of salinity PA, compared to E-P PA is a topic to pursue.

In models where there is not a high correlation between E-P and the surface salinity PA, significant changes to ocean mixing/velocity may be responsible for the decoupling of the forcing (E-P) and response (salinity change) fields. Attribution of the causes of this decoupling is a key area for future research (analysis of freshwater redistribution and their timescales). Recent work has analysed the contribution of mesoscale eddies to subduction of ocean properties in the Southern Ocean. Sallée & Rintoul (2011) suggest that current coarse-

resolution climate models regionally underestimate near surface diffusion by an order of magnitude in frontal regions of strong mixing. This result is supported by a new modelling study, using a climate model with higher resolution than a CMIP3-generation coarse resolution model, this suggests that the response of earlier generation models may overly damp eddy-induced transports preventing faithful representation of variability and change responses due to GHG forcing (Farneti *et al.*, 2010). Other studies have suggested that the surface-enhanced observed warming, when compared to similar coarse-resolution climate models overestimate vertical diffusivity in mid-ocean layers (Wijffels *et al.*, in prep). Clearly there is more research required to understand both observed and modelled ocean changes in response to climate change.

An enhanced water cycle has occurred over the 20th century, supported strongly by new global surface salinity estimates, which largely agree with atmospheric observations. Salinity does appear to be a reliable marker of long-term water cycle change, with models suggesting this to be a robust and coherent estimator.

Summary and Future Directions

This study is the first to look in detail at both observed and modelled global salinity changes. Although models do not provide a flawless representation of the observed ocean water cycle operation, when using a technique to extract the basin-scale zonal changes, modelled surface salinity appears to perform better than other aspects of water cycle changes (rainfall and E-P). From this analysis, it was found that modelled surface salinity shows stronger pattern correlations (PC) between mean and perturbation fields than the noisier E-P fields. This is likely due to the spatial and temporal integration of E-P fluxes by the ocean's salinity field. If this is true of the real world, ocean salinity changes may be a sensitive diagnostic to multi-decadal changes in the surface water balance such as those expected under anthropogenic climate change.

The observed ocean salinity field acts as an integrator of spatially and temporally noisy E-P fluxes, and it is fair to assume this will hold for the multi-decadal timescale. In CMIP3, salinity appears to provide a more coherent and robust estimate of long-term water cycle changes. The relationship between E-P changes, and surface salinity changes reported by the CMIP3 model suite for 1950-2000 (20C3M; and future SRES-forced realisations) suggest ocean salinity pattern amplification (PA) is a more sensitive marker of water cycle change than freshwater flux (E-P) pattern amplification (PA). This result was unexpected, but it suggests the observed robust pattern of amplification of the mean salinity field can be used to infer water cycle changes over the past 50-years – something that is nearly impossible to discern using direct measurements of precipitation due to the paucity and sparse distribution of historical rain gauge records. The new salinity estimates however implies observed 20th century E-P changes of 4% over the past 50 years or 8±5% K^{-1} of global warming corresponding to the observed and robust salinity changes of 8% (16±7% K^{-1}). These new estimates correspond closely to the anticipated response due to Clausius-Clapeyron (CC), are supported by direct observed estimates (Figure 3.10) and observed changes to ocean surface warming which suggest a 4% increase in column water vapour has occurred (Trenberth *et al*., 2007; 1970-2005).

It is important to validate magnitudes of observed change with observations, with the key question being the rate of reported changes in the 20th century, and the accurate simulation of rates and spatial patterns by CMIP3 models. It is important to note that projections of 21st century climate, undertaken using the same CMIP3 suite, with different climate forcing priors, are not directly comparable to 20C3M-derived rates. While it is true that, compared to new estimates of ocean change, the 20C3M model realisations provide conservative estimates of this change, future climate projections for the 21st century may not provide similar underestimations.

This analysis has focused on global ocean surface changes as expressed both in new observed estimates and CMIP3 model realisations. Clearly, changes are not only occurring at the surface, but also in the subsurface ocean, as surface changes are subducted and circulated by the ocean's mean flow (Chapter 2). It would be prudent to extend this analysis to examine the full three dimensional nature of oceanic water cycle change in CMIP3 models, while explicitly accounting for model drift which is particularly a problem in the deep ocean. Another fruitful area for new research would be to explore the sub-annual evolution of changes, and explicitly investigate ocean circulation, its changes over time and throughout the seasons, and these

contributions to multi-decadal trends. Laliberté & Pauluis (2010) have investigated mid-latitude atmospheric circulation changes using CMIP3 SRES A1B projected realisations and suggested a seasonal asymmetry is apparent, with a strengthening occurring over winter months, which is largely absent during summer. Enhanced seasonal amplitudes for the western Pacific Warm Pool surface salinity has also been described by Cravatte *et al*. (2009), particularly in recent decades.

In order to improve our understanding of water cycle changes into the future with anthropogenic climate change, more attention needs to be focused on the ocean component of the water cycle. This will be achieved by developing a better understanding the ocean's role in the water cycle and obtaining a better understanding of climate (and ocean) variability – with these new insights improving model representations of reality in ongoing work. Such steps are currently being made to progress the observational coverage of ocean surface salinity through a dedicated satellite system scheduled for launch in 2011 (e.g. Lagerloef *et al.*, 2008). It is likely that these future observations will provide better observational coverage which will lead to an improved understanding of ocean variability and water cycle operation. It is essential that the Argo array be maintained to continue to monitor how three dimensional global salinities evolve in the future.

The new ocean estimates of change (Chapter 2) provide a globally coherent and stringent target for coupled modelling systems when undertaking 20th century hindcast simulations. These new estimates suggest large, robust, spatially coherent and potentially larger rates of ocean changes have occurred in the 20th century than from previous estimates, and modelling studies. We intend to provide this new dataset to researchers to aid in evaluation of the upcoming CMIP5 model suite. These new observed estimates provide a benchmark by which to assess the poorly known water cycle intensification and robust ocean changes expressed in the 20th century and beyond.

References

Adachi, K., S.H. Chung and P.R. Buseck (2010) Shapes of soot aerosol particles and implications for their effects on climate. *Journal of Geophysical Research*, **115**, D15206. doi: 10.1029/2009JD012868

Allan, R.P. and B.J. Soden (2008) Atmospheric Warming and the Amplification of Precipitation Extremes. *Science*, **321**, pp 1481-1484. doi: 10.1126/science.1160787

Allan, R.P., B.J. Soden, V.O. John, W. Ingram and P. Good (2010) Current changes in tropical precipitation. *Environmental Research Letters*, **5**, 0525205. doi: 10.1088/1748-9326/5/2/025205

Allen, M.R. and W.J. Ingram (2002) Constraints on future changes in climate and the hydrologic cycle. *Nature*, **419**, pp 224-232. doi: 10.1038/nature01092

Andrews, T. and P.M. Forster (2010) The transient response of global-mean precipitation to increasing carbon dioxide levels. *Environmental Research Letters*, **5**, 025212. doi: 10.1088/1748-9326/5/2/025212

Andrews, T., P.M. Forster, O. Boucher, N. Bellouin and A. Jones (2010) Precipitation, radiative forcing and global temperature change. *Geophysical Research Letters*, **37**, L14701. doi: 10.1029/2010GL043991

Barnett, T. P., D.W. Pierce, H.G. Hidalgo, C. Bonfils, B.D. Santer, T. Das, G. Bala, A.W. Wood, T. Nozawa, A.A. Mirin, D.R. Cayan and M.D. Dettinger (2008) Human-Induced Changes in the Hydrology of the Western United States. *Science*, **319**, pp 1080-1083. doi: 10.1126/science.1152538

Bates, B.C., Z.W. Kundzewicz, S.Wu and J.P Palutikof, Eds. (2010) *Climate Change and Water*. Technical Paper of the Intergovernmental Panel on Climate Change, IPCC Secretariat, Geneva, 210 pp. Available online: http://www.ipcc.ch/publications_and_data/publications_and_data_technical_papers_climate_change_and_water.htm

Bellucci, A., S. Gualdi and A. Navarra (2010) The Double-ITCZ Syndrome in Coupled General Circulation Models: The Role of Large-Scale Vertical Circulation Regimes. *Journal of Climate*, **23**, pp 1127-1145. doi: 10.1175/2009JCLI3002.1

Boucher, O. and M. Pham (2002) History of sulfate aerosol radiative forcings. *Geophysical Research Letters*, **29** (9), 1308. doi: 10.1029/2001GL014048

Boyer, T.P., S. Levitus, J. Antonov, R. Locarnini, and H. Garcia (2005) Linear trends in salinity for the World Ocean, 1955-1998. *Geophysical Research Letters*, **32**, L01604. doi: 10.1029/2004GL021791

Brohan, P., J.J. Kennedy, I. Harris, S.F.B. Tett and P.D. Jones (2006) Uncertainty estimates in regional and global observed temperature changes: A new data set from 1850. *Journal of Geophysical Research*, **111**, D12106. doi: 10.1029/2005JD006548

Church, J.A., N.J. White and J.M. Arblaster (2005) Significant decadal-scale impact of volcanic eruptions on sea level and ocean heat content. *Nature*, **438**, pp 74-77. doi: 10.1038/nature04237

Cravatte, S., T. Delcoix, D. Zhang, M. McPhaden and J. LeLoup (2009) Observed freshening and warming of the western Pacific Warm Pool. *Climate Dynamics*, **33**, pp 565-589. doi: 10.1007/s00382-009-0526-7

Curry, R., B. Dickson and I. Yashayaev (2003) A change in the freshwater balance of the Atlantic Ocean over the past four decades. *Nature*, **426**, pp 826-829. doi: 10.1038/nature02206

de Szoeke, S.P. and S. Xie (2008) The Tropical Eastern Pacific Seasonal Cycle: Assessment of Errors and Mechanisms in IPCC AR4 Coupled Ocean-Atmosphere General Circulation Models. *Journal of Climate*, **21**, pp 2573-2590. doi: 10.1175/2007JCLI1975.1

Durre, I., C.N. Williams Jr, X. Yin and R.S. Vose (2009) Radiosonde-based trends in precipitable water over the Northern Hemisphere: An update. *Journal of Geophysical Research*, **114**, D05112. doi: 10.1029/2008JD010989

Dyurgerov, M. (2003) Mountain and subpolar glaciers show an increase in sensitivity to climate warming and intensification of the water cycle. *Journal of Hydrology*, **282**, pp 164-176. doi: 10.1016/S0022-1694(03)00254-3

Emori, S. and S.J. Brown (2005) Dynamic and thermodynamic changes in mean and extreme precipitation under changed climate. *Geophysical Research Letters*, **32**, L17706. doi: 10.1029/2005GL023272

Farneti, R., T.L. Delworth, A.J. Rosati, S.M. Griffies and F. Zeng (2010) The Role of Mesoscale Eddies in the Rectification of the Southern Ocean Response to Climate Change. *Journal of Physical Oceanography*, **40**, pp 1539-1557. doi: 10.1175/2010JPO4353.1

Forster, P., V. Ramaswamy, P. Artaxo, T. Berntsen, R. Betts, D.W. Fahey, J. Haywood, J. Lean, D.C. Lowe, G. Myhre, J. Nganga, R. Prinn, G. Raga, M. Schulz and R. Van Dorland (2007) Changes in Atmospheric Constituents and in Radiative Forcing. In: *Climate Change 2007: The Physical Science Basis. Contribution to Working Group I to the Fourth Assessment Report of the Intergovernmental Panel on Climate Change*. Solomon, S., D. Qin, M. Manning, Z. Chen, M. Marquis, K.B. Averyt, M. Tignor and H.L. Miller (Eds.). Cambridge University Press, Cambridge, United Kingdom and New York, NY, U.S.A. pp 129-234

Gillett, N.P., A.J. Weaver, F.W. Zwiers and M.F. Wehner (2004) Detection of volcanic influence on global precipitation. *Geophysical Research Letters*, **31**, L12217. doi: 10.1029/2004GL020044

Hack, J.J., J.M. Caron, S.G. Yeager, K.W. Oleson, M.M. Holland, J.E. Truesdale and P.J. Rasch (2006) Simulation of the Global Hydrological Cycle in the CCSM Community Atmosphere Model Version 3 (CAM3): Mean Features. *Journal of Climate*, **19**, pp 2199-2221. doi: 10.1175/JCLI3755.1

Hagemann, S., K. Arpe and E. Roeckner (2006) Evaluation of the Hydrological Cycle in the ECHAM5 Model. *Journal of Climate*, **19**, pp 3810-3827. doi: 10.1175/JCLI3831.1

Hansen, J., M. Sato, R. Ruedy, L. Nazarenko, A. Lacis, G.A. Schmidt, G. Russell, I. Aleinov, M. Bauer, S. Bauer, N. Bell, B. Cairns, V. Canuto, M. Chandler, Y. Cheng, A. Del Genio, G. Faluvegi, E. Fleming, A., Friend, T. Hall, C. Jackman, M. Kelley, N. Kiang, D. Koch, J. Lean, J. Lerner, K. Lo, S. Menon, R. Miller, P. Minnis, T. Novakov, V. Oinas, Ja. Perlwitz, Ju. Perlwitz, D. Rind, A. Romanou, D. Shindell, P. Stone, S. Sun, N. Tausnev, D. Thresher, B. Wielicki, T. Wong, M. Yao, Z. Zhang (2005) Efficacy of climate forcings. *Journal of Geophysical Research*. **110**, D18104. doi: 10.1029/2005JD005776

Held, I.M. and B.J. Soden (2006) Robust Responses of the Hydrological Cycle to Global Warming. *Journal of Climate*, **19**, pp 5686-5699. doi: 10.1175/JCLI3990.1

Helm, K.P., N.L. Bindoff and J.A. Church (2010) Changes in the global hydrological-cycle inferred from ocean salinity. *Geophysical Research Letters*, **37**, L18701. doi: 10.1029/2010GL044222

Hosoda, S., T. Suga, N. Shikama and K. Mizuno (2009) Global Surface Layer Salinity Change Detected by Argo and Its Implication for Hydrological Cycle Intensification. *Journal of Oceanography*, **65**, pp 579-586.

IPCC (2007). Summary for Policymakers. In *Climate Change 2007: The Physical Science Basis. Contribution of Working Group I to the Fourth Assessment Report of the Intergovernmental Panel on Climate Change*. Solomon, S., D. Qin, M. Manning, Z. Chen, M. Marquis, K.N. Averyt, M. Tignor and H.L. Miller (Eds) Cambridge University Press, Cambridge, U.K. pp 1-18

Johnson, E.S., G.S.E. Lagerloef, J.T. Gunn and F. Bonjean (2002) Surface salinity advection in the tropical oceans compared with atmospheric freshwater forcing: A trial balance. *Journal of Geophysical Research*, **107,** (C12) 8014. doi: 10.1029/2001JC001122

Josey, S.A., E.C. Kent and P.K. Taylor (1998) The Southampton Oceanography Centre (SOC) Ocean – Atmosphere Heat, Momentum and Freshwater Flux Atlas. Southampton Oceanography Centre Report No. 6, 30 pp. Available online: http://www.noc.soton.ac.uk/ooc/REFERENCES/PREPRINTS/SOC_flux_atlas.pdf

Keihm, S., S. Brown, J. Teixeira, S. Desai, W. Lu, E. Fetzer, C. Ruf, X. Huang and Y. Yung (2009) Ocean water vapor and cloud liquid water trends from 1992 to 2005 TOPEX Microwave Radiometer data. *Journal of Geophysical Research*, **114**, D18101. doi: 10.1029/2009JD012145

Laliberté, F. and O. Pauluis (2010) Winter intensification of the moist branch of the circulation in simulations of 21st century climate. *Geophysical Research Letters*, **37**, L20707. doi: 10.1029/2010GL045007

Lagerloef, G., F.R. Colomb, D. Le Vine, F. Wentz, S. Yueh, C. Ruf, J. Lilly, J. Gunn, Y. Chao, A. Decharon, G. Feldman and C. Swift (2008) The AQUARIUS/SAC-D Mission: Designed to meeting the salinity remote-sensing challenge. *Oceanography*, **21** (1), pp 68-81

Liepert, B.G. and M. Previdi (2009) Do Models and Observations Disagree on the Rainfall Response to Global Warming? *Journal of Climate*, **22**, pp 3156-3166. doi: 10.1175/2008JCLI2472.1

Lin, J. (2007) The Double-ITCZ Problem in IPCC AR4 Coupled GCMs: Ocean-Atmosphere Feedback Analysis. *Journal of Climate*, **20**, pp 4497-4525. doi: 10.1175/JCLI4272.1

Meehl, G.A., C. Covey, T. Delworth, M. Latif, B. McAvaney, J.F.B. Mitchell, R.J. Stouffer and K.E. Taylor (2007a) The WCRP CMIP3 Multimodel Dataset: A New Era in Climate Change Research. *Bulletin of the American Meteorological Society*, **88**, pp 1383-1394. doi: 10.1175/BAMS-88-9-1383

Meehl, G.A., T.F. Stocker, W.D. Collins, P. Friedlingstein, A.T. Gaye, J.M. Gregory, A. Kitoh, R. Knutti, J.M. Murphy, A. Noda, S.C.B. Raper, I.G. Watterson, A.J. Weaver and Z.-C. Zhao (2007b) Global Climate Projections. In: *Climate Change 2007: The Physical Science Basis. Contribution of the Working Group I to the Fourth Assessment Report of the Intergovernmental Panel on Climate Change*. Solomon, S., D. Qin, M. Manning, Z. Chen, M. Marquis, K.B. Averyt, M. Tignor and H.L. Miller (Eds). Cambridge University Press, Cambridge, United Kingdom and New York, NY, U.S.A. pp 747-845

Mieruch, S., S. Noël, H. Bovensmann and J.P. Burrows (2008) Analysis of global water vapour trends from satellite measurements in the visible spectral range. *Atmospheric Chemistry and Physics*, **8**, pp 491-504. doi: 10.5194/acp-8-491-2008

Ming, Y., V. Ramaswamy and G. Persad (2010) Two opposing effects of absorbing aerosols on global-mean precipitation. *Geophysical Research Letters*, **37**, L13701. doi: 10.1029/2010GL042895

Palmer, T.N. and J. Räisänen (2002) Quantifying the risk of extreme seasonal precipitation events in a changing climate. *Nature*, **415**, pp 512-514. doi: 10.1038/415512a

Panin, G.N. and V.S. Brezgunov (2007) Influence of the Salinity of Water on Its Evaporation. *Izvestiya, Atmospheric and Oceanic Physics*, **43**, pp 663-665. doi: 10.1134/S0001433807050143

Pardaens, A.K., H.T. Banks, J.M. Gregory and P.R. Rowntree (2003) Freshwater transports in HadCM3. *Climate Dynamics*, **21**, pp 177-195. doi: 10.1007/s00382-003-0324-6

Patz, J.A., D. Campbell-Lendrum, T. Holloway and J. A. Foley (2005) Impact of regional climate change on human health. *Nature*, **438**, pp 310-317. doi: 10.1038/nature04188

Petrone, K.C., J.D. Hughes, T.G. Van Niel and P. Silberstein (2010) Streamflow decline in southwestern Australia, 1950-2008. *Geophysical Research Letters*, **37**, L11401. doi: 10.1029/2010GL043102

Ramanathan, V., P.J. Crutzen, J.T. Kiehl and D. Rosenfeld (2001) Aerosols, Climate, and the Hydrological Cycle. *Science*, **294**, pp 2119-2124. doi: 10.1126/science.1064034

Reichler, T. and J. Kim (2008) How Well Do Coupled Models Simulate Today's Climate? *Bulletin of American Meteorological Society*, **89**, pp 303-311. doi: 10.1175/BAMS-89-3-303

Robock, A. (2000) Volcanic Eruptions and Climate. *Reviews of Geophysics*, **38**, pp 191-219. doi: 10.1029/1998RG000054

Roeckner, E., K. Bengtsson, J. Feichter, J. Lelieveld and H. Rodhe (1999) Transient Climate Change Simulations with a Coupled Atmosphere-Ocean GCM Including the Tropospheric Sulfur Cycle. *Journal of Climate*, **12**, pp 3004-3032. doi: 10.1175/1520-0442(1999)012<3004:TCCSWA>2.0.CO;2

Roemmich, D. and J. Gilson (2009) The 2004-2008 mean and annual cycle of temperature, salinity, and steric height in the global ocean from the Argo Program. *Progress in Oceanography*, **82**, pp 81-100. doi: 10.1016/j.pocean.2009.03.004

Sallée, J. and S.R. Rintoul (2011) Parameterization of eddy-Induced subduction in the Southern Ocean surface-Layer. *Ocean Modelling*, (Article in Press). doi: 10.1016/j.ocemod.2011.04.001

Santer, B.D., C. Mears, F.J. Wentz, K.E. Taylor, P.J. Gleckler, T.M.L. Wigley, T.P. Barnett, J.S. Boyle, W. Bruggemann, N.P. Gillett, S.A. Klein, G.A. Meehl, T. Nozawa, D.W. Pierce, P.A. Stott, W.M Washington and M.F. Wehner (2007) Identification of human-induced changes in atmospheric moisture content. *Proceedings of the National Academy of Sciences*, **104**, pp 15248-15253. doi: 10.1073/pnas.0702872104

Schanze, J.J., R.W. Schmitt and L.L. Yu (2010) The Global Oceanic Freshwater Cycle: A Best-Estimate Quantification. *Journal of Marine Research*, **68**, pp 569-595. doi: 10.1357/002224010794657164

Schneider, T., P.A. O'Gorman and X.J. Levine (2010) Water vapor and the dynamics of climate changes. *Review of Geophysics*, **48**, RG3001. doi: 10.1029/2009RG000302

Seager, R., N. Naik and G.A. Vecchi (2010) Thermodynamic and Dynamic Mechanisms for Large-Scale Changes in the Hydrological Cycle in Response to Global Warming. *Journal of Climate*, **23**, pp 4651-4668. doi: 10.1175/2010JCLI3655.1

Sherwood, S.C., J.R., Lanzante and C.L. Meyer (2005) Radiosonde Daytime Biases and Late-20th Century Warming. *Science*, **309**, pp 1556-1559. doi: 10.1126/science.1115640

Shiogama, H., S. Emori, K. Takahashi, T. Nagashima, T. Ogura, T. Nozawa and T. Takemura (2010) Emission Scenario Dependency of Precipitation on Global Warming in the MIROC3.2 Model. *Journal of Climate*, **23**, pp 2404-2417. doi: 10.1175/2009JCLI3428.1

Stephens, G.L. and T.D. Ellis (2008) Controls of Global-Mean Precipitation Increases in Global Warming GCM Experiments. *Journal of Climate*, **21**, pp 6141-6155. doi: 10.1175/2008JCLI2144.1

Stott, P.A., N.P. Gillett, G.C. Hegerl, D.J. Karoly, D.A. Stone, X. Zhang and F. Zwiers (2010) Detection and attribution of climate change: a regional perspective. *Wiley Interdisciplinary Reviews: Climate Change*, **1**, pp 192-211. doi: 10.1002/wcc.34

Stott, P.A., D.A. Stone and M.R. Allen (2004) Human contribution to the European heatwave of 2003. *Nature*, **432**, pp 610-614. doi: 10.1038/nature03089

Trenberth, K.E., J. Fasullo and L. Smith (2005) Trends and variability in column-integrated atmospheric water vapor. *Climate Dynamics*, **24**, pp 741-758. doi: 10.1007/s00382-005-0017-4

Trenberth, K.E., P.D. Jones, P. Ambenje, R. Bojariu, D. Easterling, A. Klein Tank, D. Parker, F. Rahimzadeh, J.A. Renwick, M. Rusticucci, B. Soden and P. Zhai (2007) Observations: Surface and Atmospheric Climate Change. In: *Climate Change 2007: The Physical Science Basis. Contribution of Working Group I to the Fourth Assessment Report of the Intergovernmental Panel on Climate Change*. Solomon, S., D. Qin, M. Manning, Z. Chen, M. Marquis, K.B. Averyt, M. Tignor and H.L. Miller (Eds). Cambridge University Press, Cambridge, United Kingdom and New York, NY, U.S.A. pp 235-336

Wentz, F.J., L. Ricciardulli, K. Hilburn and C. Mears (2007) How Much More Rain Will Global Warming Bring? *Science*, **317**, pp 233-235. doi: 10.1126/science.1140746

Wijffels, S.E. *et al.* (in prep) Detection and Anatomy of Linear Ocean Warming from 1960 to 2010

World Water Assessment Programme (2009) *The United Nations World Water Development Report 3: Water in a Changing World*. Paris: UNESCO, and London: Earthscan, 348 pp. Available online: http://www.unesco.org/water/wwap/wwdr/wwdr3/

Yin, X., A. Gruber and P. Arkin (2004) Comparison of the GPCP and CMAP Merged Gauge-Satellite Monthly Precipitation Products for the Period 1979-2001. *Journal of Hydrometeorology*, **5**, pp 1207-1222. doi: 10.1175/JHM-392.1

Yu, L. (2007) Global Variations in Oceanic Evaporation (1958-2005): The Role of the Changing Wind Speed. *Journal of Climate*, **20**, pp 5376-5390. doi: 10.1175/207JCLI1714.1

Zhang, X., F.W. Zwiers, G.C. Hegerl, F.H. Lambert, N.P. Gillett, S. Solomon, P.A. Stott and T. Nozawa (2007) Detection of human influence on twentieth-century precipitation trends. *Nature*, **448**, pp 461-465. doi: 10.1038/nature06025

Supplementary

Appendix 1: Model Drift

Model (or climate) drift is an inherent problem in current state-of-the-art climate modelling systems. Drift is the term applied to a systematic bias in model fields which can be attributed to deficiencies in the modelling system, with this feature primarily a problem with ocean simulations. These can manifest due to many different reasons, primarily on two timescales. Rapid drift occurs and is most likely due to errors introduced when coupling the ocean and atmosphere subcomponents, and is referred to as “coupling shock”. Longer term drift can be attributed to the slow adjustment of the deep ocean, and the most likely causes can be linked to unquantified/sub-grid scale physics (exclusion of eddies, localised boundary flows), poor initialisation (deficiencies with “first/best guess” climatologies), imposed flux adjustments (mostly deprecated in CMIP3) and insufficient model “spin-up” (not running the model integration out until a pseudo-equilibrium is reached).

In order to effectively obtain the pure transient forced signal from a climate model, and in particular in the “low” externally forced 20C3M realisations, it is necessary to attempt to account for drift, and additionally to attempt to account for high and low-frequency variability which can influence trends obtained from climate model data. It is for this reason that multi-decadal trends over 50-years (1950-2000) are considered in this analysis, with an expectation that model (or climate) variability will be fairly small over 50-year timescales when compared to the transient forced greenhouse gas response.

Drift was determined from the 1900-2049 period associated with the initial (run1: 1950-2000) 20C3M realisation, and the spatial pattern and magnitude was then extracted and removed from all the transient 20C3M realisations. A test was undertaken to ensure that differences in the time of 20C3M initialisation off the corresponding PICNTRL did not largely affect the result, and this was a sound assumption for most of the realisations, with the exception of gfdl_cm2_0 run1, as a strong initial drift was present.

The third row (if present) in Figure 3.S3A-L indicates the associated 50-year surface salinity drift as expressed in the 1900-2049 (or nearest time period) pre-industrial control (PICNTRL) realisation corresponding to the 1950-2000 20th century (20C3M) realisation.

More information:

Sen Gupta, A., L.C. Muir, J.N. Brown, S.J. Phipps, P.J. Durack, D.P. Monselesan and S.E. Wijffels, (submitted) Climate Drift in CMIP3 Models. *Journal of Climate*.

Cai, W. and H.B. Gordon (1999) Southern High-Latitude Ocean Climate Drift in a Coupled Model. *Journal of Climate*, **12**, pp 132-146. doi: 10.1175/1520-0442(1999)012<0132:SHLOCD>2.0.CO;2

Covey, C. *et al.* (2006) Secular trends and climate drift in coupled ocean-atmosphere general cirulation models. *Journal of Geophysical Research*, **111**, D03107. doi: 10.1029/2005JD006009

Table 3.S1. Forcings and flux corrections used in CMIP3 simulations of 20th century climate change (Updated from Santer *et al.*, 2007). The letter 'Y' denotes inclusion of the specific forcing for the selected model. G: well-mixed greenhouse gases; O: tropospheric and stratospheric ozone; SD: sulphate aerosol direct effects; SI: sulphate aerosol indirect effects; BC: black carbon; OC: organic carbon; MD: mineral dust; SS: sea salt; LU: land use change; SO: solar irradiance; VL: volcanic aerosols. For flux corrections (FC) the following notation is used; Freshwater: F; Heat/momentum: H. For ocean temperature, global surface temperature and global precipitation a larger number of models appear in Table 3.2 than are included below, these include the models: BCC-CM1 (China), INM-CM3.0 (Russia) and were excluded from the analysis as the primary variable of this study, ocean salinity were not available for analysis.

Model	Representative numbers	G	O	SD	SI	BC	OC	MD	SS	LU	SO	VL	FC
bccr_bcm2.0	1	Y	-	Y	-	-	-	-	-	-	-	-	-
cccma_cgcm3_1_t47	2,3,4,5,6	Y	-	Y	-	-	-	-	-	-	-	-	F,H
cccma_cgcm3_1_t63	7	Y	-	Y	-	-	-	-	-	-	-	-	F,H
cnrm_cm3	8	Y	Y	Y	-	Y	-	-	-	-	-	-	-
csiro_mk3_0	9,10,11	Y	Y	Y	-	-	-	-	-	-	-	-	-
csiro_mk3_5	12,13,14	Y	Y	Y	-	-	-	-	-	-	-	-	-
gfdl_cm2_0	15	Y	Y	Y	-	Y	Y	-	-	Y	Y	Y	-
gfdl_cm2_1	16	Y	Y	Y	-	Y	Y	-	-	Y	Y	Y	-
giss_aom	17,18	Y	-	Y	-	-	-	-	Y	-	-	-	-
giss_model_e_h	19,20,21,22,23	Y	Y	Y	Y	Y	Y	Y	Y	Y	Y	Y	-
giss_model_e_r	24,25,26,27,28,29,30,31,32	Y	Y	Y	Y	Y	Y	Y	Y	Y	Y	Y	-
iap_fgoals1_0	33,34,35	Y	-	Y	-	-	-	-	-	-	-	-	-
ingv_echam4	36	Y	Y	Y	-	-	-	-	-	-	-	-	-
ipsl_cm4	37	Y	-	Y	Y	-	-	-	-	-	-	-	-
miroc3_2_hires	38	Y	Y	Y	Y	Y	Y	Y	Y	Y	Y	Y	-
miroc_3_2_medres	39	Y	Y	Y	Y	Y	Y	Y	Y	Y	Y	Y	-
miub_echo_g	40,41,42	Y	-	Y	Y	-	-	-	-	-	Y	Y	F,H
mpi_echam5	43,44,45	Y	Y	Y	Y	-	-	-	-	-	-	-	
mri_cgcm2_3_2a	46,47,48,49,50	Y	-	Y	-	-	-	-	-	-	Y	Y	F,H
ncar_ccsm3_0	51,52	Y	Y	Y	-	Y	Y	-	-	-	Y	Y	
ncar_pcm1	53,54,55	Y	Y	Y	-	-	-	-	-	-	Y	Y	
ukmo_hadcm3.run1	56	Y	Y	Y	Y	-	-	-	-	-	Y	Y	
ukmo_hadcm3.run1	57	Y	Y	Y	Y	Y	Y	-	-	-	Y	-	
ukmo_hadgem1	58	Y	Y	Y	Y	Y	Y	-	-	Y	Y	Y	

Table 3.S2. Some representative observed water cycle changes for the 20th century, as expressed in Figure 3.10 for various observational products (salinity change estimates are scaled by 50% to represent E-P changes, see text, this table contains unscaled values). All global warming trends were obtained from the HadCRUT3 data product (Brohan *et al.*, 2006) as a linear trend over the period of analysis, following the Met Office smoothed annual average temperature technique described at http://hadobs.metoffice.com/hadcrut3/smoothing.html (Accessed 28/10/2010). Error estimates in the last column indicate formal errors resolved from the linear warming trend combined with water cycle error bounds (if available). Estimates are presented at 99% confidence for the warming estimate plus the water cycle error.

	Author	Instrument	Region	Period	Change per Decade	Change per K
1	Trenberth *et al.*, 2005	SSMI	Global PW	1987-2004	1.3±0.3%	7±16% K^{-1}
2	Durre *et al.*, 2009	Radiosondes	Northern Hemisphere PW	1973-2006	2.4%	14% K^{-1}
3	Keihm *et al.*, 2009	TMR	global PW 60°S-60°N	1992-2005	1.8±0.4%	6±9% K^{-1}
4	Mieruch *et al.*, 2008	GOME & SCIAMACHY	Global PW	1996-2002	1.9±0.7%	7±4% K^{-1}
5	Wentz *et al.*, 2007	SSMI	Tropical PW	1987-2006	1.2±0.4%	6±11% K^{-1}
6	Wentz *et al.*, 2007	SSMI	Tropical P	1987-2006	1.4±0.5%	7±14% K^{-1}
7	Wentz *et al.*, 2007	SSMI	Tropical E	1987-2006	1.3±0.5%	7±13% K^{-1}
8	Liepert & Previdi, 2009	OAFlux	Global Ocean E	1987-2004	1.6±0.8%	8±27% K^{-1}
9	Liepert & Previdi, 2009	HOAPS	Global Ocean E	1987-2004	4.6±3.6%	24±95% K^{-1}
10	Allan *et al.*, 2010	GPCP_V2.1/SSM/I	Tropical Hi-P	1988-2008	1.8±0.5%	10±23% K^{-1}
11	Allan *et al.*, 2010	GPCP_V2.1/SSM/I	Tropical Lo-P	1988-2008	-2.6±0.8%	-15±9% K^{-1}
12	Zhang *et al.*, 2007	GHCN	Land P 30°S-0	1925-1999	0.006%	<1% K^{-1}
13	Zhang *et al.*, 2007	GHCN	Land P 0-30°N	1925-1999	-0.007%	<1% K^{-1}
14	Zhang *et al.*, 2007	GHCN	Land P 40-70°N	1925-1999	0.01%	<1% K^{-1}
15	Yu, 2007 (updated)	OAFlux	Global Ocean E	1958-2008	1.2±0.5%	10±8% K^{-1}
16	Curry *et al.*, 2003	Ocean profile data	Atlantic Ocean salinity	1950-1990	1.9% (5-10)	22% K^{-1}
17	Hosoda *et al.*, 2009	Ocean profile data	Global Ocean surface salinity	1974-2005	1.2±1.5%	7±14% K^{-1}
18	Hosoda *et al.*, 2009	Ocean profile data	Southern Ocean surface salinity	1974-2005	2.7±2.1%	15±22% K^{-1}
19	Helm *et al.*, 2010	Ocean profile data	Southern Ocean salinity	1970-2005	4.6±1.7%	28±25% K^{-1}
20	Helm *et al.*, 2010	Ocean profile data	Northern Hemisphere Hi-latitude salinity	1970-2005	2.0±1.1%	12±14% K^{-1}
21	Helm *et al.*, 2010	Ocean profile data	Subtropical gyres salinity	1970-2005	-0.9±0.6%	-5±4% K^{-1}
22	Boyer *et al.*, 2005	Ocean profile data	Global Ocean surface salinity	1955-1998	1.0±0.1%	10±7% K^{-1}
23	This study	Ocean profile data	Global Ocean surface salinity	1950-2000	1.6±0.1%	16±7% K^{-1}
-	This study	Ocean profile data	Pacific Ocean surface salinity	1950-2000	1.4±0.1%	15±7% K^{-1}
-	This study	Ocean profile data	Atlantic Ocean surface salinity	1950-2000	1.4±0.1%	15±7% K^{-1}
-	This study	Ocean profile data	Indian Ocean surface salinity	1950-2000	1.2±0.1%	12±7% K^{-1}

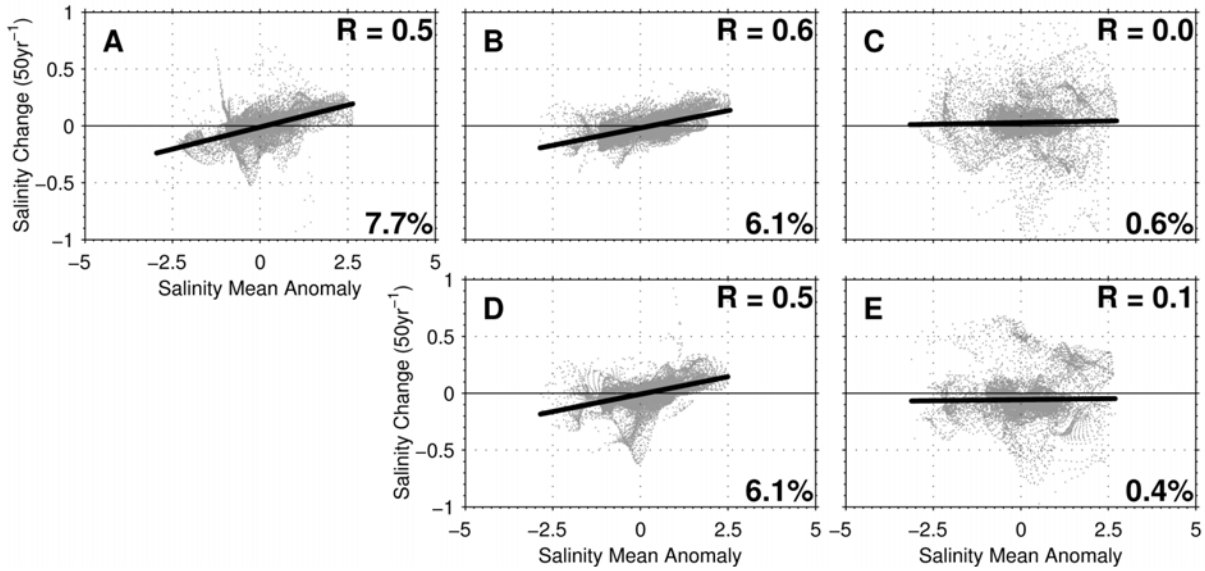

Figure 3.S1. Examples of pattern amplification for global ocean surface salinity for A) the 1950-2000 observed result (Chapter 2) B) Canadian Centre for Climate Modelling & Analysis: CGCM3.1 (T63) for 1950-2000 C) United Kingdom MetOffice: HadGEM1 for 1950-2000 D) Canadian Centre for Climate Modelling & Analysis: CGCM3.1 (T63) for 1850-2000 E) United Kingdom MetOffice: HadGEM1 for 1860-2000

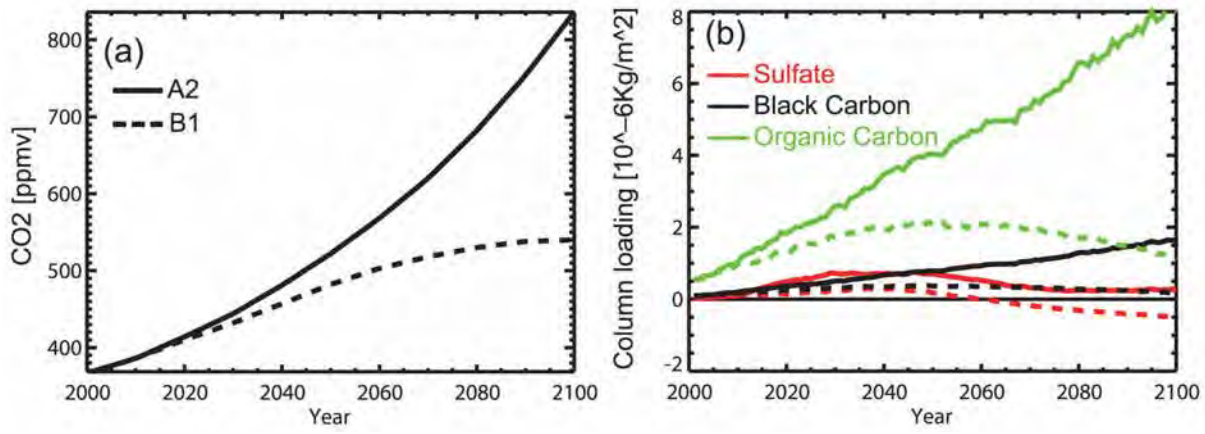

Figure 3.S2. External forcing agents in the SRES A2 (solid lines) and B1 (dashed lines) scenarios. (A) concentrations of well mixed CO_2 (ppmv) and (B) changes in the column loading of sulphate (red), black carbon (black) and organic carbon (green) aerosols from the 1981-2000 mean. Reproduced from Shiogama *et al.* (2010).

Table 3.S3. Integrated global surface values for 1950-2000 trends resolved from available 20th century (20C3M) CMIP3 experiments, de-drifted by their corresponding pre-industrial control in: sea surface salinity (basin zonal-mean) pattern amplification (PA; %), ocean freshwater flux (E-P) (basin zonal-mean) pattern amplification (PA; %), area-weighted global ocean surface temperature (°C), area-weighted global surface temperature (°C) and area-weighted global surface mean precipitation change (%). A non-exhaustive selection of observational estimates from available data products are found in the lower section of the table for comparison. Trends have been obtained over the period in parentheses and scaled to represent directly comparable 50yr changes.

#	Model	Salinity (%PA)	E-P (%PA)	Ocean Temperature (°C)	Global Temperature (°C)	Rainfall (ΔP)
1	bccr_bcm2_0.20c3m.run1	+2.5	-	-	+0.41	+0.1
2	cccma_cgcm3_1_t47.20c3m.run1	+4.0	+3.4	+0.73	+1.10	+2.0
3	cccma_cgcm3_1_t47.20c3m.run2	+4.7	+3.7	+0.66	+1.04	+1.7
4	cccma_cgcm3_1_t47.20c3m.run3	+5.9	+4.9	+0.66	+0.96	+2.0
5	cccma_cgcm3_1_t47.20c3m.run4	+4.9	+6.5	+0.67	+1.01	+2.1
6	cccma_cgcm3_1_t47.20c3m.run5	+6.3	+5.1	+0.61	+0.90	+1.8
7	cccma_cgcm3_1_t63.20c3m.run1	+6.6	+5.5	+0.74	+1.10	+1.8
8	cnrm_cm3.20c3m.run1	+8.3	+5.1	-	+0.74	+1.1
9	csiro_mk3_0.20c3m.run1	+2.2	+2.6	+0.42	+0.63	+1.0
10	csiro_mk3_0.20c3m.run2	+1.7	+0.4	+0.45	+0.69	+0.9
11	csiro_mk3_0.20c3m.run3	+2.2	+2.2	+0.38	+0.58	+0.8
12	csiro_mk3_5.20c3m.run1	+2.8	+2.1	+0.44	+0.71	+1.5
13	csiro_mk3_5.20c3m.run2	+6.8	+2.3	+0.59	+0.87	+1.4
14	csiro_mk3_5.20c3m.run3	+3.9	+2.0	+0.47	+0.64	+1.1
15	gfdl_cm2_0.20c3m.run1	+4.3	+0.5	+0.02	+0.09	-0.7
16	gfdl_cm2_1.20c3m.run2	+2.6	+1.6	+0.21	+0.29	-0.6
17	giss_aom.20c3m.run1	+2.5	-	+0.35	+0.49	+0.5
18	giss_aom.20c3m.run2	+3.7	-	+0.27	+0.39	+0.4
19	giss_model_e_h.20c3m.run1	+4.7	-	-	+0.34	-0.2
20	giss_model_e_h.20c3m.run2	+6.0	-	-	+0.24	-0.6
21	giss_model_e_h.20c3m.run3	+5.2	-	-	+0.25	-0.4
22	giss_model_e_h.20c3m.run4	+3.4	-	-	+0.25	-0.7
23	giss_model_e_h.20c3m.run5	+5.9	-	-	+0.31	-0.7
24	giss_model_e_r.20c3m.run1	-0.1	+0. 9	+0.13	+0.18	-0.8
25	giss_model_e_r.20c3m.run2	+4.9	+2.9	+0.13	+0.27	-0.9
26	giss_model_e_r.20c3m.run3	+2.3	+0.1	+0.12	+0.23	-1.1
27	giss_model_e_r.20c3m.run4	-0.1	-0.2	+0.22	+0.39	-0.7
28	giss_model_e_r.20c3m.run5	+0.9	+0.8	+0.20	+0.37	-0.6
29	giss_model_e_r.20c3m.run6	+3.2	+0.1	+0.15	+0.27	-0.8
30	giss_model_e_r.20c3m.run7	+0.6	-0.0	+0.15	+0.34	-0.7
31	giss_model_e_r.20c3m.run8	+2.3	+1.4	+0.18	+0.32	-0.8
32	giss_model_e_r.20c3m.run9	+2.7	+1.5	+0.13	+0.26	-0.9
33	iap_fgoals1_0_g.20c3m.run1	+9.4	+0.5	+0.48	+0.80	+0.8
34	iap_fgoals1_0_g.20c3m.run2	+7.5	-	-	+0.83	+1.2
35	iap_fgoals1_0_g.20c3m.run3	+10.2	-	-	+0.74	+0.7
36	ingv_echam4.20c3m.run1	+2.2	-	+0.53	+0.73	+1.4
37	ipsl_cm4.20c3m.run1	+5.4	-	+0.42	+0.60	+0.9

#	Model (cnt'd)	Salinity (%PA)	E-P (%PA)	Ocean Temperature (°C)	Global Temperature (°C)	Rainfall (ΔP)
38	miroc3_2_hires.20c3m.run1	+1.7	-0.4	+0.37	+0.48	-0.1
39	miroc3_2_medres.20c3m.run1	+4.8	+2.3	+0.16	+0.23	-0.5
40	miub_echo_g.20c3m.run1	+0.4	+0.00	+0.13	+0.29	-0.3
41	miub_echo_g.20c3m.run2	+4.4	+2.0	+0.21	+0.32	-0.4
42	miub_echo_g.20c3m.run3	+1.0	+0.2	+0.16	+0.22	-0.5
43	mpi_echam5.20c3m.run1	-	-	-	+0.48	+0.6
44	mpi_echam5.20c3m.run2	-	-	-	+0.24	-0.2
45	mpi_echam5.20c3m.run3	-	-	-	+0.44	+0.9
46	mri_cgcm2_3_2a.20c3m.run1	+3.5	+3.3	-	+0.65	+1.1
47	mri_cgcm2_3_2a.20c3m.run2	+1.9	+3.8	-	+0.62	+1.1
48	mri_cgcm2_3_2a.20c3m.run3	+2.0	+3.3	-	+0.69	+1.5
49	mri_cgcm2_3_2a.20c3m.run4	+1.6	+3.0	-	+0.59	+0.8
50	mri_cgcm2_3_2a.20c3m.run5	+4.2	+4.2	-	+0.63	+1.4
51	ncar_ccsm3_0.20c3m.run1	-	-	-	+0.32	-0.2
52	ncar_ccsm3_0.20c3m.run3	-	-	-	+0.52	+0.2
53	ncar_pcm1.20c3m.run1	-	-	-	-	-
54	ncar_pcm1.20c3m.run3	-	-	-	-	-
55	ncar_pcm1.20c3m.run4	-	-	-	-	-
56	ukmo_hadcm3.20c3m.run1	+0.1	+1.7	-	+0.60	+0.5
57	ukmo_hadcm3.20c3m.run2	+4.7	+4.3	-	+0.67	+0.3
58	ukmo_hadgem1.20c3m.run1	+1.1	+1.3	+0.40	+0.60	+0.2
20C3M Models		20	16	16	23	23
20C3M Realisations		58	47	63	78	73
20C3M De-drifted Realisations		50	44	41	70	68
Ensemble Mean		+3.7	+2.0	+0.33	+0.50	+0.3
Ensemble Standard Deviation		+2.4	+1.8	+0.20	+0.25	+0.9
Observational Estimates		**Salinity (%PA)**	**E-P (%PA)**	**Ocean Temperature (°C)**	**Global Temperature (°C)**	**Rainfall (ΔP)**
Durack & Wijffels (2010; 1950-2000)		+8.0		+0.49		
Boyer *et al.* (2005; 1955-1998)		+5.2				
Wijffels *et al.* (in prep; 1960-2008)				+0.56		
HadCRUT3 (1950-2009)					+0.54	
GISTEMP (1950-2009)					+0.53	
Levitus *et al.* (2009; 1955-2009)				+0.25		
HadSST2 (1950-2009)				+0.37		
Kaplan V2 (1950-2009)				+0.24		
ERSST V3b (1950-2009)				+0.31		
OAFlux V3 (1958-2008)			+6.4			
GPCP V2.1 (1979-2008)						-3.7
CMAP (1979-2008)						-6.0

Figure 3.S3A-L. Ocean salinity amplification is expressed by 23 CMIP3 global climate models in their 20C3M realisations for the period 1950-2000. Top vertical panel represents surface mean salinity for 1950-2000, second vertical panel represents 20C3M surface salinity change for 1950-2000, third vertical panel represents the corresponding PICNTRL drift as determined for 1900-2049 and the lowest vertical panel represents surface mean freshwater flux (E-P) for 1950-2000. Panel numbers represent each model as numbered in Table 3.S1.

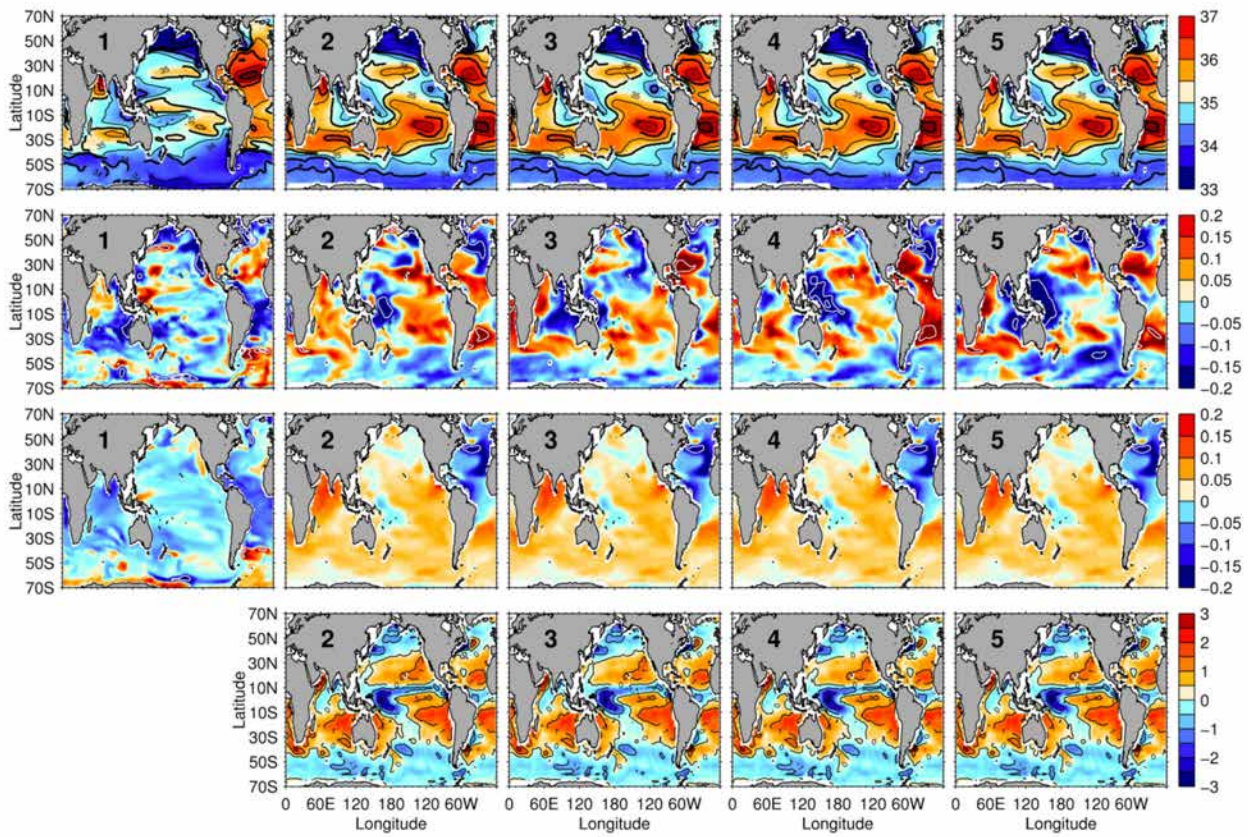

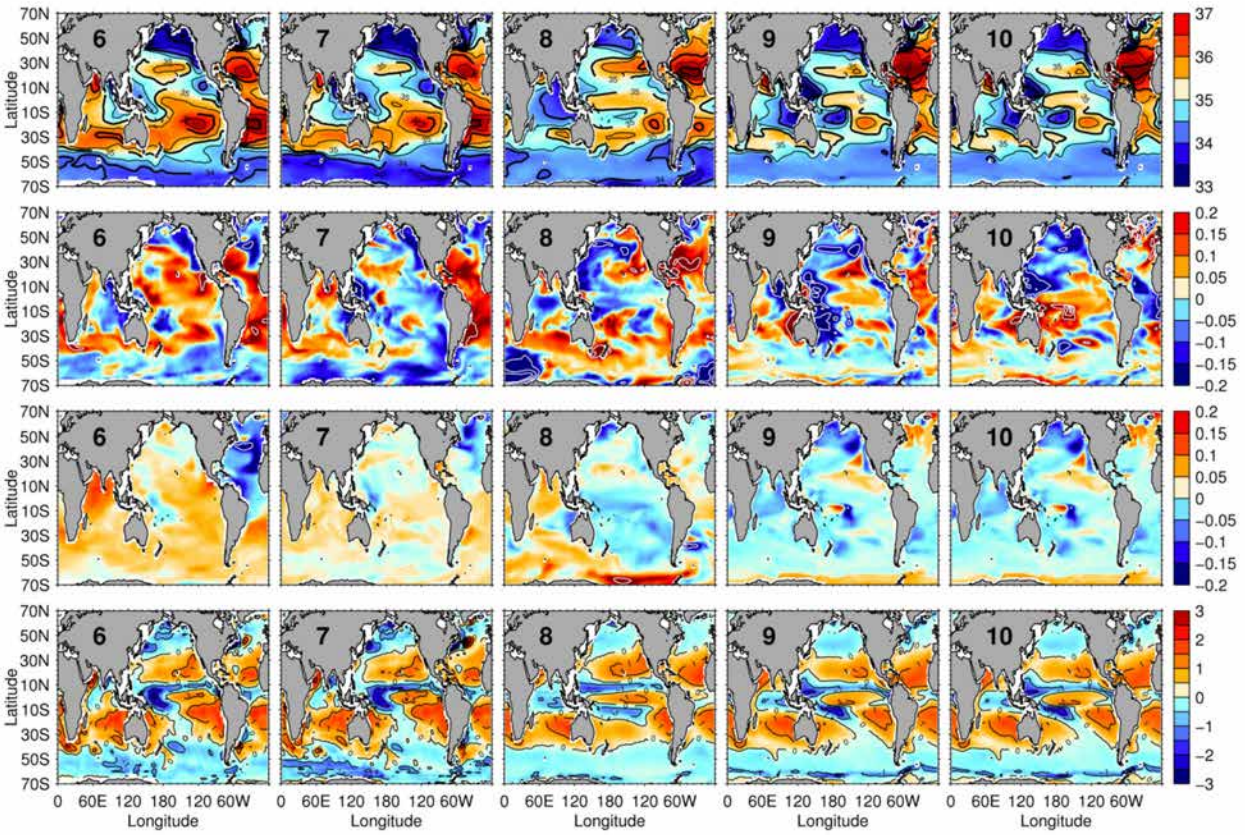
6
7
8
9
10
70N
50N
30N
10N
10S
30S
50S
70S
Latitude
0 60E 120 180 120 60W
Longitude
37
36
35
34
33
0.2
0.15
0.1
0.05
0
−0.05
−0.1
−0.15
−0.2
3
2
1
0
−1
−2
−3

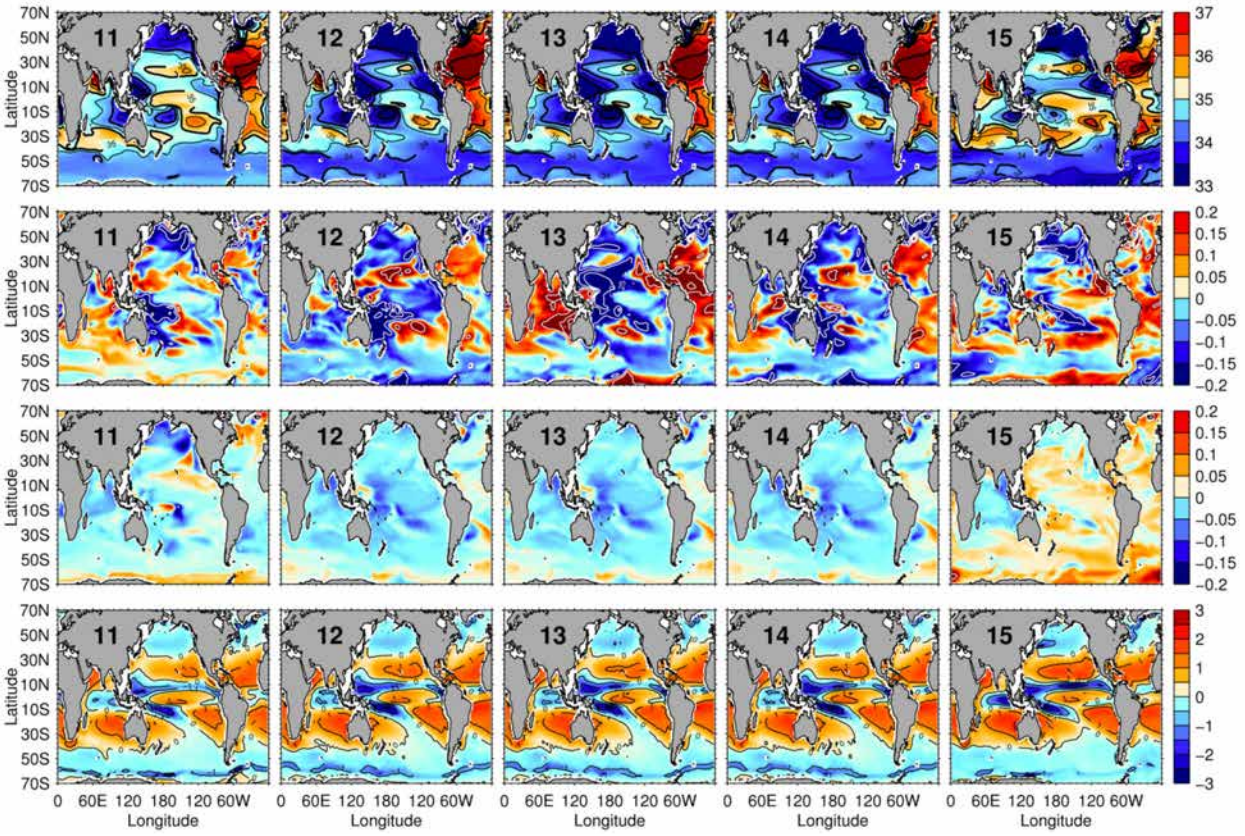
11
12
13
14
15
70N
50N
30N
10N
10S
30S
50S
70S
Latitude
0 60E 120 180 120 60W
Longitude
37
36
35
34
33
0.2
0.15
0.1
0.05
0
−0.05
−0.1
−0.15
−0.2
3
2
1
0
−1
−2
−3

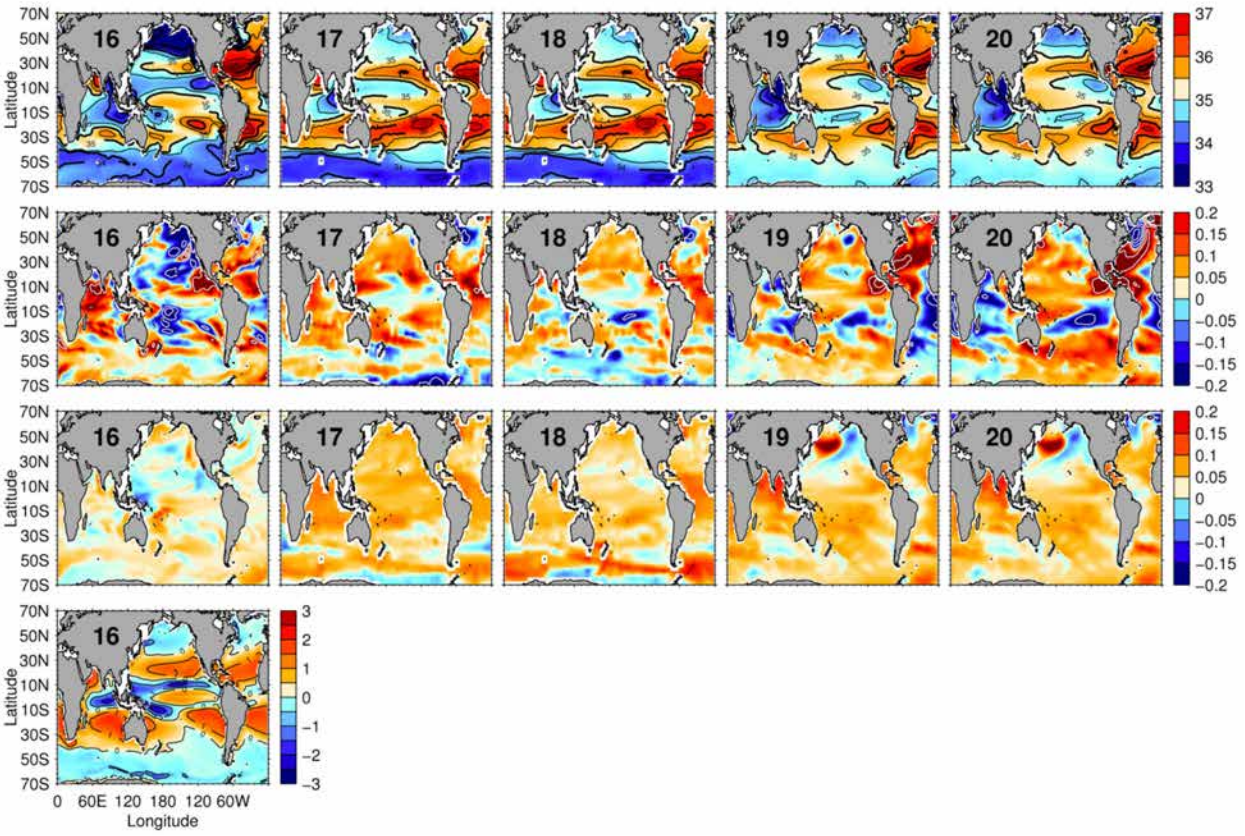
16
17
18
19
20
Latitude
70N
50N
30N
10N
10S
30S
50S
70S
0 60E 120 180 120 60W
Longitude
37
36
35
34
33
0.2
0.15
0.1
0.05
0
−0.05
−0.1
−0.15
−0.2
3
2
1
0
−1
−2
−3

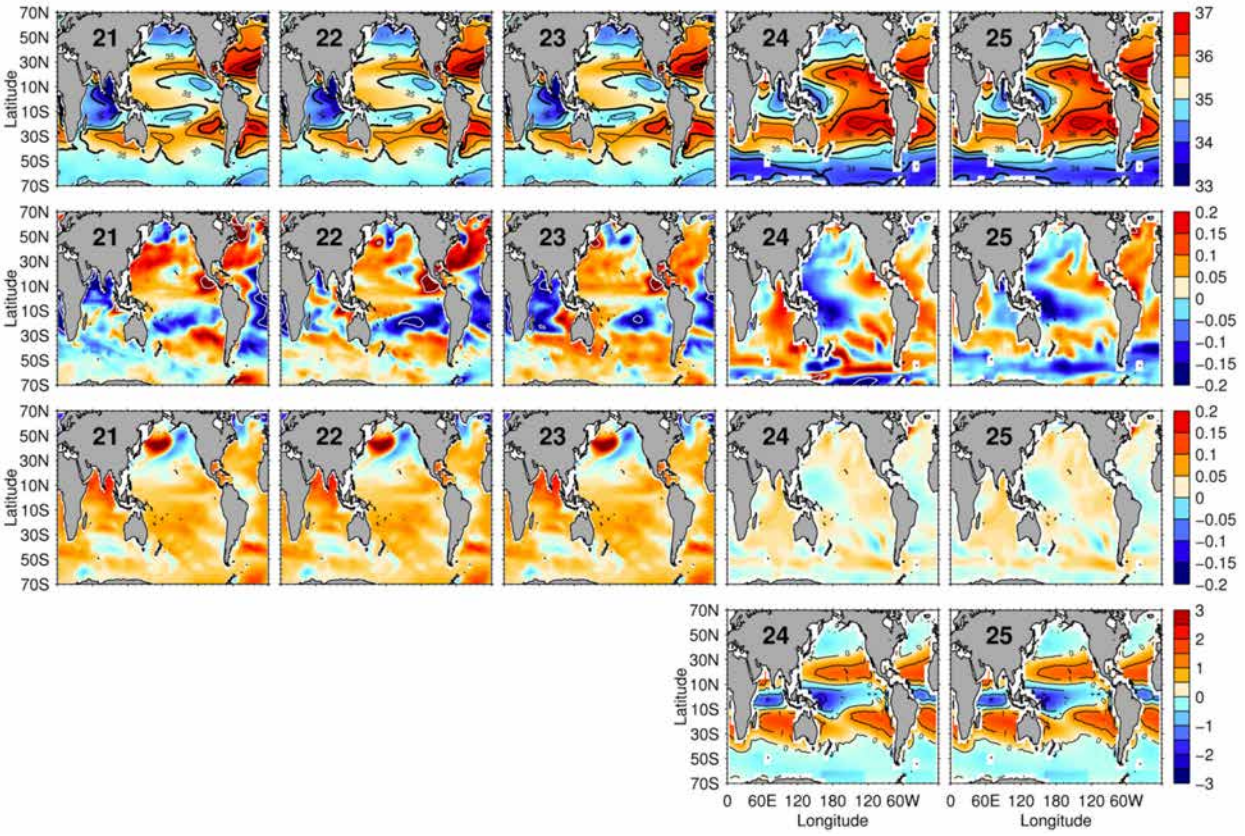
21
22
23
24
25
Latitude
70N
50N
30N
10N
10S
30S
50S
70S
0 60E 120 180 120 60W
Longitude
37
36
35
34
33
0.2
0.15
0.1
0.05
0
−0.05
−0.1
−0.15
−0.2
3
2
1
0
−1
−2
−3

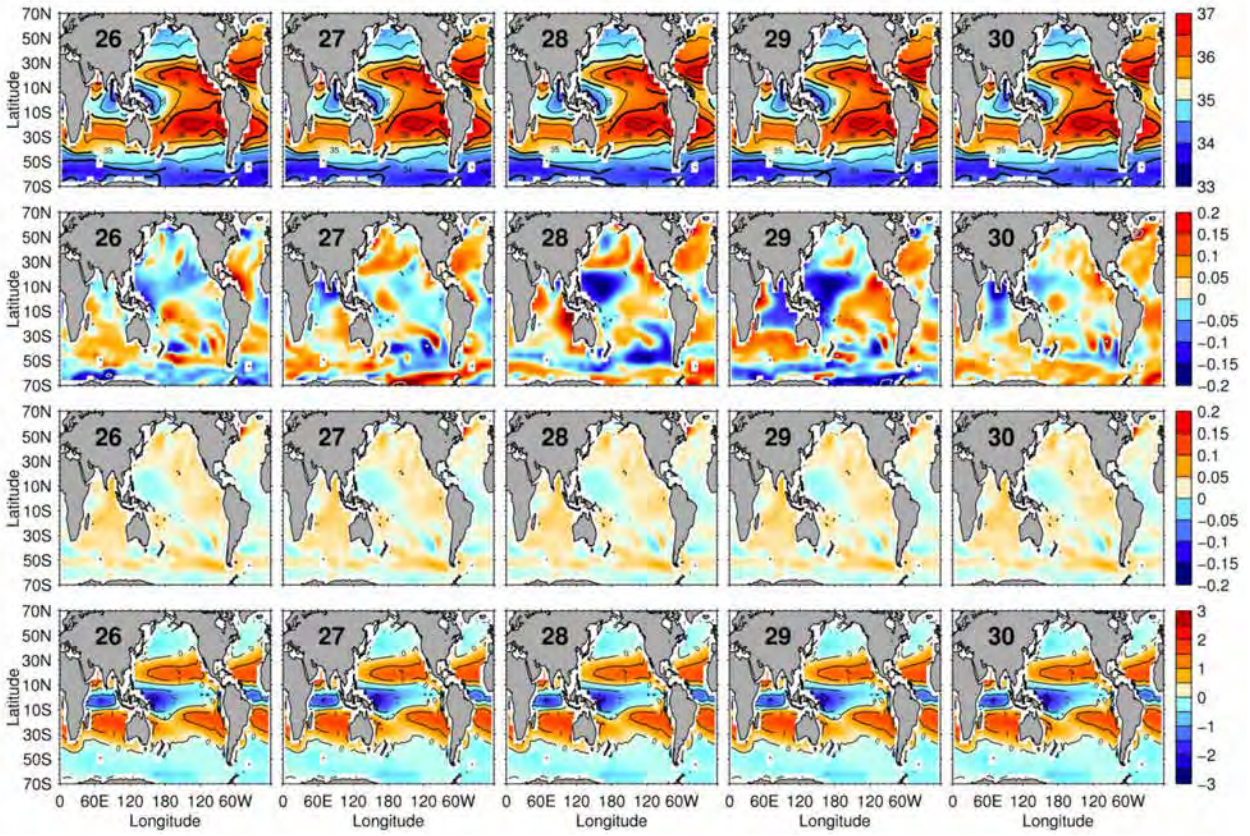
26
27
28
29
30
Latitude
70N
50N
30N
10N
10S
30S
50S
70S
0 60E 120 180 120 60W
Longitude
37
36
35
34
33
0.2
0.15
0.1
0.05
0
−0.05
−0.1
−0.15
−0.2
3
2
1
0
−1
−2
−3

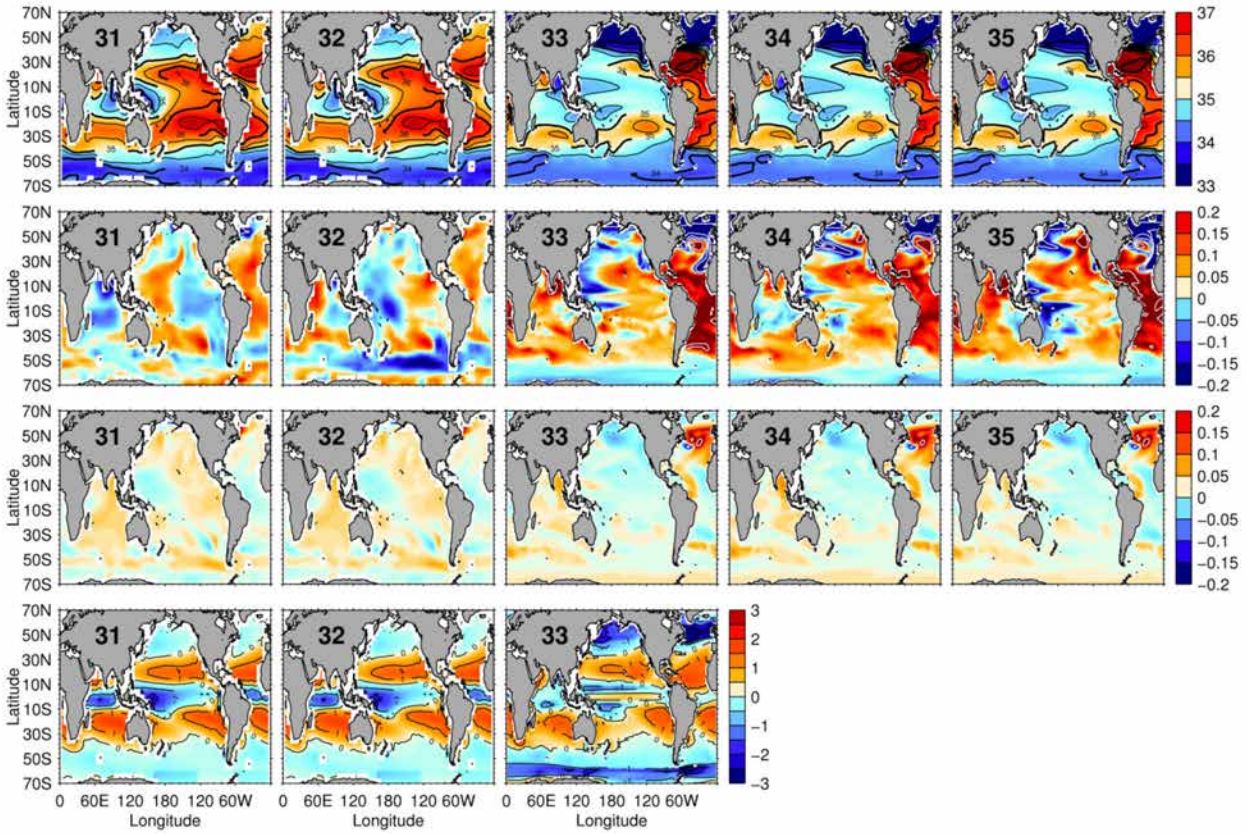
31
32
33
34
35
Latitude
70N
50N
30N
10N
10S
30S
50S
70S
0 60E 120 180 120 60W
Longitude
37
36
35
34
33
0.2
0.15
0.1
0.05
0
−0.05
−0.1
−0.15
−0.2
3
2
1
0
−1
−2
−3

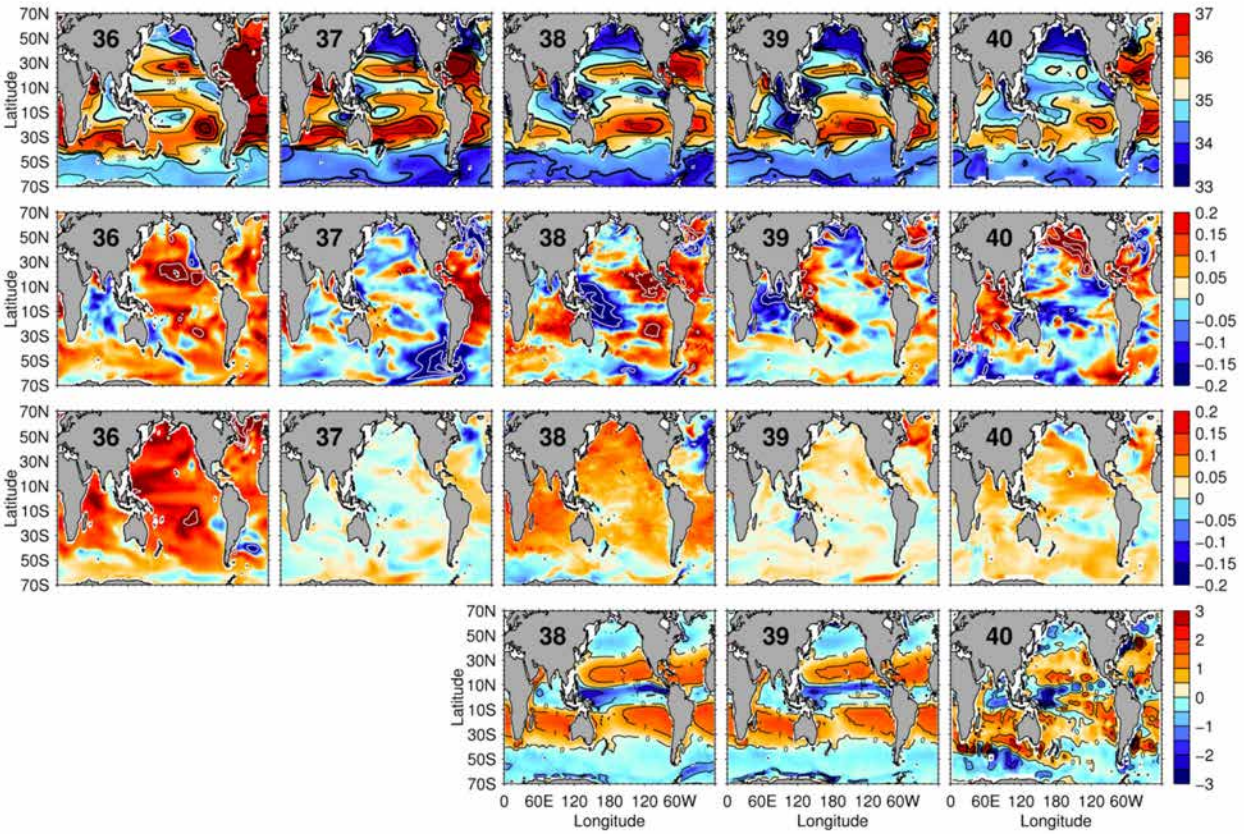
36
37
38
39
40
Latitude
70N
50N
30N
10N
10S
30S
50S
70S
0 60E 120 180 120 60W
Longitude
37
36
35
34
33
0.2
0.15
0.1
0.05
0
−0.05
−0.1
−0.15
−0.2
3
2
1
0
−1
−2
−3

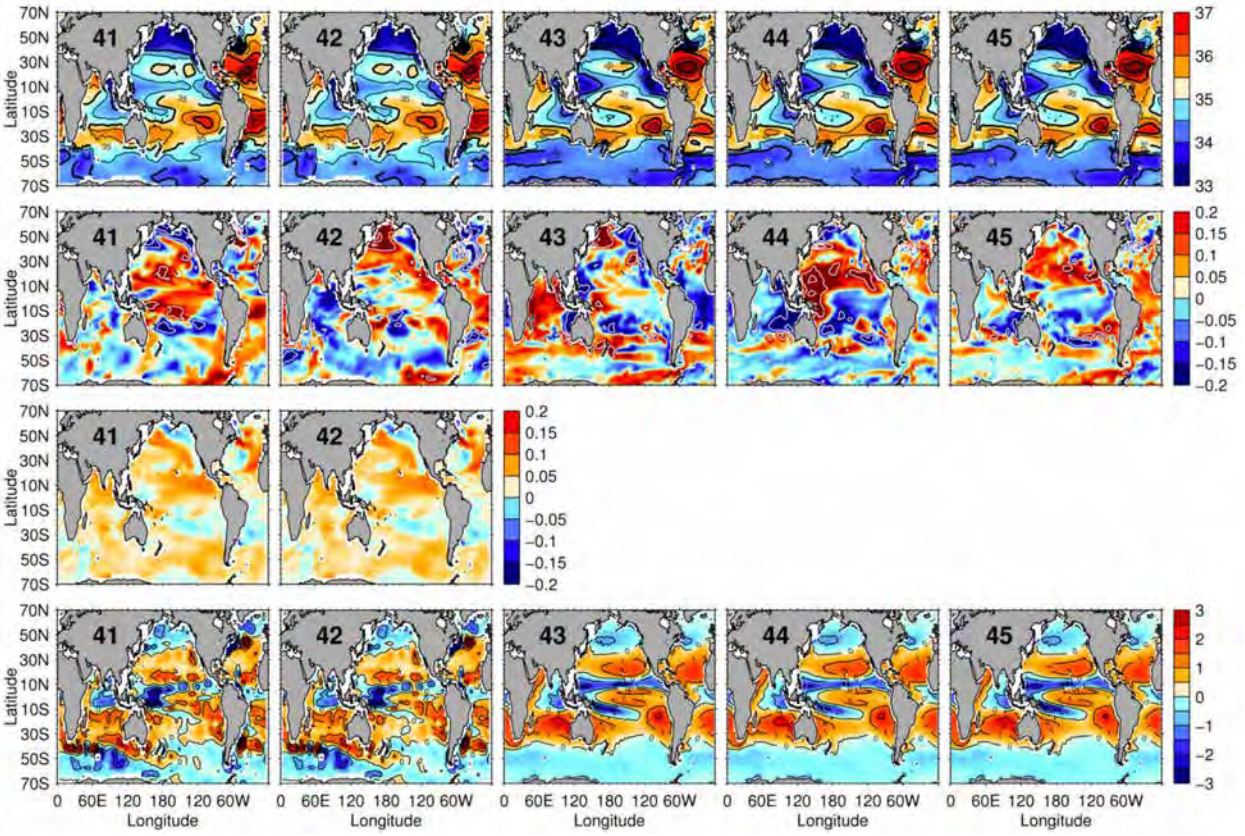
41
42
43
44
45
Latitude
70N
50N
30N
10N
10S
30S
50S
70S
0 60E 120 180 120 60W
Longitude
37
36
35
34
33
0.2
0.15
0.1
0.05
0
−0.05
−0.1
−0.15
−0.2
3
2
1
0
−1
−2
−3

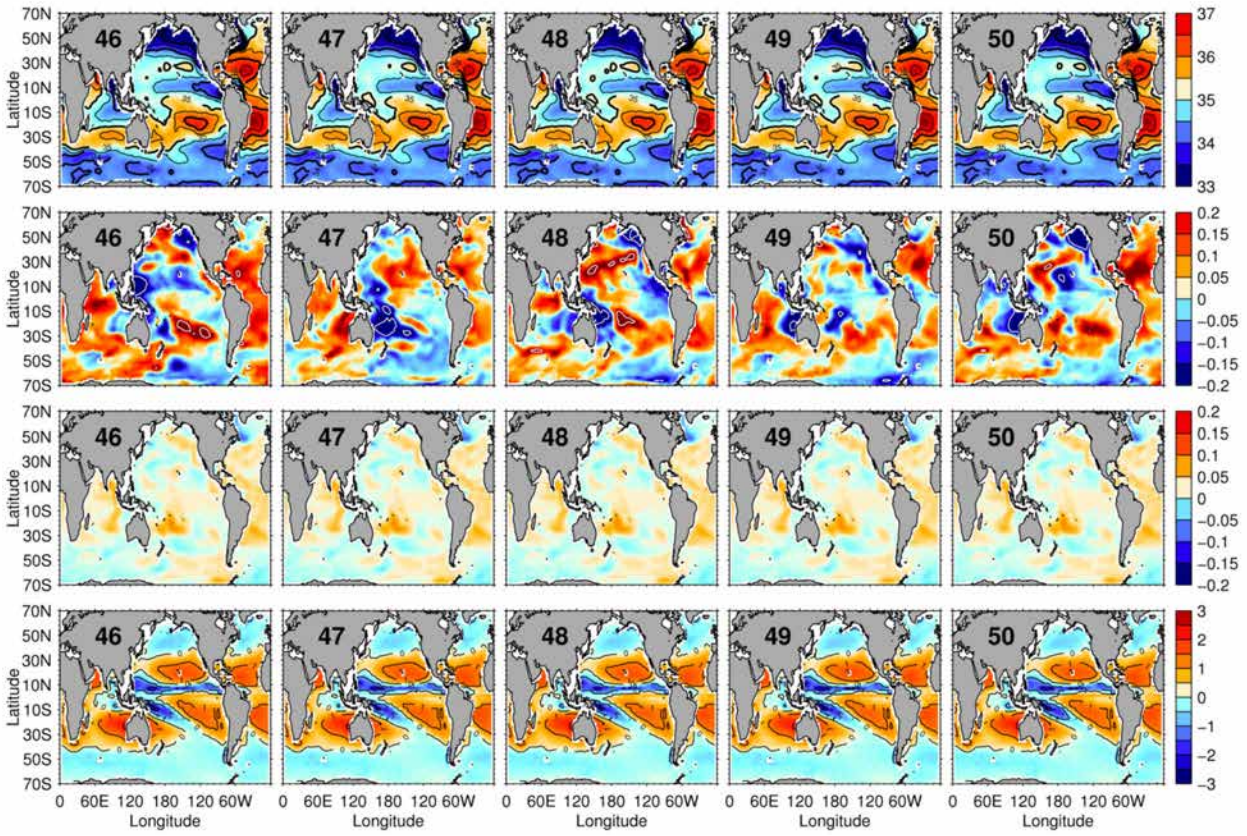
46
47
48
49
50
Latitude
70N
50N
30N
10N
10S
30S
50S
70S
0 60E 120 180 120 60W
Longitude
37
36
35
34
33
0.2
0.15
0.1
0.05
0
−0.05
−0.1
−0.15
−0.2
3
2
1
0
−1
−2
−3

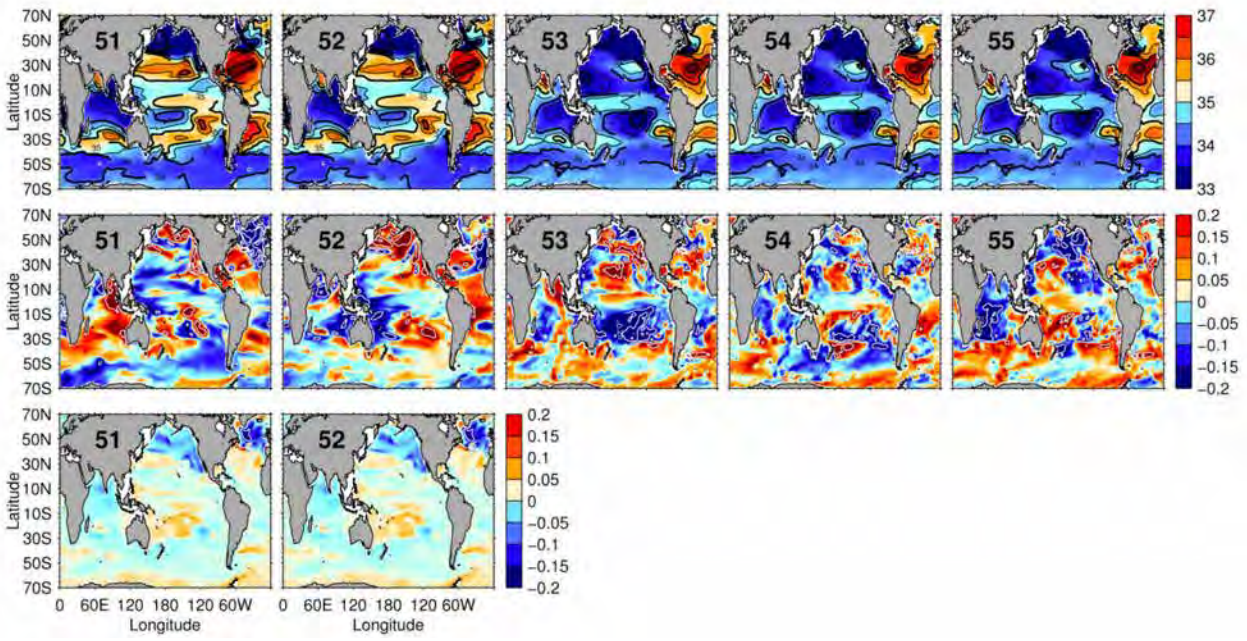
51
52
53
54
55
Latitude
70N
50N
30N
10N
10S
30S
50S
70S
0 60E 120 180 120 60W
Longitude
37
36
35
34
33
0.2
0.15
0.1
0.05
0
−0.05
−0.1
−0.15
−0.2

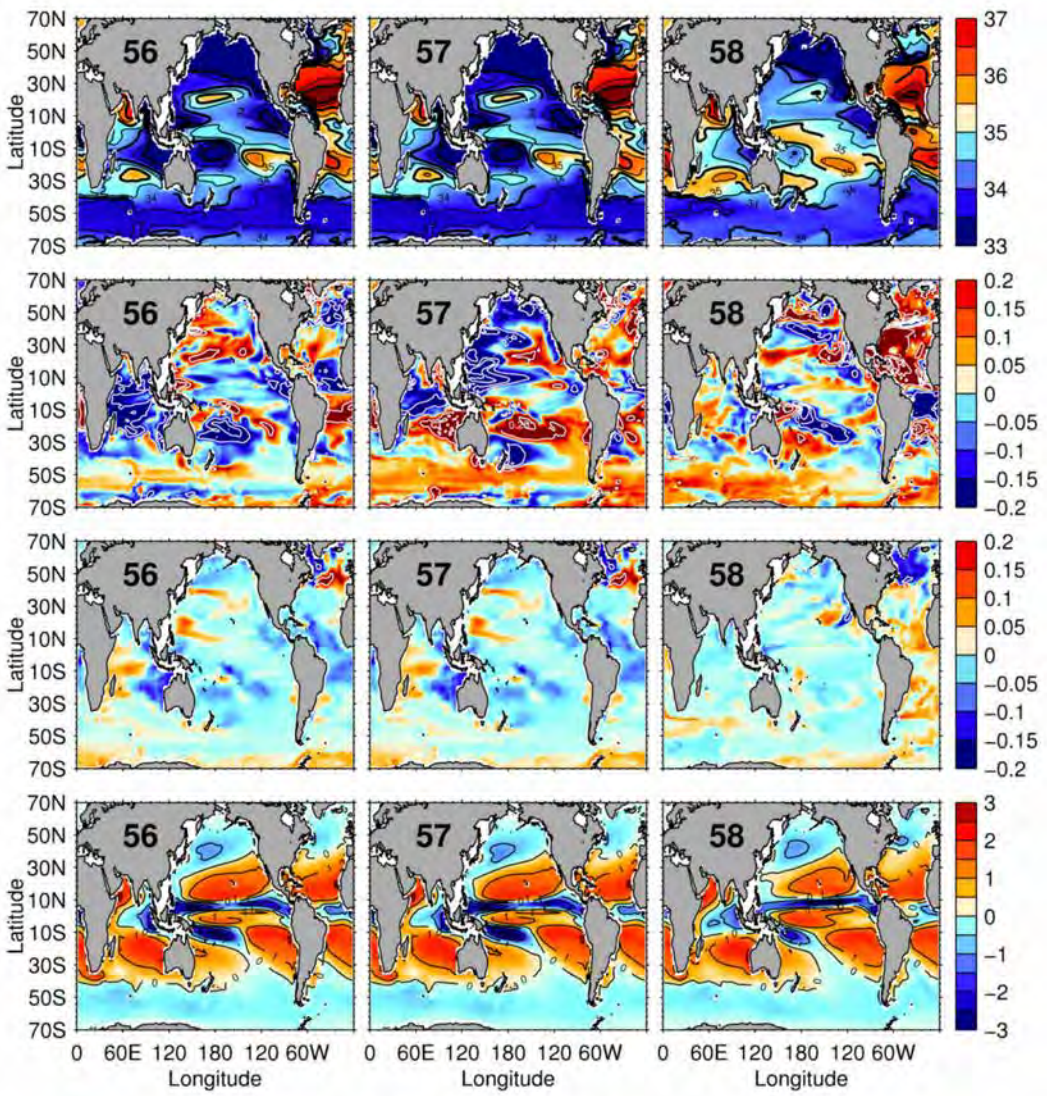
56
57
58
Latitude
70N
50N
30N
10N
10S
30S
50S
70S
37
36
35
34
33
0.2
0.15
0.1
0.05
0
−0.05
−0.1
−0.15
−0.2
3
2
1
0
−1
−2
−3
0 60E 120 180 120 60W
Longitude

Chapter 4

50-Years of Integrated Ocean Changes: Sea-level Rise

Abstract

A new global analysis of linear trends in historical and Argo Program ocean profile data quantifies both the halosteric and thermosteric changes in sea-level down to 1800m over the past 50-years, and more importantly their regional patterns. Total steric change for 1950-2000 is 35mm (27mm) integrated to a depth of 1800m (700m). These are consistent with the current best steric estimates accounting for around half of total 20th century observed sea-level rise, with the remainder attributed to mass contributions from the cryosphere. Of this 6mm or 20% (3mm or 10%) is due to halosteric effects.

The halosteric integrated global average presented by this analysis contains clear errors. The error may be partly compensated by signals from unobserved regions (high latitude, marginal seas and the deep ocean) and eustatic sea-level rise from terrestrial ice melt. In a global sense, redistribution of salinity in the ocean and the integrated halosteric effect must sum to zero, as eustatic (mass addition) contributions are too small over the observed record to be recorded accurately in an observed salinity derived halosteric global average.

There is more certainty for regional halosteric effects however. In parts of the regional ocean such as the South Pacific, South Indian and North Atlantic basins, depth integrated halosteric changes can account for around 50% of the total steric signal. In the Atlantic basin this halosteric contraction strongly counteracts a thermosteric expansion. Regional patterns of steric change show highs along the axis of the Antarctic Circumpolar Current (likely associated with its southward shift) and in the North Pacific and Atlantic subtropical gyres. Reduced steric sea-level is found around northern Australia, the eastern Indian Ocean and the subpolar North-western Pacific.

Halosteric changes are shown to be the leading steric regional change for 34% of the depth-integrated global ocean by area. Contraction (enhanced salinity) is observed throughout the Atlantic between 45°N and 45°S and the North Indian Ocean. Expansion is observed through most of the Pacific and Southern Oceans associated with Mode Water freshening. The patterns of halosteric change largely reflect a strengthening of inter-basin salinity contrasts (both surface and subsurface) and mean salinity pattern amplification likely due to an enhanced water cycle.

This chapter is to be submitted:

Durack, P.J. and S.E. Wijffels (in prep) Revisiting Halosteric and Thermosteric Sea-level Rise 1950-2000

Introduction

Sea-level rise (SLR) associated with anthropogenic climate change and its subsequent impacts on the coastal zone have been identified as one of the major challenges facing humankind into the 21st century. Likely impacts on coastal communities are expected to be significant (e.g. Nicholls *et al.*, 2007), considering over 80% of Australians are living within the coastal zone (Harvey & Caton, 2003). This number is not dissimilar to other developed countries, and global population projections suggest that 75% of the global population will reside in coastal areas by 2025 (Hinrichsen, 1995). Expected sea-level rise will therefore have large effects on humankind in the near future. However, estimates of rates of change and their magnitudes into the future vary considerably, and our understanding of regional changes is poor (IPCC, 2010). Obtaining the best estimates of past sea-level changes guides our current understanding of processes that influence global (and regional) variations, thus improving our ability to estimate changes into the future.

The warming ocean accounts for around 90% of additional planetary heat storage over 1961-2008 (1450 x 10^{21} joules; Church *et al.*, in prep), associated with increasing temperatures recorded over the Earth surface during this time (Trenberth *et al.*, 2007). As a response to increased heat storage, an expansion of the ocean, elevating mean sea-level has been observed (Ishii *et al.*, 2006; Domingues *et al.*, 2008; Levitus *et al.*, 2009). Seawater density (volume) is a fundamental physical property which decreases (increases) when heat is added (removed), and expands (contracts) with decreasing (increasing) salinity concentrations for a contained water parcel. These steric (density) components are termed the thermosteric (heat) and halosteric (salt) properties of seawater.

New estimates of halosteric changes to ocean properties (associated with observed salinity changes; Chapter 2) have been recorded over comparable periods to the thermosteric estimates noted above. These halosteric estimates are more spatially complex than the broad-scale (basin-scale) warming expressed over the 20th century (Trenberth *et al.*, 2007). Changes to the ocean freshwater budget, which manifests in observed salinity changes, is largely driven by ocean-atmosphere fluxes (Chapter 3) and compensating inter-basin ocean transports (Wijffels, 2001). After these, the much smaller transient contributions from terrestrial storage and sea-ice reservoirs play a role (a sense of transport scales is expressed in Table 4.1). However, with a 4% observed increase to ocean-atmosphere freshwater fluxes (expressed as evaporation minus precipitation [E-P]), inferred from the 1950-2000 salinity changes (Chapter 3), these are many orders of magnitude larger than other contributions to the regional halosteric SLR budget from the cryosphere.

Table 4.1. Freshwater transports and the long-term sea-level budget. Upper: Observed time-varying estimates of cryospheric freshwater contributions and their sources (Adapted from Steffen *et al.*, 2010), sea-level equivalent and inferred global ocean salinity change (0-1800m). Middle: an estimate of sea-ice coverage loss in the Beaufort Sea (Arctic) from Kwok & Cunningham (2010) and inferred global salinity change (0-200m). Lower: estimates of ocean-atmosphere-land fluxes on an annual timescale from Schanze *et al.* (2010) – these estimates balance in globally-integrated volumes within errors (not shown).

Freshwater source	Period	Volume loss (Gt = 1.09 km^3)	Sverdrups (10^6 m^3 s^{-1})	SLE (mm yr^{-1})	Inferred Salinity change
Glaciers and Ice-caps	1960-1990	~3000	0.000003	-	0.0002
Glaciers and Ice-caps	1990-2000	~2500	0.000009	-	0.0001
Glaciers and Ice-caps	2000-	~3000	0.000010	-	0.0002
Glaciers and Ice-caps (total)	1960-	~8500	0.000006	2	0.0005
Greenland	2005-	>1000	0.000007	1.4	0.0001
Antarctica	2005-	>500	0.000003	5.1	0.0000
TOTAL	**1960-**	**>10000**	**0.000007**	**-**	**0.0006**
Arctic sea-ice (Beaufort Sea)	2004-2008	~5800	0.000050	0	0.003
Arctic sea-ice (Beaufort Sea)	1993-2009	~900000 (area, km^2)	-	-	-
Global ocean evaporation	Annual mean	-	-13.04	-	-
Global ocean rainfall	Annual mean	-	+12.18	-	-
Global ocean terrestrial runoff	Annual mean	-	+1.25	-	-

Observed globally-averaged SLR over the 20th century is comprised of many components. These components include steric (both thermosteric and halosteric), and eustatic changes (mass changes: addition/subtraction of freshwater). Global SLR contributions for the second half of the 20th century have recently been updated by Church *et al.* (in prep) who attempt to close the sea-level and planetary energy budgets for this period in a self-consistent way. The observed SLR trend of 1.7±0.3 mm yr^{-1} comprises the following contributions over the 1970-2008 period: thermal expansion (47% of the total change; +0.8 mm yr^{-1}), terrestrial glaciers and ice caps (41%; +0.7 mm yr^{-1}), Greenland and Antarctica (24%; +0.4 mm yr^{-1}) and terrestrial storage (-12%; -0.2 mm yr^{-1}; Figure 4.1). These new estimates are supported by Dyurgerov & Meier (2005) who suggest a eustatic SLR of 0.3-0.45 mm yr^{-1} from glaciers and ice-caps have been recorded over the last 50-years, rising to 0.8 mm yr^{-1} over the last decade. The observed increasing trend in the last 20-years is reproduced by Shepherd & Wingham (2007), Velicogna (2009), Chen *et al.* (2010) and Sasgen *et al*. (2010) using updated techniques and observing platforms. These studies independently concluded that SLR is occurring at an increasing rate from the 20th and into the 21st century.

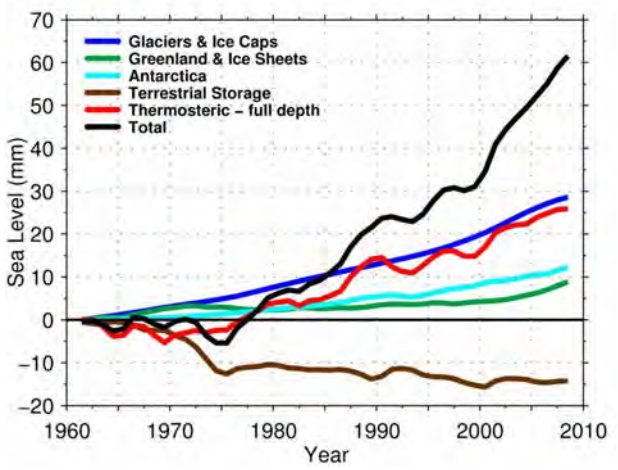

Figure 4.1. The best estimate of the global sea-level rise budget 1961-2008. Reproduced from Church *et al.* (in prep)

Thermal expansion is the largest single term in this updated global sea-level budget (47%), however steric changes in the global (and regional) oceans are also attributable to salinity changes on short and long timescales (e.g. Pattullo *et al.*, 1955; Tabata *et al.*, 1986; Maes, 1998; Sato *et al.*, 2000; Antonov *et al.*, 2002; Ishii *et al.*, 2006). Halosteric (salinity) changes have not been considered directly in the updated global SLR budget as expressed in Figure 4.1.

Unlike thermosteric SLR, halosteric SLR is much more complex to accurately diagnose, as it comprises freshwater (and salt) redistribution as well as freshwater addition (eustatic SLR). There is a need therefore to approach estimates of halosteric SLR cautiously, so as not to double count freshwater changes in sea-level budgets (e.g. Munk, 2003).

Eustatic SLR estimates have been made for the 20th and early 21st century, based on observed cryosphere changes, and more recently from satellite estimates of sea surface height and mass changes to ice sheets (e.g. Nerem *et al*., 1997; Shepherd & Wingham, 2007; Velicogna, 2009; Chen *et al*., 2010; Steffen *et al*., 2010; Sasgen *et al*., 2010). Contributions from terrestrial groundwater stores and cryospheric estimates (land-based ice, glaciers and ice-caps) affect both regional halosteric and total sea-level, adding freshwater mass to the total ocean mass (eustatic SLR). These freshwater contributions have a clear spatially varying footprint and are very regional in their short-term effects, with anomalies circulated throughout the global ocean on long timescales. What salinity changes have these freshwater additions to the global ocean caused?

Using observed estimates of global freshening, and after accounting for their estimate of (Arctic and Antarctic) sea-ice contributions, Wadhams & Munk (2004) suggest that a eustatic contribution of 220 km^3 yr^{-1} has occurred from terrestrial runoff, which implies a 0.6 mm yr^{-1} mean eustatic SLR for the period 1955-1995. More recent estimates, by Church *et al.* (in prep) suggest a total eustatic freshwater contribution of 0.95 mm yr^{-1} (45.6 mm) over 1961-2008 has occurred. If evenly mixed over the global ocean down to 1800m (the analysis depth of this study), salt conservation (4.1) allows salinity changes to be inferred for this 48-year period.

$$\overline{S} \times 1800m = (\overline{S} + \Delta S_{Global}) \times (1800m + 0.0456m)$$
$$\Delta S_{Global} = \frac{\overline{S} \times 1800m}{1800.0456m} - \overline{S}$$
$$\Delta S_{Global} \approx -0.0009 \qquad (4.1)$$

Where $\overline{S}$ is the mean ocean salinity derived from the analysis presented in Chapter 2 (34.6 PSS-78), and ΔS_{Global} is the integrated 0-1800m global salinity change 1961-2008. From their analysis the resolved depth-integrated global freshening yields -0.0009.

The expected change in global salinity of -0.0009 is not measurable given poor accuracy of historical instruments (0.02 PSS-78) and more limiting, sampling error of past change. Thus, measurements of globally average ocean salinity changes cannot be used to constrain eustatic contributions to SLR (Munk, 2003). However, *regionally*, terrestrial ice melt is likely to impact salinity and thus through the halosteric effect, sea-level patterns. As shown in Table 4.1, the inferred changes to E-P (and corresponding regional freshwater and salt budgets) of 4% over the past 50-years will dominate over cryospheric contributions for most of the global oceans. Regions proximate to melting ice sources, such as Antarctica and Greenland, may however see more dominant ice melt effects.

Recent estimates made by Kwok & Cunningham (2010) for the period 1993-2009 suggest multi-year Arctic sea-ice coverage has been reducing over this period, a reduction of around 50%, with a peak loss of 6300 km^3 over 2004-2008 (Table 4.1; single year losses peak in 2008). While melting of sea-ice contributes to regional halosteric patterns, it does not affect total sea-level (eustatic SLR) as it already contributes to the global oceans mass budget. If we consider this sea-ice melt for the Arctic Basin alone, and constrain this to the upper ocean (0-200m), and following the calculation presented in (4.1) a regional salinity change of -0.06 results, a value within currently measurable limits. If this freshwater contribution is considered globally (an unlikely scenario, considering ocean circulation timescales much greater than the 4 years over which their observations are available would be required to propagate the anomaly globally), a salinity anomaly of -0.003 would be recorded (assuming 0-200m). While small and considering a reduced ocean volume, these salinity changes are larger than (or if considered for 0-1800m: -0.0003; approximately equal to) the best eustatic contribution estimates to the global sea-level budget (0-1800m) described in (4.1) and Table 4.1. This serves to illustrate that contributions from sea-ice while not measurable in global mean salinity, could significantly contribute to regional anomalies, and as a consequence halosteric contributions to the total steric mean sea-level.

Antonov *et al.* (2002) suggested that salinity (halosteric contraction) in the Atlantic is of key importance in quantifying the total steric sea-level budget. Ignoring halosteric components when interpreting total steric change calculated from altimetric (satellite) observations can cause erroneous heat content change estimates, a result supported by Tabata *et al.* (1986), Maes (1998) and Sato *et al.* (2000).

In previous chapters large and coherent salinity changes were described for the global oceans from 1950-2000 (Chapter 2). Along with the companion analysis of ocean temperature change (free from observational biases associated with XBTs, more information below), these will now

be used to revisit the rates of total steric, thermosteric and halosteric SLR for this period. First, previously reported estimates of steric sea-level change will be described.

Past Estimates: Strengths and Weaknesses

Three key periods of analysis dominate the majority of past sea-level change studies. These include: the long-term budget (1950/60-), with most studies focussing primarily on the steric (ocean property changes) components (e.g. Antonov *et al.*, 2002; Antonov *et al.*, 2005; Levitus *et al.*, 2005b; Ishii *et al.*, 2006; Domingues *et al.*, 2008; Levitus *et al.*, 2009); the altimeter period (1980-), which allows direct estimates of rates and patterns of total (steric and eustatic components) sea surface height anomalies (e.g. Church *et al.*, 2004; Lombard *et al.*, 2005); and the Gravity Recovery and Climate Experiment (GRACE) period (2002-), which provides direct estimates of the Earth's gravity field to ascertain mass changes (eustatic sea-level contributions from the cryosphere) on monthly timescales (e.g. Shepherd & Wingham, 2007; Velicogna, 2009; Chen *et al*., 2010; Sasgen *et al.*, 2010).

Previous estimates of global mean multi-decadal SLR have been obtained from numerous sources, using varied analysis methods and techniques. Church *et al.* (2004) constructed a time history of past patterns of global sea level by combining the sparse global tide gauge network, reanalysis products and patterns of variability from satellite altimeter data. These data sources were merged to determine spatial patterns over 1993-2000, and these patterns were then extrapolated backwards in time. Sources of uncertainty and error include inadequate geographical distribution of tide gauges, particularly in the southern hemisphere, inadequate correction for gravitational effects (glacial isostatic adjustment [GIA] – Earth crustal effects where uplift and subsidence can confound in-situ tide gauge estimates relative to mean sea level) in gauge data, and a short altimetric record (<10-years) from which to reconstruct patterns of corresponding variability.

Many steric estimates have been based on subsurface ocean property changes (e.g. Antonov *et al.*, 2002; Antonov *et al.*, 2005; Levitus *et al.*, 2005b; Ishii *et al.*, 2006; Domingues *et al.*, 2008; Levitus *et al.*, 2009), primarily focussing on thermosteric effects as temperature profile data are far more numerous than salinity observations. A major source of uncertainty in past estimates is due to sampling errors due to poor data coverage in historical observations (Lyman & Johnson, 2008). Another major source of errors are the still poorly quantified biases with one of the historical observation platforms, eXpendable BathyThermographs (XBTs) which comprises around 70% of available historical profiles. A time varying bias in XBTs has confounded past attempts to close the thermosteric component of the global sea-level budget over the past 50-years (e.g. Gouretski & Koltermann, 2007; Wijffels *et al*., 2008). Lyman *et al*. (2010) show that the poor understanding of these biases dominates spread in current estimates of the evolution of global thermosteric SLR over the past decade.

Additionally, most previous global steric estimates have concentrated on the upper 0-700m (e.g. Domingues *et al.*, 2008; Ishii *et al.*, 2006; Antonov *et al.*, 2005; Levitus *et al.*, 2009) with the exception of a few deeper (0-3000m) studies (e.g. Antonov *et al.*, 2002; Levitus *et al.*, 2005b). Since the average depth of the ocean is close to 4000m, most steric assessments are missing a very large portion of the global ocean volume. Results from these studies are generally presented in globally-integrated estimates, with a high unresolved variance

associated with the regional patterns of change. New estimates of deep (3000m-) thermosteric contributions based on repeat deep ocean measurements made since the 1980s (Purkey & Johnson, 2010) show consistent and broad-scale near bottom warming, concentrated in abyssal pathways fed by Antarctic Bottom Water (AABW). These weak but detectable warming patterns are significant contributors to full depth global thermosteric change (13%; 0.09±0.06 mm yr^{-1} 1961-2008; Church *et al*., in prep).

The impact of poor historical observational coverage ensures that estimates of past change are sensitive to the methods used to fill gaps. Many past estimates of steric SLR used an optimal interpolation technique in order to deal with sparse temporal and spatial data coverage provided by the observational record (e.g. Antonov *et al.*, 2002; Antonov *et al.*, 2005; Levitus *et al.*, 2005b; Lombard *et al.*, 2005; Ishii *et al.*, 2006; Levitus *et al.*, 2009). Gille (2008) showed that assuming a zero anomaly in data-void regions when using optimal interpolation methods significantly biased change estimates low, particularly in the Southern Ocean. She concluded that the real thermosteric SLR is likely to have been significantly larger than previous estimates (which used this optimal interpolation technique). Lyman & Johnson (2008) reached similar conclusions, with their focus on temporal (and spatial) data coverage, and again concluded that techniques employing optimal interpolation with a zero initial guess, biases change estimates low.

Likely due to the even sparser coverage of salinity observations, there have been fewer studies concentrating on halosteric contributions to the long-term SLR budget. Of these, only two independent research groups have approached the question, with Ishii *et al.* (2006) focussing on 0-700m changes from 1945-2003, and Levitus *et al.* (2005b & Antonov *et al.*, 2002) focussing on 0-3000m for 1957-1996 (and 1957-1994 period respectively). Both used the optimal interpolation technique described above.

This study focuses on the long-term 50-year changes using new estimates of ocean property changes, in an attempt to provide more rigorous estimates of regionally and spatially varying steric contributions for the long-term. New estimates of salinity and temperature changes (Chapter 2) contrast with those above in the following way:

1. XBT data are not used and thus thermosteric change estimates are free from the uncertainty associated with poorly know biases in these data
2. Salinity and temperature data are mapped concurrently using the same methods and scale resolution so that directly comparable thermosteric and halosteric estimates are obtained
3. The parametric fit performed does not suffer from the low “zero initial guess” bias of previous optimal averaging studies – it essentially uses surrounding data in space and time to infill observational gaps (a better assumption, given that most global change signals are broad-scale; Chapter 2)

Some of the impacts of this different approach are evident when comparing raw temperature and salinity changes on single levels from that of previous studies which used optimal averaging (Figure 4.2).

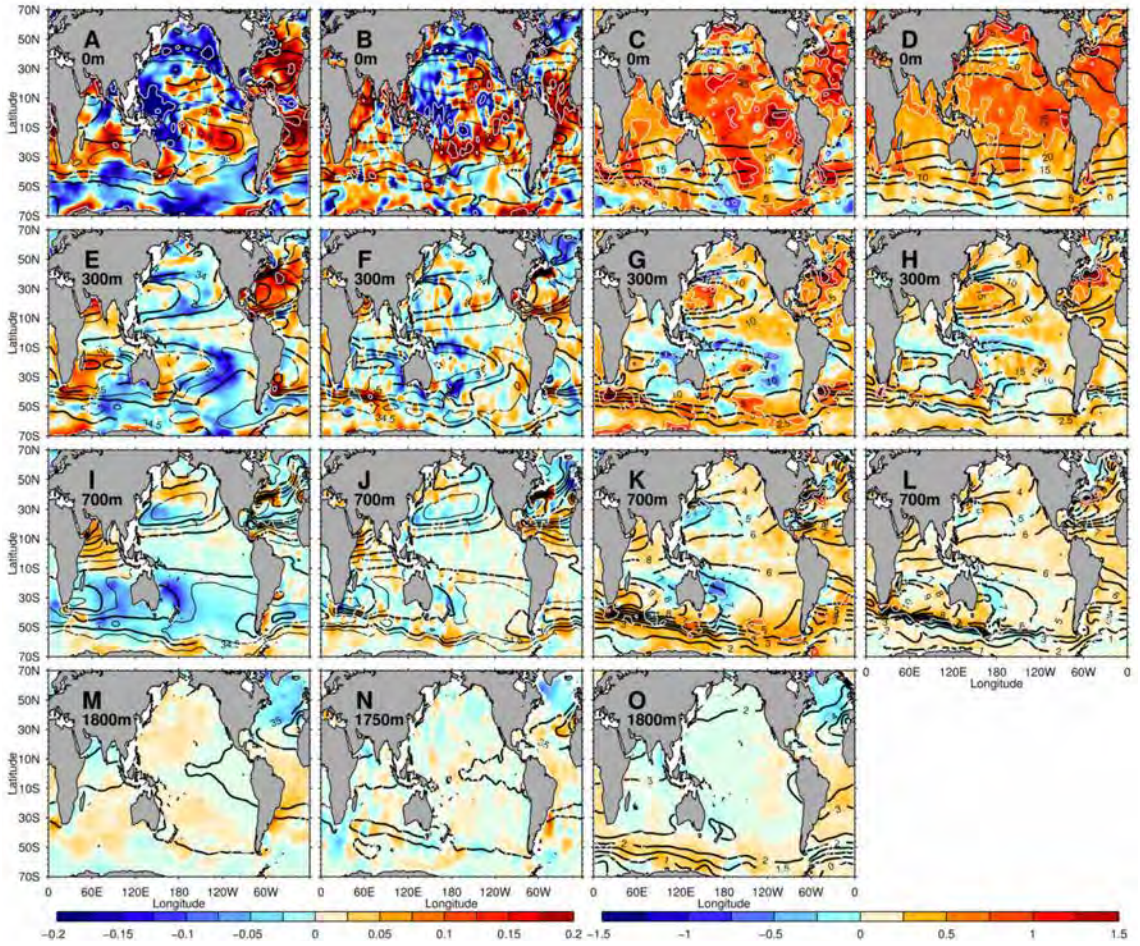

Figure 4.2. Observational change estimates at selected depth levels for salinity (as per Chapter 2 1950-2000: A, E, I, M) and the results of Boyer *et al.* (2005; 1955-1998: B, F, J, N) and temperature from Chapter 2 (1950-2000 not previously shown: C, G, K, O) and the results of Levitus *et al.* (2009; 1955-2009: D, H, L – only extend to 700m). For salinity changes climatological mean salinity is contoured in black (A & B: every 0.5, bold every 1 pss; E & F: every 0.025, bold every 0.5 pss; I & J: every 0.125, bold every 0.25 pss; M & N: bold every 0.125 pss) for temperature changes climatological mean temperature is contoured in black (C & D: bold every 5°; G & H: bold every 2.5°; K & L: bold every 1°; O: bold every 0.5°).

Salinity and temperature change estimates mostly agree in data-rich regions, however new results provide more coherent estimates of the broad-scale trends, particularly in data sparse regions. In this study, surface salinity largely represents an enhancement to mean climatological salinity patterns (Figure 4.2A). These spatial patterns are more difficult to ascertain in Figure 4.2B. Thorough descriptions of key salinity changes over 1950-2000 for the surface and subsurface are included in Chapter 2 & 3.

Broad-scale warming is apparent in the surface plots (Figure 4.2C & D), with area-weighted global integrals of +0.27°C (Levitus *et al.*, 2009; Figure 4.2D) and +0.49°C (this study; Figure 4.2C – See Chapter 3, Table 3.S3 for additional observed and modelled estimates). The broad-scale warming has a larger magnitude almost everywhere and is more spatially widespread in the Southern Ocean (Figure 4.2C vs D). It is interesting to note the cooling trend in the North Pacific subpolar gyre (40-50°N) apparent in both surface temperature estimates. This region expresses the largest magnitudes of change due to the Pacific Decadal Oscillation (PDO). The

PDO is a mode of long-term climate variability that shifts phases on inter-decadal timescales of 20-30 years (Mantua *et al.*, 1997), a time period long enough to influence the 1950-2000 trends.

Subsurface salinity change patterns do not appear to share much in common between the two studies. The broad-scale zonal patterns which express similarities with the geographical water mass distributions (Figure 4.2E, I, M) are largely absent in the result of Boyer *et al*. (2005; Figure 4.2 F, J, N). More detailed descriptions of salinity changes are included in Chapter 2.

Subsurface temperature changes appear to share more features in common with previous estimates than salinity changes. This study (Figure 4.2G & K) shows slightly larger warming magnitudes in the lower thermocline and Mode Waters, however features are broadly consistent between both analyses. The previously documented southward shift of the Antarctic Circumpolar Current (ACC; Gille, 2002; Alory *et al.*, 2007) is seen in both studies as a subsurface warming band following the ACC pathway (Figure 4.2G, H, K, L). However, the shift appears more circumpolar in nature in this study, with a more coherent warming present across the entire Southern Ocean (Figure 4.2G, K vs H, L). Persistent warming of the North Atlantic is also present in both analyses, with the magnitude and coherence of this warming trend decreasing at 700m and below.

Deep changes (1750-1800m) are weaker than in the upper ocean for both analyses; however there does appear to be a consistent pattern of increased salinity in the western South Atlantic off southern Brazil and Argentina, and a hint of warming. A consistent deep reaching freshening also appears to be present in the high latitude North Atlantic, with a more pervasive pattern resolved by this study (Figure 4.2M vs N). An apparent cooling anomaly appears to coincide with the freshening in the North Atlantic, and the southward shift of the deep ACC is also suggested south of 50°S (Figure 4.2O).

New Estimates of Steric Sea-level Change

The data sources, quality control and the method used to extract broad-scale patterns of change in salinity and temperature are described in detail in Chapter 2. From this analysis, mean climatological fields of salinity and temperature were available, along with the 1950-2000 linear trend estimates of *in-situ* change on both pressure and density grids for the global ocean. In order to ascertain halosteric (salinity) and thermosteric (temperature) components of the total steric (density) sea-level budget, it was necessary to calculate mean climatological steric height and then the changes due to salinity and temperature, together and then separately.

Mean climatological steric height was computed using mean fields of salinity and temperature for 1950-2000 as presented in Chapter 2 on pressure surfaces.

$$h_{steric} = \int_{p0}^{p1} \alpha(\overline{S}, \overline{T}, p) \qquad (4.2)$$

for (4.2) h_{steric} is the climatological dynamic height, obtained from using the 50-year mean $\overline{S}$ salinity and $\overline{T}$ temperature for selected p pressure surfaces, across the 2° longitude and 1° latitude grid of analysis, and α is the specific volume. Using the salinity and temperature anomaly fields for 1950-2000 we then calculate the halosteric and thermosteric anomalies from the climatological mean steric height, using the trapezoidal rule of depth integration for selected pressure levels.

$$\Delta h_{halosteric} = \int_{p0}^{p1} \alpha(\overline{S} + \Delta S, \overline{T}, p) - h_{steric}$$

$$\Delta h_{thermosteric} = \int_{p0}^{p1} \alpha(\overline{S}, \overline{T} + \Delta T, p) - h_{steric}$$

$$\Delta h_{steric} \cong \Delta h_{halosteric} + \Delta h_{thermosteric} \qquad (4.3)$$

In (4.3) ΔS is the salinity anomaly, ΔT is the temperature anomaly and $\Delta h_{halosteric}$ and $\Delta h_{thermosteric}$ are the salinity and temperature-driven changes to total steric height over 1950-2000. The arithmetic sum of $\Delta h_{halosteric}$ and $\Delta h_{thermosteric}$ is then approximately equal to the total steric height Δh_{steric} as non-linear effects are small.

In order to calculate basin or globally-integrated totals, an area-weighted mask is applied which ensures that polar contributions are appropriately down-weighted compared to equatorial contributions to the integrals.

Data from marginal seas are excluded (see Chapter 2 Figure 2.1), as historical coverage is poor and averaging issues across sea margins complex. The primary focus is chiefly on broad-scale open ocean changes. Regions poleward of 70° in both hemispheres were excluded, primarily due to poor data coverage. Vertically, sparse deep ocean coverage both historically and in modern times has ensured that large portions of the global ocean deeper than 1800m lack sufficient spatial or temporal data coverage for a meaningful broad-scale analysis. For spatial maps presented here we focus on changes down to 1800m.

These new results provide the only other complete long-term salinity and temperature analysis to Boyer *et al.* (2005; salinity 0-3000m), Levitus *et al.* (2009; temperature 0-3000m) and Ishii *et al.* (2006; salinity & temperature 0-700m), all of which use optimal averaging techniques and include XBT data in their thermosteric estimates. Comparisons to the zonally-integrated global salinity changes of Boyer *et al.* (2005) are made in Chapter 2 (Figure 2.6).

Thermosteric components of the sea-level budget are more commonly reported upon than halosteric effects, steric components will be presented separately in the following sections.

Global Steric Sea-level Change

Thermosteric

New estimates of globally-integrated thermosteric changes from 1950-2000 presented in this study agree well with most previous estimates. This confirms that the 50-year increase in upper ocean heat content is somewhat robust to the data and analysis methods used. Time histories of thermosteric sea level rise from 1950 to the present, for both 0-700m and 0-1800m depth are presented in Figure 4.3. The new linear trend estimates presented by this study agree well with Domingues *et al.* (2008) which considered the period 1950-2003 using new correction estimates for XBT biases. Their calculated thermosteric SLR estimate for this period is +0.52±0.08 mm yr^{-1}, with our new rate of +0.50±0.09 mm yr^{-1} agreeing within error bounds. For the deep component (0-1800m), the new estimate of +0.58±0.05 mm yr^{-1} agrees well with the Church *et al.* (in prep) rate of +0.59±0.16 mm yr^{-1} (1961-2008) though their estimate includes coverage between 700-3000m depth using linear scaling derived from previous estimates (Antonov *et al.*, 2005; Levitus *et al.*, 2005a). Quantitative comparisons to other estimates are provided in Table 4.2.

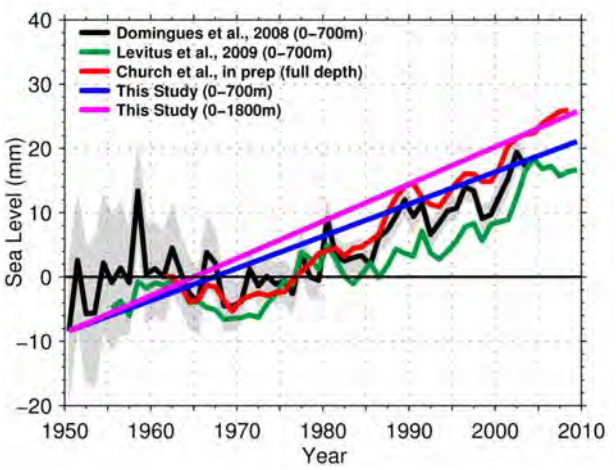

Figure 4.3. Observed globally-integrated thermosteric sea-level rise estimates 1950-2010. The Church *et al.* (in prep) full depth estimate uses linear scaling for the full depth global ocean.

The new, direct 700-1800m thermosteric estimate is consistent with previous independent analyses and validates the magnitude of other deeper (depth > 700m) observational estimates. This supports the scaling used in the SLR and energy budget approach of Church *et al.* (in prep; magenta this study 0-1800m vs red full depth).

Table 4.2. Observed estimates of thermosteric sea-level rise

Author	Period	Depth (metres)	Thermosteric (mm yr^{-1})
Antonov *et al.* (2005)	1955-2003	0-700	0.33±0.04
Ishii *et al.* (2006)	1955-2003	0-700	0.31±0.07
Domingues *et al.* (2008)	1961-2003	0-700	0.52±0.08
Levitus *et al.* (2009)	1955-2008	0-700	0.39
Church *et al.* (in prep)	1961-2008	0-700	0.52±0.06
This study	1950-2000	0-700	0.50±0.09
This study	1950-2000	0-1800	0.58±0.05
Antonov *et al.* (2005)	1957-1996	0-3000	0.40±0.05
This study	1950-2000	700-1800	0.08±0.03
Church *et al.* (in prep)	1961-2008	700-3000	0.07±0.1
Church *et al.* (in prep)	1961-2008	Full depth	0.68±0.13
Domingues *et al.* (2008)	1961-2003	700-	0.2±0.1
Purkey & Johnson (2010)	1980-2010	3000-	0.09±0.06

Values presented in Table 4.2 are largely representative of similar long-term (>40-years) trends, where the same rate of SLR has been observed in the thermosteric record. Of the shallow (0-700m) and deep (700m-) estimates presented above, the lowest trends are expressed by studies which used optimal interpolation to infill spatial and temporally sparse global ocean data. These studies: Antonov *et al.* (2005), Ishii *et al.* (2006) and Levitus *et al.* (2009); express SLR rates of around two-thirds of other best estimates (Domingues *et al.*, 2008; Church *et al.*, in prep) and the new independently analysed rates of this study.

It is interesting to note the differences in sea surface temperature trends reported by different analyses (Chapter 3, table 3.S3). Using available sea surface temperature data products to

form a point-wise linear trend over time and area-weighting these global surface warming trend estimates, provides a comparison to the estimates presented in this study. Some of these include HadSST2 (+0.37°C: 1950-2009 – scaled to represent 50yr^{-1} changes consistent with this study); ERRST_V3b (+0.31°C: 1950-2009); and Kaplan_V2 (+0.24°C: 1950-2009). Using ocean profile data, Levitus *et al.* (2009) obtain a warming estimate 1955-2009 of +0.25°C (scaled to represent 50yr^{-1}), which is much lower than the estimate from data analysed in Chapter 2 (+0.49°C) and the result of Wijffels *et al.* (in prep; +0.56°C) who use a similar method optimised to determine broad-scale temporal changes. Similarly, thermosteric SLR trend estimates from Levitus *et al.* (2009) also express smaller trends (Table 4.2), with some of the potential reasons for low-biases discussed above.

The regional pattern of steric changes is more relevant for understanding impacts than the global average. Spatial patterns for the thermosteric and halosteric contributions to total steric changes 1950-2000 will now be considered.

Regional Thermosteric and Halosteric Patterns of Sea-level Change

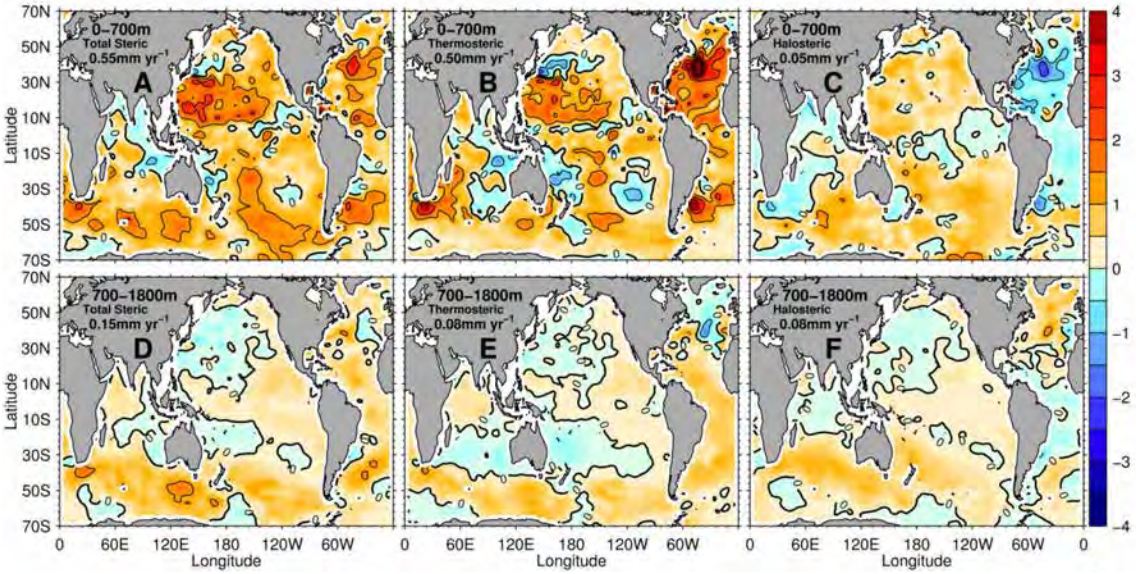

Figure 4.4. Observed 1950-2000 estimates of all steric sea-level rise contributions (mm yr^{-1}). Total steric for 0-700m (A) and 700-1800m (D), thermosteric 0-700m (B) and 700-1800m (E) and halosteric 0-700m (C) and 700-1800m (F). Steric changes are contoured in black every 1, bold contours represent -4, 0, 4 mm yr^{-1}.

Relative to other basins, strong thermosteric expansion is expressed in the upper Atlantic basin similar to the previous results of Antonov *et al.* (2002) and Ishii *et al.* (2006). In fact, in new estimates presented here, the Atlantic basin is warming more than three times stronger than the other basins in area-weighted mean to 1800m depth (more detailed comparisons are contained in Table 4.3).

Spatial maps of long-term thermosteric SLR are rarely published, with regional maps of SLR expressed over the altimeter time period more common. Long-term estimates presented by Antonov *et al.* (2002; their Figure 2: 0-3000m) and Ishii *et al.* (2006; their Figure 8: 0-700m) are

not directly comparable due to the inclusion of deeper components (700-3000m) in the Antonov *et al.* (2002) analysis. Both estimates however, tend to suggest a strong warming driven thermosteric expansion in the Atlantic south of 50°N. Opposing trends are found in the western Pacific, with a thermosteric contraction reported by Antonov *et al.* (2002), and expansion for Ishii *et al.* (2006). The inverse opposing patterns are expressed for the eastern Pacific basin respectively.

Table 4.3. Total steric, thermosteric and halosteric components of sea-level rise for 1950-2000, for global average and ocean basins 0-1800m depth. Units are mm yr^{-1}; Percentage values in parentheses indicate contribution to the total steric SLR. Positive thermosteric components indicate a temperature increase; positive halosteric components indicate a freshening.

Basin	Total steric	Thermosteric	Halosteric
Global	+0.71	+0.58 (82%)	+0.13 (18%)
Northern Hemisphere	+0.73	+0.76 (105%)	-0.03 (-5%)
Southern Hemisphere	+0.69	+0.46 (66%)	+0.24 (34%)
Pacific	+0.70	+0.38 (54%)	+0.32 (46%)
Atlantic	+0.85	+1.18 (139%)	-0.33 (-39%)
Indian	+0.56	+0.34 (60%)	+0.22 (40%)
North Pacific	+0.74	+0.50 (67%)	+0.24 (33%)
North Atlantic	+0.96	+1.38 (145%)	-0.43 (-45%)
North Indian	-0.22	+0.21 (-94%)	-0.43 (194%)
South Pacific	+0.66	+0.28 (42%)	+0.39 (58%)
South Atlantic	+0.75	+0.99 (131%)	-0.24 (-31%)
South Indian	+0.70	+0.36 (52%)	+0.34 (48%)
Southern Ocean (>40°S)	+1.02	+0.65 (64%)	+0.37 (36%)

Some clear features are prominent in regional spatial patterns of change (Figure 4.4). The dominance of the upper oceans in setting spatial patterns of change is clear, with 0-700m broad-scale spatial patterns very similar to their corresponding 0-1800m patterns (not shown). Steric changes, particularly the thermosteric component are surface-intensified; 0-200m (not shown) contains 60% (+0.35 mm yr^{-1}) of the 0-1800m globally-integrated area-weighted mean thermosteric signal.

Increased salinity in the Atlantic basin (Chapter 2) drives as a halosteric contraction across most of the upper 0-700m (Figure 4.4C). This contraction is more than offset by a thermosteric expansion, the strongest of the regional basin responses, particularly in the North Atlantic extending full depth (0-1800m). The deeper halosteric contribution (700-1800m; Figure 4.4F) suggests high latitude Atlantic freshening is expanding into the northern basin, a feature also expressed in Figure 4.2O. Complex interactions can be seen in the waters around Australia, with a deep cooling (contraction; Figure 4.2K, Figure 4.4E), partially offset by a Mode Water freshening (expansion; Figure 4.2I, Figure 4.4F) particularly south of Australia. Enhanced salinities, particularly in upper layers (Figure 4.2E, Figure 4.4C) are driving a clear halosteric contraction along the western boundary of the Indian Ocean, diminishing at depth. The southward shift of the ACC is most clearly evident in the total steric response (Figure 4.4D) south of Africa and Australia. A hint of western intensification is apparent, particularly in the Atlantic and Pacific basins, and may suggest circulation changes have occurred following a

Sverdrup response to wind changes as reported by Cai (2006). Interestingly, a pervasive (though patchy) halosteric contraction expressed by Antonov *et al.* (2002; their Figure 2), in the Pacific basin is not replicated in this study.

While halosteric contributions to the regional steric budget are normally assumed small, and insignificant to the total long-term steric sea-level budget (Church *et al.*, 2010), the new results presented in Figure 4.4 and Table 4.3 above suggest otherwise. On basin-scales, halosteric contributions can be 50% or larger of the total steric change (Table 4.3), and in regions of strong salinity changes (Chapter 2), it can be the leading term in the depth-integrated total (Figure 4.5).

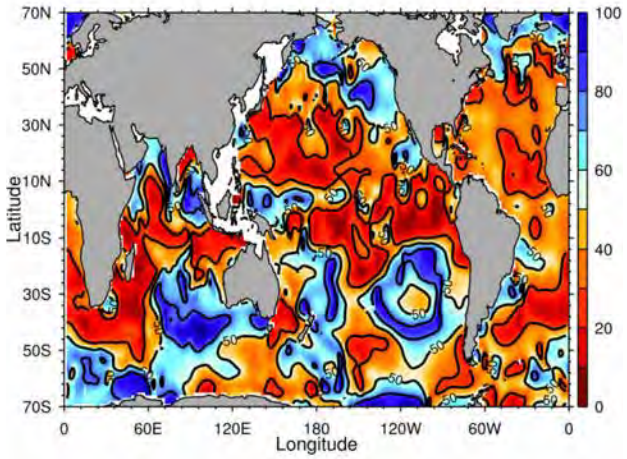

Figure 4.5. Observed 1950-2000 0-1800m halosteric contribution (%) to the depth-integrated steric total. Contours represent 25%, 50% (labelled) and 75% respectively. Regions in red are where thermosteric effects comprise more than 50% of the steric total, whereas regions of blue indicate salinity is the leading term in the steric total (>50% of total steric change).

In this analysis, 34% of the global ocean by area is dominated by depth-integrated halosteric effects (either by strong local freshening or enhanced salinity; Figure 4.5). This is the case even though most of the global ocean has undergone broad-scale warming over the corresponding period (Figure 4.2 & 4.4). Key regions dominated by freshening-driven halosteric expansion are where the Antarctic Mode Waters (South Pacific and South Indian waters around Australia) are prevalent in the thermocline, directly beneath the West Pacific and East Indian Warm Pools along the equator, and the high latitude subpolar North Atlantic and North Pacific. The vertical structure of salinity changes underlying the halosteric patterns can be complicated (Figure 4.5). For example, surface salinity increases overlying a deeper freshening beneath the South Pacific subtropical gyre (100-750m; Chapter 2 Figure 2.5B & 2.7D) along with a localised weak cooling, ensure that halosteric effects dominate in this region (Figure 4.5). In the South Indian, strong contrasts are also found depth integrated, with a surface salinity increase dominated by a very strong Mode Water freshening at depth (400-1500m; Chapter 2 Figure 2.9C & 2.7G). Figure 4.5 shows considerably more structure than the equivalent plot of Ishii *et al.* (2006; their Figure 9).

Zonal Averages for Thermosteric and Halosteric Sea-level Change

Levitus *et al.* (2005b) presented zonally-averaged linear trends in thermosteric and halosteric contributions for the global ocean 1955-2003 for 0-3000m (their Figure 1). Their results suggested that compensating halosteric and thermosteric changes were present in many latitude bands throughout the global ocean. They also undertook thermosteric analyses including and excluding additional XBT and Mechanical BathyThermograph (MBT) data which do not provide a corresponding salinity observation. They noted, that due to salinity observations only being available for 30% of the full temperature database, steric effects are most likely underestimated when this subset of data is used. The problems with XBTs as described in the previous section had not been discovered at the time of their assessment, and consequently biasing from this observational platform may have affected their results.

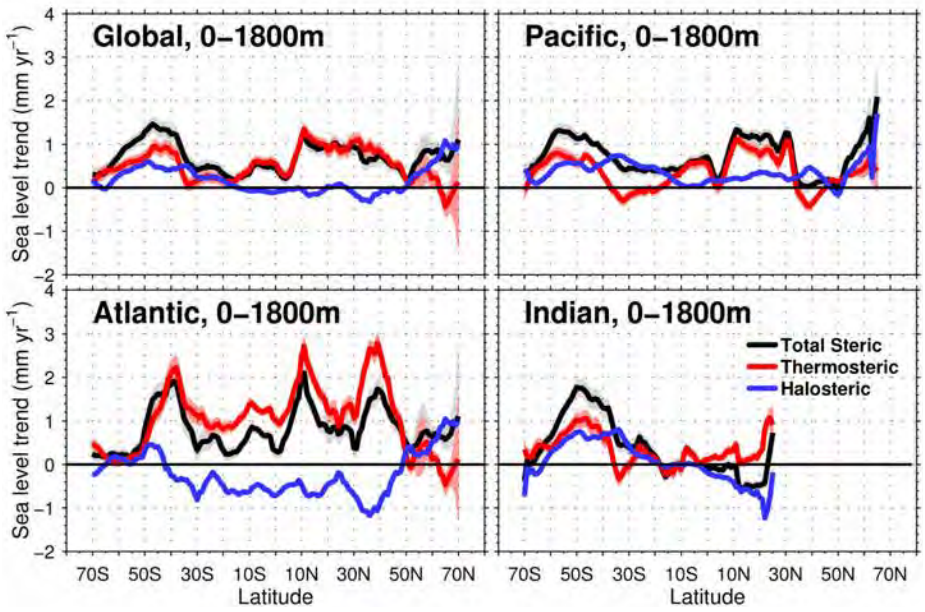

Figure 4.6. Observed 1950-2000 zonally integrated steric contributions for 0-1800m. Positive (negative) thermosteric effects express a temperature increased (decreased) local steric sea-level, and positive (negative) halosteric effects express a freshening-driven expansion (enhanced-saline contraction).

The new results presented here (Figure 4.6) agree qualitatively with Levitus *et al.* (2005b; their Figure 1), with a strong thermosteric expansion associated with warming expressed for each independent ocean basin. Similarities in the halosteric responses are also apparent, the Levitus *et al*. (2005b) result suggesting; an expansion for the entire Pacific basin, and a strong tropical and subtropical contraction, counteracting a strong thermosteric expansion in the Atlantic basin. The Indian basin however shares less similarity with the Levitus (2005b) result, the mode water freshening centred around 50°S and expressed as a clear expansion is not apparent in their analysis. However even though there is broad spatial agreement between results, the magnitudes of change are consistently larger, likely associated with the bias in the optimal average technique they employed.

Focussing on halosteric components, it is clear that a basin-scale contraction is occurring in the Atlantic from 40°S to 50°N associated with the strong enhanced salinity change expressed in

this basin (Figure 4.6). The Pacific however shows signs of a freshening driven expansion for almost the entire basin. Most high latitude southern basins experience a marked freshening-driven expansion, extending from 70°S to 10°S in the Pacific, and 60°S to 20°S in the Indian basins. Both these features are associated with the Antarctic Mode Water freshening patterns described above. The halosteric contraction of the northern Indian basin is also captured in this analysis, and extends southward to the equator. The strong contraction expressed throughout the Atlantic, and a weaker expansion in the Pacific tends to sum to zero in the global integral (Figure 4.6).

The large halosteric contractions are often offset by density compensating thermosteric expansion, particularly in the Atlantic. Most thermosteric components indicate a warming-driven expansion throughout the global ocean, aside from high latitude cooling (contraction) expressed in the North Pacific and Atlantic basins. In every basin, except the North Indian, a positive total steric effect is evident and is dominated by thermosteric expansion. The strong halosteric SLR near 30°S in the South Pacific and South Indian basin zonal means (Figure 4.6) is also clearly seen in Figure 4.5. It is clear from Figure 4.6 that the largest magnitudes of both halosteric and thermosteric components are recorded in the Atlantic basin.

Mechanisms Driving Steric Change

The new estimates of broad-scale warming and salinity changes (Chapter 2) over 1950-2000 will be used to investigate the mechanisms driving long-term steric changes. To obtain a simplified view of basin changes, zonal-mean depth changes are expressed in Figure 4.7.

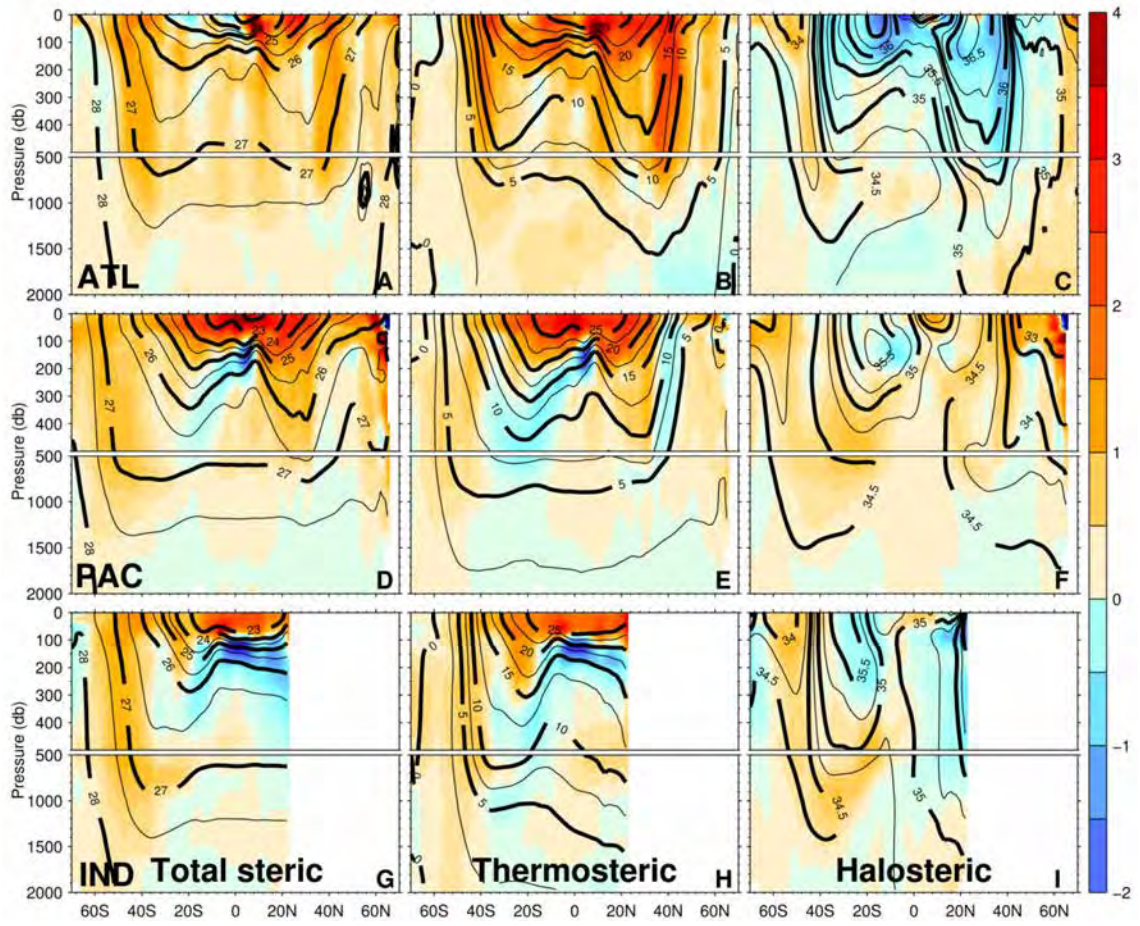

Figure 4.7. Observed 1950-2000 basin zonal mean total steric (A, D, G), thermosteric (B, E, H) and halosteric (C, F, I) contributions for the Atlantic, Pacific and Indian Ocean basins respectively in mm yr^{-1}. Left column, mean density 1950-2000 is contoured in black (every 0.5, bold every 1 kg m^{-3}), middle column, mean temperature (contoured every 2.5°, bold every 5°C) and right column, mean salinity (contoured every 0.25, bold every 0.5 pss). Halosteric totals present zonal-mean salinity changes for each of the basins, and provide the inverse of the pattern expressed in Chapter 2 (Figure 2.7A, D, G correspond to this chapter: Figure 4.7C, F, I), with freshening (blue; Chapter 2 Figure 2.7) expressing a halosteric expansion (yellow/orange) in Figure 4.7 above.

A common pattern of surface intensified warming largely confined above the main thermocline over 1950-2000 is clearly visible in the thermosteric components for each basin, particularly in the Pacific and Indian basins (Figure 4.7, centre column). Any positive (yellow to red) values indicate a warming, with the Atlantic showing the largest, deepest and broadest warming (Figure 4.7B) compared to the Pacific and Indian basins (Figure 4.7E & H respectively). All subtropical gyre bowls suggest a deepening of isopycnals has occurred in both hemispheres (Figure 4.7; Chapter 2 Figure 2.7). A deepening of isopycnals in the northern hemisphere Atlantic and Pacific, suggests broad-scale warming is penetrating into the ocean interior driven

by the subduction by the ocean circulation of the heating from above (Figure 4.7B, E, H) in agreement with the results of Palmer & Haines (2009). The south Indian subtropical gyre appears to indicate a deepening of isopycnals (Figure 4.7H), equivalent in magnitude to the northern responses in other basins, and the strongest of the southern basin responses. These results show that on shallow pressure surfaces a broad-scale density decrease has occurred.

Northern subtropical gyres appear to have broadened northwards, with a shift apparent in the Atlantic and Pacific. This feature is clearly evident in the thermosteric change (Figure 4.7B, E) and strongly reflected in the total steric changes (Figure 4.7A, D). The strength of the thermosteric (halosteric) response reflects the climatological mean horizontal temperature (salinity) gradient. This correspondence is stronger in the North Atlantic than in the North Pacific. Southern subtropical gyres have shifted south, visible in the thermosteric and total steric components for the Pacific and Indian basins on the equatorward side of the gyre bowls (20°S -> 25°S). The cooling anomaly, which has a maximum just off the equator between 100-200m in the Pacific and Indian basins (Figure 4.7E, H) suggests a southward shift, rather than a broadening has occurred. This result agrees with the reported southward shift of the ACC over a similar time period (Gille, 2002; Alory *et al.*, 2007).

In all Southern Ocean subduction zones (~30°-50°S) isopycnal migration-driven freshening (Chapter 2, Figure 2.9) has occurred. It is clearly visible as a halosteric expansion following the mean subduction pathway along the vertical contours of mean temperature and salinity. As described in Chapter 2, the complexity of temperature and salinity changes over this time period make attribution of change to specific processes difficult, as surface E-P changes along with isopycnal outcrop migration is occurring concurrently. However, this freshening anomaly which follows the mean circulation pathways does appear clearly for all basins (Figure 4.7C, F, I).

Broad-scale halosteric responses have also been found in this analysis, with a dominant contraction in the Atlantic upper 500m and expansion in the upper 1000m for the Pacific. For the Atlantic, in both southern and northern hemispheres, the halosteric contraction (0-1800m) is counteracting around 30% of the strong thermosteric expansion (Table 4.3). Understanding the dynamics of these changes, and why the strongest steric responses are expressed in the Atlantic is a key question. One explanation is that the strong halosteric response, in the Atlantic, is strongly tied to the horizontal gradient of mean salinity found at 40°S and 40°N, regions where strong compensating thermosteric and halosteric changes are found. In the Atlantic, a very steep ~2 (pss) gradient is apparent at the southern and northern boundaries of the subtropical gyres (Figure 4.7C), much stronger than that in the Pacific (Figure 4.7F). This strong salinity gradient means that an equivalent vertical (or horizontal) shift of an isopycnal will lead to much larger halosteric (salinity) anomalies being recorded in the Atlantic than in the Pacific, when viewed on pressure levels. While density-compensating thermosteric and halosteric responses are important, we suggest that the mean climatological gradients are a key reason why much larger change magnitudes in the Atlantic are found.

Discussion

This study has emphasised the importance of halosteric (salinity) effects in long-term regional SLR. On basin-scales, halosteric contributions to the steric total can be 50% or larger (Table 4.3) of total steric change. Depth-integrated halosteric contributions can locally be the leading term in the total steric change (Figure 4.5 – 34% of ocean area is dominated by halosteric effects).The new estimates of change presented here are more spatially coherent and interpretable, and express larger change magnitudes than previous estimates. The coherent nature of the spatial changes encourages confidence in the regional patterns of change, with the broad basin-scale changes (freshening Pacific, increasing salinity in Atlantic) suggested by many other studies (e.g. Boyer *et al.*, 2005; Levitus *et al.*, 2005b; Ishii *et al.*, 2006).

While regionally halosteric components can be a significant contributor to the steric total, halosteric contributions to the total global long-term steric sea-level budget have previously been considered insignificant (Church *et al.*, 2010). While this must be true in globally-integrated totals (aside from small eustatic contributions (Table 4.1) the system is closed and regional halosteric contributions must cancel in the global mean), it may not be true in regional totals. In the depth integrated global analysis presented here, errors remain due to incomplete data coverage and the unobserved regions which include the deep ocean (>1800m), high latitude (>70°) and marginal seas. There is more certainty in regional estimates however, and the 4% inferred change to E-P (Chapter 3) and its associated changes to regional E-P fluxes may drive strong regional halosteric responses. Halosteric SLR as expected from inferred E-P changes are expressed in the Atlantic (halosteric contraction) and Pacific (halosteric expansion) Oceans. For this reason, we would strongly suggest regional halosteric effects should be considered in future budget studies of long-term steric SLR. The results presented in Table 4.2 quantify these effects, with the Atlantic total steric SLR (0-1800m) suppressed by 39% (-0.33 mm yr^{-1}), the North Atlantic by 44% (-0.43 mm yr^{-1}) and 31% for the South Atlantic (-0.24 mm yr^{-1}). If not accounted for, halosteric effects could lead to an underestimate of heat content changes being derived from direct altimetric measurements of sea surface height (SLR).

This new observational estimate of steric SLR provides a coherent and consistent benchmark of 20th century ocean change through which both Coupled Model Intercomparison Project Phase 3 (CMIP3) 20th century (20C3M) and 21st century future scenarios run under the Intergovernmental Panel on Climate Change (IPCC) Special Report Emissions Scenarios (SRES) can be compared.

So how do these new observed estimates compare in spatial patterns and magnitudes to modelling studies of the global ocean? Pardaens *et al.* (2011) undertook an analysis of 13 coupled climate models from the CMIP3 suite, which were forced with the SRES A1B scenario into the 21st century. Accounting for climate drift in these models (see Chapter 3), they examined total (steric and eustatic), total steric and the halosteric and thermosteric contributions using an ensemble mean approach for the 13 models. Their results, comparing 20-year means of 2080-2099 (future) and 1980-1999 (present) are presented in Figure 4.8. Two more in depth studies of long-term SLR using a single model analysis was undertaken by Yin *et al.* (2010) and Landerer *et al*. (2007) with their conclusions agreeing broadly with the ensemble mean results presented by Pardaens *et al.* (2011).

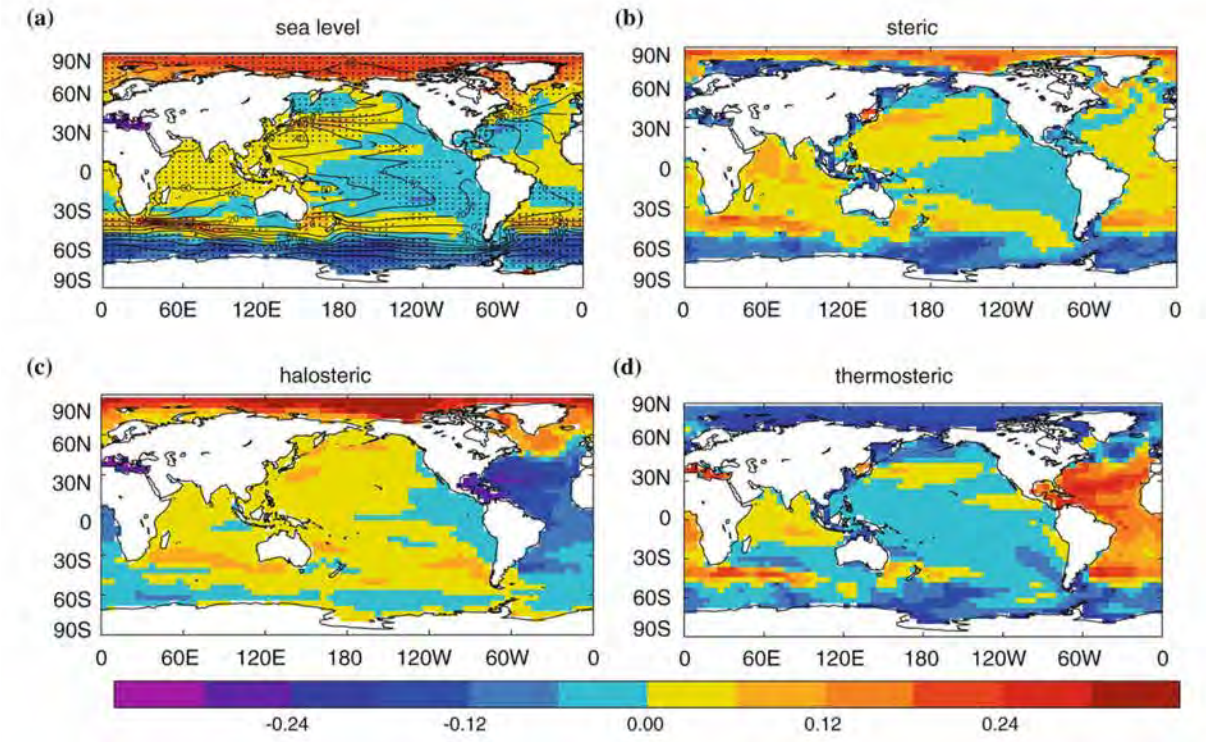

Figure 4.8. 21st century projected total and steric changes as captured by an ensemble average of 13 CMIP3 models. Fields represent the anomaly from the global mean between the periods 2080-2099 minus 1980-1999 in units of metres for (A) total sea-level (B) total steric (C) halosteric and (D) thermosteric reproduced from Pardaens *et al.* (2011).

As these results express the 13 model ensemble mean response, quantitatively comparing these to the new 1950-2000 observed estimates is not directly possible, however a comparison between the clear spatial patterns from models and observations will now be undertaken. Figure 4.9 contains the 1950-2000 observed equivalent plots to Figure 4.8 above.

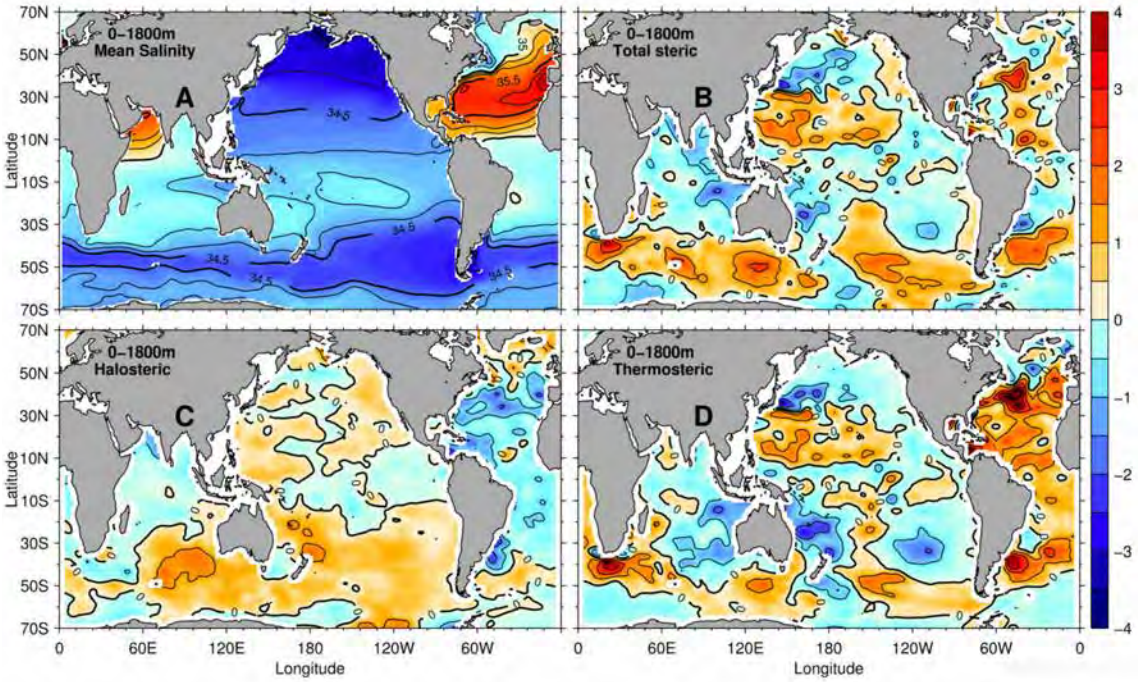

Figure 4.9. Observed 1950-2000 steric sea-level changes, following Pardaens *et al.* (2011) fields represent the anomaly from the global mean for (B) total steric (C) halosteric (D) thermosteric and (A) represents the 0-1800m vertical mean salinity. Steric changes are contoured in black (every 1, bold contours represent -4, 0, 4 mm yr^{-1}). For (A) climatological mean salinity is contoured in black every 0.125, bold every 0.5 pss. Units of steric sea-level changes is mm yr^{-1}; climatological mean salinity in pss.

While not directly quantitatively comparable, a remarkable broad-scale spatial similarity is apparent between 20th century observed (Figure 4.9) and 21st century modelled results (Figure 4.8). The thermosteric warming pattern expressed in the models shows a marked warming response in the entire subtropical Atlantic basin extending approximately from 50°S to 50°N (Figure 4.8D). This feature is captured almost identically in the equivalent observational estimate (Figure 4.9D). The thermosteric contraction poleward of 50° in both hemispheres in also seen in both estimates. In the Southern Hemisphere, however, this contraction is circumpolar in observations, and patchy in models. In the North Pacific the modelled contraction extends much closer to the equator than observed. Largely, the Pacific basin is experiencing a slower thermosteric expansion than the global mean, a feature consistent between observations (Figure 4.9D) and models (Figure 4.8D). Patterns expressed in the Indian basin seem not to agree. However, the southward shift of the ACC, and associated thermosteric expansion stands out clearly in this basin also (Figure 4.8D vs Figure 4.9D).

Halosteric changes are also similar between the observational estimates and CMIP3 projections. In the Atlantic, strong halosteric contraction (enhanced salinity) is occurring in the models (Figure 4.8C) with this feature extending from 50°N southward. Largely, observations (Figure 4.9C) agree, with maxima around 40°N and 30-40°S also captured by observations. Models express a weak halosteric expansion (freshening) for most of the Pacific and Indian basins (Figure 4.8C), with corresponding weak freshening pervading a large portion of the observed North and South Pacific and southeast Indian basin (Figure 4.9C).

The compensating nature of the steric responses in the Atlantic is clearly evident (Figure 4.8B), agreeing well with observations (Figure 4.9B), and also suggesting a western intensification of SLR is present (e.g. Cai, 2006). The North Pacific total steric expansion is similar in both models (Figure 4.8B) and observations (Figure 4.9B), except for the Indian Ocean. In the models, steric changes account for most of the change in total sea-level between 50°S and 50°N (Figure 4.8A).

As discussed in Chapter 3, observed surface mean salinity pattern amplification has occurred over the 1950-2000 period. This pattern amplification is also captured in strongly forced (SRES) models of projected 21st century climate (Chapter 3); however these express a weaker rate of change than do ocean observations. This mean pattern amplification is also apparent in 0-1800m depth-integrated salinity, with the broad-scale salinity pattern expressed in Figure 4.9A largely replicated in the broad-scale halosteric pattern of Figure 4.9C (regions of high salinity; red and light blue (Figure 4.9A) correspond broadly with regions of halosteric contraction; blue (Figure 4.9C)).

Summary and Future Directions

Robust multi-decadal linear trends describing global and spatially consistent patterns of halosteric and thermosteric SLR have been described for the period 1950-2000. These changes largely report a broad-scale warming and amplification to the global water cycle (Chapters 2 & 3) expressed in ocean salinity change. The techniques employed in this analysis are optimised to extract the broad-scale, long-term multi-decadal linear trends, with a key focus to reduce seasonal, eddy and sampling biases which can reduce signal to noise ratios in resolved trend estimates. These new change estimates do not suffer from the low-bias problems of previous analyses (e.g. Gille, 2008; Lyman & Johnson, 2008), or suffer from observational (XBT) platform biases (e.g. Wijffels *et al.*, 2008; Lyman *et al.*, 2010). Concurrent temperature and salinity analyses "independently" suggest consistent broad-scale changes are robust within this analysis.

The globally-integrated 0-700m thermosteric analysis agrees within error estimates of the best current data-corrected estimates of long-term thermosteric SLR, using the highest quality data which is unaffected by any currently known biases, and provide new spatial patterns of change. New deep (700-1800m) long-term thermosteric SLR rates also agree, and express coherent spatial patterns of change; a deep ocean warming (particularly in the Atlantic basin), a southerly shift in the ACC in the south Pacific and Indian basins, and small changes elsewhere.

New estimates of long-term halosteric components to the total SLR budget show this component of regional change cannot be excluded when attempting to account for long-term regional sea-level change. Atlantic thermosteric expansion (warming; the largest in any basin) is directly offset by halosteric contraction (enhanced salinity). The large magnitudes reported for this basin are linked to the strong mean climatological gradients in salinity, which are the strongest gradients in any basin. The spatial patterns from these estimates agree well with modelled estimates of future changes in the 21st century. Depth-integrated changes (Figure 4.9) reflect an enhancement to mean salinity contrasts, providing agreement with the surface (models versus observation) comparison presented in Chapter 3, and the model-based sea-level results of Pardaens *et al.* (2011), Yin *et al.* (2010) and Landerer *et al*. (2007). These changes are most closely represented in the strong greenhouse gas forcing experiments using the SRES scenarios for 21st century future climate, which simulate remarkably well most broad-scale features presented in the 1950-2000 observational estimates. This strongly suggests that change patterns reported for the past 50-years are driven by anthropogenic greenhouse gas (GHG) forcing and its associated broad-scale warming.

This new observational analysis provides a globally consistent and stringent target for coupled modelling systems that are being developed and used to project future climate. As reported in Chapter 3, these modelling systems tend to underestimate surface salinity changes when compared to new surface estimates of 20th century water cycle changes captured by global ocean salinity. It would be useful, using the full-depth modelled ocean to determine the rates at which modelling systems are responding to greenhouse gas forcing, and quantitatively compare these to the new rates of SLR expressed by this analysis. We would hope that modelling systems are providing us with robust estimates of global ocean responses to change, and that future projections of climate change are not overly conservative in their magnitudes.

References

Alory, G., S. Wijffels and G. Meyers (2007) Observed temperature trends in the Indian Ocean over 1960-1999 and associated mechanisms. *Geophysical Research Letters*, **34**, L02606. doi: 10.1029/2006GL028044

Antonov, J.I, S. Levitus and T.P. Boyer (2002) Steric sea-level variations during 1957-1994: The importance of salinity. *Journal of Geophysical Research*, **107** (C12), 8013. doi: 10.1029/2001JC000964

Antonov, J.I., S. Levitus and T.P. Boyer (2005) Thermosteric sea level rise, 1955-2003. *Geophysical Research Letters*, **32**, L12602. doi: 10.1029/2005GL023112

Boyer, T.P., S. Levitus, J.I. Antonov, R.A. Locarnini and H.E. Garcia (2005) Linear trends in salinity for the World Ocean, 1955-1998. *Geophysical Research Letters*, **32**, L01604. doi: 10.1029/2004GL021791

Cai, W. (2006) Antarctic ozone depletion causes an intensification of the Southern Ocean super-gyre circulation. *Geophysical Research Letters*, **33**, L03712. doi: 10.1029/2005GL024911

Chen, J.L., C.R. Wilson, D. Blankenship and B.D. Tapley (2010) Accelerated Antarctic ice loss from satellite gravity measurements. *Nature Geoscience*, **2**, pp 859-862. doi: 10.1038/NGEO694

Church, J.A., N.J. White, R. Coleman, K. Lambeck and J. Mitrovica (2004) Estimates of the Regional Distribution of Sea Level Rise over the 1950-2000 Period. *Journal of Climate*, **17**, pp 2609-2625. doi: 10.1175/1520-0442(2004)017<2609:EOTRDO>2.0.CO;2

Church, J.A., D. Roemmich, C.M. Domingues, J.K. Willis, N.J. White, J.E. Gilson, D. Stammer, A. Köhl, D.P. Chambers, F.W. Landerer, J. Marotzke, J.M. Gregory, T. Suzuki, A. Cazenave and P. Le Traon (2010) Ocean Temperature and Salinity Contributions to Global and Regional Sea-Level Change. In *Understanding Sea-Level Rise and Variability*, Church, J.A., P.L. Woodworth, T. Aarup and W.S. Wilson (Eds) Wiley-Blackwell, Oxford, U.K. pp 143-176

Church, J.A., N.J. White, L.F. Konikow, C.M. Domingues, J.G. Cogley, E. Rignot, J.M. Gregory, M.R. van den Broeke, A. Monaghan and I. Velicogna (in prep) The Earth's sea-level and energy budgets from 1961 to 2008.

Domingues, C.M., J.A. Church, N.J. White, P.J. Gleckler, S.E. Wijffels, P.M. Barker and J.R. Dunn (2008) Improved estimates of upper-ocean warming and multi-decadal sea-level rise. *Nature*, **453**, pp 1090-1093. doi: 10.1038/nature07080

Dyurgerov, M.B. and Meier, M.F. (2005) Glaciers and the Changing Earth System: a 2004 Snapshot. Occasional Paper No. 58. Institute of Arctic and Alpine Research, University of Colorado, Boulder, CO. Available online: http://instaar.colorado.edu/other/occ_papers.html

Gille, S.T. (2002) Warming of the Southern Ocean Since the 1950s. *Science*, **295**, pp 1275-1277. doi: 10.1126/science.1065863

Gille, S. (2008) Decadal-Scale Temperature Trends in the Southern Hemisphere Ocean. *Journal of Climate*, **21**, pp 4749-4765. doi: 10.1175/2008JCLI2131.1

Gouretski, V. and K.P. Koltermann (2007) How much is the ocean really warming? *Geophysical Research Letters*, **34**, L01610. doi: 10.1029/2006GL027834

Harvey, N. and B. Caton (2003) Coastal Management in Australia. Oxford University Press, Melbourne, 342 pp

Hinrichsen, D. (1995) Coasts in Crisis: Coasts and the Population Bomb. *American Association for the Advancement of Science (AAAS)*. Available online: http://www.aaas.org/international/ehn/fisheries/hinrichs.htm

IPCC (2010) Workshop Report of the Intergovernmental Panel on Climate Change Workshop on Sea Level Rise and Ice Sheet Instabilities. Stocker, T.F., D. Qin, G.-K. Plattner, M. Tignor, S. Allen and P.M. Midgley (Eds.). IPCC Working Group I Technical Support Unit, University of Bern, Bern, Switzerland, 227 pp. Available online: http://www.ipcc-wg1.unibe.ch/publications/supportingmaterial/SLW_WorkshopReport.pdf

Ishii, M., M. Kimoto, K. Sakamoto and S. Iwasaki (2006) Steric Sea Level Changes Estimated from Historical Ocean Subsurface Temperature and Salinity Analyses. *Journal of Oceanography*, **62**, pp 155-170

Kwok, R. and G.F. Cunningham (2010) Contribution of melt in the Beaufort Sea to the decline in Arctic multiyear sea ice coverage: 1993-2009. *Geophysical Research Letters*, **37**, L20501. doi: 10.1029/2010GL044678

Landerer, F.W., J.H. Jungclaus and J. Marotzke (2007) Regional Dynamic and Steric Sea-level Change in Response to the IPCC-A1B Scenario. *Journal of Climate*, **37**, pp 296-312. doi: 10.1175/JPO3013.1

Levitus, S., J.I. Antonov, T.P. Boyer, H.E. Garcia and R.A. Locarnini (2005a) Warming of the world ocean, 1955-2003. *Geophysical Research Letters*, **32**, L02604. doi: 10.1029/2004GL021592

Levitus, S., J.I. Antonov, T.P. Boyer, H.E. Garcia and R.A. Locarnini (2005b) Linear trends of zonally averaged thermosteric, halosteric, and total steric sea-level for individual ocean basins and the world ocean, (1955-1959)-(1994-1998). *Geophysical Research Letters*, **32**, L16601. doi: 10.1029/2005GL023761

Levitus, S. J.I. Antonov, T.P. Boyer, R.A. Locarnini, H.E. Garcia and A.V Mishonov (2009) Global ocean heat content 1955-2008 in light of recently revealed instrumentation problems. *Geophysical Research Letters*, **36**, L070608. doi: 10.1029/2008GL037155

Lombard, A., A. Cazenaze, P. Le Traon and M. Ishii (2005) Contribution of thermal expansion to present-day sea-level change revisited. *Global and Planetary Change*, **47**, pp 1-16. doi: 10.1016/j.gloplacha.2004.11.016

Lyman, J.M., S.A. Good, V.V. Gouretski, M. Ishii, G.C. Johnson, M.D. Palmer, D.M. Smith and J.K. Willis (2010) Robust warming of the global upper ocean. *Nature*, **465**, pp 334-337. doi: 10.1038/nature09043

Lyman, J.M. and G.C. Johnson (2008) Estimating Annual Global Upper-Ocean Heat Content Anomalies despite Irregular In Situ Ocean Sampling. *Journal of Climate*, **21**, pp 5629-5641. doi: 10.1175/2008JCLI2259.1

Maes, C. (1998) Estimating the influence of salinity on sea level anomaly in the ocean. *Geophysical Research Letters*, **25**, 19. doi: 10.1029/98GL02758

Mantua, N.J., S.R. Hare, Y. Zhang, J.M. Wallace and R.C. Francis (1997) A Pacific Interdecadal Climate Oscillation with Impacts on Salmon Production. *Bulletin of the American Meteorological Society*, **78**, pp 1069-1079. doi: 10.1175/1520-0477(1997)078<1069:APICOW>2.0.CO;2

Munk, W. (2003) Ocean Freshening, Sea-level Rising. *Science*, **300**, pp 2041-2043. doi: 10.1126/science.1085534

Nerem, R.S., B.J. Haines, J. Hendricks, J.F. Minster, G.T. Mitchum and W.B. White (1997) Improved determination of global mean sea level variations using TOPEX/POSEIDON altimeter data. *Geophysical Research Letters*, **24** (11), pp 1331-1334. doi: 10.1029/97GL01288

Nicholls, R.J., P.P. Wong, V.R. Burkett, J.O. Codignotto, J.E. Hay, R.F. McLean, S. Ragoonaden and C.D. Woodroffe (2007) Coastal systems and low-lying areas. In *Climate Change 2007: Impacts, Adaptation and Vulnerability. Contribution of Working Group II to the Fourth Assessment Report of the Intergovernmental Panel on Climate Change*, M.L. Parry, O.F. Canziani, J.P. Palutikof, P.J. van der Linden and C.E. Hanson (Eds) Cambridge University Press, Cambridge, U.K. pp 315-356

Palmer, M.D. and K. Haines (2009) Estimating Oceanic Heat Content Change Using Isotherms. *Journal of Climate*, **22**, pp 4953-4969. doi: 10.1175/2009JCLI2823.1

Pardaens, A.K., J.M. Gregory and J.A. Lowe (2011) A model study of factors influencing projected changes in regional sea-level over the twenty-first century. *Climate Dynamics*, **36**, pp 2015-2033. doi: 10.1007/s00382-009-0738-x

Pattullo, J. W. Munk, R. Revelle and E. Strong (1955) The Seasonal Oscillation in Sea Level. *Journal of Marine Research*, **14**, pp 88-156

Purkey, S.G. and G.C. Johnson (2010) Warming of Global Abyssal and Deep Southern Ocean Waters Between the 1990s and 2000s: Contributions to Global Heat and Sea Level Rise Budgets. *Journal of Climate*, **26**, pp 6336-6351. doi: 10.1175/2010JCLI3682.1

Sasgen, I., Z. Martinec and J. Bamber (2010) Combined GRACE and InSAR estimate of West Antarctic ice mass loss. *Journal of Geophysical Research*, **115**, F04010. doi: 10.1029/2009JF001525

Sato, O.T., P.S. Polito and W.T. Liu (2000) Importance of salinity measurements in the heat storage estimation from TOPEX/POSEIDON. *Geophysical Research Letters*, **27**, 4. doi: 10.1029/1999GL011003

Schanze, J.J., R.W. Schmitt and L.L. Yu (2010) The Global Oceanic Freshwater Cycle: A Best-Estimate Quantification. *Journal of Marine Research*, **68**, pp 569-595. doi: 10.1357/002224010794657164

Shepherd, A. and D. Wingham (2007) Recent Sea-Level Contributions of the Antarctic and Greenland Ice Sheets. *Science*, **315**, pp 1527-1532. doi: 10.1126/science.1136776

Steffen, K., R.H. Thomas, E. Rignot, J.G. Cogley, M.B. Dyurgerov, S.C.B. Raper, P. Huybrechts and E. Hanna (2010) Cryospheric Contributions to Sea-Level Rise and Variability. In *Understanding Sea-Level Rise and Variability*, Church, J.A., P.L. Woodworth, T. Aarup and W.S. Wilson (Eds) Wiley-Blackwell, Oxford, U.K. pp 178-225

Tabata, S., B. Thomas and D. Ramsen (1986) Annual and Interannual Variability of Steric Sea Level along Line P in the Northeast Pacific Ocean. *Journal of Physical Oceanography*, **16**, pp 1378-1398. doi: 10.1175/1520-0485(1986)016<1378:AAIVOS>2.0.CO;2

Tomczak, M. and J.S. Godfrey (1994) Regional Oceanography: An Introduction. Pergamon Press, Oxford OX3 0BW, U.K. 422pp

Trenberth, K.E., P.D. Jones, P. Ambenje, R. Bojariu, D. Easterling, A. Klein Tank, D. Parker, F. Rahimzadeh, J.A. Renwick, M. Rusticucci, B. Soden and P. Zhai (2007) Observations: Surface and Atmospheric Climate Change. In *Climate Change 2007: The Physical Science Basis. Contribution of Working Group I to the Fourth Assessment Report of the Intergovernmental Panel on Climate Change*, S. Solomon, D. Qin, M. Manning, Z. Chen, M. Marquis, K.B. Averyt, M. Tignor and H.L. Miller (Eds) Cambridge University Press, Cambridge, U.K. pp 235-335

Wadhams, P. and W. Munk (2004) Ocean freshening, sea level rising, sea ice melting. *Geophysical Research Letters*, **31**, L11311. doi: 10.1029/2004GL020039

Velicogna, I. (2009) Increasing rates of ice mass loss from the Greenland and Antarctic ice sheets revealed by GRACE. *Geophysical Research Letters*, **36**, L19503. doi: 10.1029/2009GL040222

Wijffels, S.E. (2001) Ocean Transport of Fresh Water. In *Ocean Circulation and Climate: Observing and Modelling the Global Ocean*, G. Siedler, J. Church and J. Gould (Eds) Academic Press, London, U.K. pp 475-488

Wijffels, S.E. *et al.* (in prep) Detection and Anatomy of Linear Ocean Warming from 1960 to 2010

Wijffels, S.E., J. Willis, C.M. Domingues, P. Barker, N.J. White, A. Gronell, K. Ridgeway and J.A. Church (2008) Changing Expendable Bathythermograph Fall Rates and Their Impact on Estimates of Thermosteric Sea Level Rise. *Journal of Climate*, **21**, pp 5657-5672. doi: 10.1175/2008JCLI2290.1

Yin, J., S.M. Griffies and R.J. Stouffer (2010) Spatial Variability of Sea-Level Rise in 21st Century Projections. *Journal of Climate*, **23**, pp 4585-4607. doi: 10.1175/2010JCLI3533.1

Chapter 5

Overview and Future Research

Research Overview

New estimates of ocean changes have been determined for 1950-2000, thanks largely to the ocean observational revolution provided by the Argo Program. For the first time, an analysis of historical observations has taken care to minimise aliasing associated with seasonal biases (particularly in the Southern Ocean, where only Austral summer observations have been available) and climate variability expressed by the major El Nino Southern Oscillation (ENSO) modes. Accounting for these modes in historical observations provides clearer, more spatially coherent and more accurate estimates of past changes to be determined from available ocean observations.

Large, robust and spatially coherent multi-decadal linear trends in both salinity and temperature are found for the global ocean to 2000 dbar. These trends are largely free from observational platform biases; Chapters 2, 4. When compared to regional estimates of salinity changes (Table 2.2), new results often agree within error bounds and in most cases provide conservative estimates of past changes, with 50-year trends accounting for most known sources of climate variability. Trends largely agree in regions of good temporal and spatial data coverage when compared to previously reported broad-scale global changes. However, the new method used by this analysis provides more representative broad-scale changes across regions of sparse data coverage. The analysis does not suffer from the low trend biases of other studies which used optimal interpolation techniques (Chapter 4), and coherent and interpretable spatial patterns of change are the result.

Surface salinity changes suggest an enhancement to the global water cycle has occurred (Chapter 2). Salinity increases are found in evaporation-dominated regions, and freshening in precipitation-dominated regions. The spatial pattern of change strongly reflects an enhancement in the mean surface salinity pattern. This in turn reflects a change in the global mean evaporation minus precipitation (E-P) pattern, consistent with a global water cycle amplification over the period. Broad-scale warming is driving poleward migration of isopycnal (density) outcrops almost everywhere. This change leads to surface salinity and temperature anomalies being subducted and circulated by the ocean's mean flow. Isopycnal outcrop migration-driven anomalies drive a clear and repeating pattern of subsurface salinity change, a feature that is particularly strong in the mid-to-high latitude Southern Ocean.

New estimates of surface salinity change provide an insight into changes to the global water cycle, with this broad-scale relationship also seen in the Coupled Model Intercomparison Project Phase 3 (CMIP3) model suite (Chapter 3). The CMIP3 suite also suggests broad-scale changes to surface salinity are expected due to warming, with this pattern particularly convincing in strongly warming realisations. Using the full CMIP3 suite of 20th century (20C3M) and a subset of the available IPCC Special Report on Emissions Scenarios (SRES) future realisations for the 21st century, a relationship between surface salinity pattern amplification (PA) and freshwater flux (E-P) PA is found. Surface salinity provides the most statistically significant PA when compared to other variables that capture global water cycle change, with E-P showing lower pattern correlations (PC). The relationship suggests modelled surface salinity responds at twice the rate of E-P changes. Using this modelled relationship allows an estimate of observed E-P change for 1950-2000 to be inferred as 4±0.5%, which correspond to a global surface warming over the corresponding period of 0.5°C (8±5% K^{-1}). These new E-P

estimates are obtained from the corresponding observed surface salinity change estimates (8±0.5%; 16±7% K^{-1}). The new estimate agrees with the Clausius-Clapeyron relation; a thermodynamic relationship which suggests lower tropospheric saturation vapour pressure will increase at ~7% K^{-1} and providing an estimate of global water cycle enhancement in response to warming.

New observed salinity change estimates, in agreement with other observed estimates, support the idea that CMIP3 underestimates past 20th and early 21st century changes. This underestimation of observed change has been suggested by many other atmospheric studies but rarely in global ocean comparisons. The underestimation has also been reported in other aspects of climate research, which haven't considered water cycle changes (e.g. Rahmstorf *et al*., 2007; global sea-level rise). Many uncertainties still remain around climate forcings and their effect on future climate, and so caution is warranted when drawing conclusions about model projections of future 21st century climate from these results.

Considering estimates of depth-integrated ocean changes and sea-level rise (SLR), new change estimates provide support for the latest SLR budget analyses (Chapter 4). The new SLR estimates extend deeper than many previous analyses (some only to 700m). The 700-1800m contributions presented in this study provide some of the first quantitative estimates, and certainly the first coherent spatial maps of deep ocean change. For the first time regional halosteric (salinity-driven) contributions are regionally quantified. In parts of the ocean halosteric changes can account for up to 50% of the total steric signal. Halosteric changes are shown to be the leading steric regional change for 34% of the depth-integrated global ocean by area, in regions strongly affected by local freshening or enhanced salinity. In these regions, the halosteric signal overrides the effect of broad-scale warming expressed across most of the global ocean. Such results strongly suggest halosteric SLR budget components cannot be ignored when attempting to account for long-term sea-level change. Counteracting halosteric and thermosteric effects (halosteric contraction and thermosteric expansion) are expressed in new observational estimates as reported by previous studies (e.g. Levitus *et al*., 2005; Ishii *et al*., 2006). The Atlantic basin is shown to express the strongest change magnitudes for both steric components, strongly counteracting to reduce the total steric response.

The PA expressed in surface salinity results both for observations and models (Chapter 3) also appear in the depth-integrated observed salinity changes (Chapter 4). This depth-integrated result has been presented in previous CMIP3 SRES model ensemble analyses which considered projected 21st century future changes. Depth-integrated (0-1800m) results suggest water cycle changes, expressed by global ocean salinity are broad-scale and coherent. Such observational results share more similarities to strongly greenhouse gas (GHG) forced SRES than to 20C3M realisations. These results provide confidence in both the new observed estimates, and the ocean change processes captured in CMIP3 realisations of future climate.

New results suggest ocean salinity is an effective diagnostic variable from which to assess global climate change (and specifically water cycle change) over the long-term. With the development of the global Argo Program, salinity observations from the near surface to 2000 dbar are being reported from over 3200 floats as at November 2010. This revolution in ocean observation, along with the new Soil Moisture and Ocean Salinity (SMOS) satellite which started streaming data in early 2010 and the AQUARIUS mission which is scheduled for launch

in 2011 will provide unprecedented coverage of ocean surface salinity, climate and water cycle changes into the future.

Future Research

New scientific results often evoke many new questions as the understanding of a system improves. Some key questions have arisen in response to the new estimates of ocean changes presented in the preceding chapters. These new questions will be briefly discussed, and are suggested as fruitful areas for further research. Answering these questions will continue to improve our understanding of the Earth's complex climate system, in turn leading to better projections of future climate due to anthropogenic influence.

A clear relationship between modelled changes to ocean surface salinity pattern amplification (PA) and E-P PA is presented in Chapter 3. This relationship appears robust, with the CMIP3 suite suggesting salinity responds at twice the rate of the E-P changes that drives it. While robust, the dynamics driving these changes are not well understood. The result appears quite counter-intuitive, with an expectation that E-P changes would induce changes to surface salinity (Chapter 3). To further attempt to understand this system, simplified linear mixed-layer models were examined, which suggested ocean circulation (subduction and advection) of salinity changes accounted for greater than 80% of the anticipated E-P-driven change. This complex system requires more quantitative examination. Dedicated dynamical model attribution studies are currently underway to attempt to better understand the dynamics of these coupled changes. It is hoped this new analysis will provide a robust explanation for the processes driving these coupled changes, explaining the dynamics that lead to the 50% relationship suggested by the CMIP3 suite.

New estimates suggest a greater rate of warming has been experienced in ocean surface temperatures than reported in previous studies (Chapter 3, Table 3.S3). Although changing ocean sea surface temperature (SST) was not a key focus of this study, new estimates of SST change were briefly presented in Chapter 3, along with surface and depth-integrated temperature changes (expressing thermosteric sea-level rise) in Chapter 4. Depth-integrated estimates expressed from this study agree well with current best-estimates of ocean heat content changes and thermosteric sea-level rise (Chapter 4). The primary difference between these analyses is the method used to obtain the change estimates (problems associated with optimal-interpolation schemes are discussed in Chapter 4). Some preliminary SST analyses of the International Comprehensive Ocean-Atmosphere Data Set (ICOADS v2.5) have been undertaken, yielding larger rates than previously reported in other SST products using this data source. However, uncertain data quality is a key issue with ICOADS and further work is required to ascertain the true rate of warming presented by this very large database. The high-quality ocean profile analysis presented in Chapter 2 provides an independent and convincing estimate of global change captured by modifications to global ocean salinity and temperature. This high-quality change estimate can provide a benchmark to guide examination of the much larger, though lower quality ICOADS database.

The complex effects of aerosols on water cycle changes were briefly described in Chapter 3. This study did not quantitatively consider the role of aerosol-forcing and their effects. Clearly, more quantitative analysis of the regional roles of these forcing agents is required to reduce

uncertainties of their effects. The expectation that aerosols provide an offsetting forcing to greenhouse gases (GHG) is well established, however the dynamics driving this response and the corresponding effect on the global water cycle is less well known. A more rigorous study dealing with the regional effects of aerosols in particular is needed, using a multi-model approach since parameterised effects can be complex to ascertain. This is a key area of fruitful research for the future, with the role of aerosols and water cycle responses a relatively unknown aspect of anthropogenic climate change.

The complex nature of climate variability is another key area for future research. The Argo Program provides unprecedented spatial and temporal observational coverage of the global oceans. A recent study by Wijffels *et al.* (in prep) has attributed ocean temperature changes over the 1960-2010 period to many broad-scale climate modes, as well as the external influence of volcanic aerosols and solar irradiance. The ability to accurately attribute changes to external forcings, and also account for modes of climate variability that are largely unforced by anthropogenic GHG, provides more certainty for long-term rates of change. Long-term ocean changes on interannual timescales have been reported for the tropical Pacific by Cravatte *et al.* (2009). Their result suggested both geographical patterns and seasonal amplitudes have enhanced. Consideration for such seasonal cycle changes, as well as changes to broad-scale climate modes have not been investigated in this study and should be considered in future analyses.

The upcoming availability of Coupled Model Intercomparison Project Phase 5 (CMIP5) data will provide a new benchmark from which to compare observed and modelled changes to the climate system. In particular, the dedicated realisations for climate change detection and attribution studies (Taylor *et al.*, 2010) will enable more clarity in determining the transient response due to forcing agents. Additionally, new model reanalysis products are also available, with these assimilating varied observational data products in dedicated ocean or atmosphere realisations. The most recent reanalysis product, the coupled ocean-atmosphere NCEP reanalysis (Saha *et al.*, 2010) provides a completely new platform from which to investigate changes to the coupled ocean-atmosphere global climate system from 1979 to the present. It would be prudent to investigate the climate changes expressed in these modelling and reanalysis systems to further quantify changes attributable to long-term GHG forcing, and changes attributable to long or short-term climate variability in the under-observed global climate system.

Clearly, ocean salinity is an effective marker of regional ocean freshwater balance changes (Chapter 2, 3, 4), expressed through ocean-atmosphere fluxes, ocean transports, cryosphere, terrestrial and other smaller contributions. The new results presented in the preceding chapters have provided quantified, coherent and interpretable estimates of change for 1950-2000. Along with new ocean observational platforms coming online, ocean changes will provide a novel new insight to global climate system change in coming years. This phase-change in ocean observation, will provide a more rigorous estimate of ocean climate variability, and consequently allow climate scientists to tighten our collective understanding of long-term climate change versus cyclical climate variability.

It is a truly exciting time to be engaging in a career involving oceanography and global climate studies!

References

Cravatte, S., T. Delcoix, D. Zhang, M. McPhaden and J. LeLoup (2009) Observed freshening and warming of the western Pacific Warm Pool. *Climate Dynamics*, **33**, pp 565-589. doi: 10.1007/s00382-009-0526-7

Ishii, M., M. Kimoto, K. Sakamoto and S. Iwasaki (2006) Steric Sea Level Changes Estimated from Historical Ocean Subsurface Temperature and Salinity Analyses. *Journal of Oceanography*, **62**, pp 155-170

Levitus, S., J.I. Antonov, T.P. Boyer, H.E. Garcia and R.A. Locarnini (2005) Linear trends of zonally averaged thermosteric, halosteric, and total steric sea-level for individual ocean basins and the world ocean, (1955-1959)-(1994-1998). *Geophysical Research Letters*, **32**, L16601. doi: 10.1029/2005GL023761

Rahmstorf, S., A. Cazenave, J.A. Church, J.E. Hansen, R.F. Keeling, D.E. Parker and R.C.J. Somerville (2007) Recent Climate Observations Compared to Projections. *Science*, **316**, pp 709. doi: 10.1126/science.1136843

Saha, S., S. Moorthi, H. Pan, X. Wu, J. Wang, S. Nadiga, P. Tripp, R. Kistler, J. Woollen, D. Behringer, H. Liu, D. Stokes, R. Grumbine, G. Gayno, J. Wang, Y. Hou, H. Chuang, H.H. Juang, J. Sela, M. Iredell, R. Treadon, D. Kleist, P. Van Delst, D. Keyser, J. Derber, M. Ek, J. Meng, H. Wei, R. Yang, S. Lord, H. van den Dool, A. Kumar, W. Wang, C. Long, M. Chelliah, Y. Xue, B. Huang, J. Schemm, W. Ebisuzaki, R. Lin, P. Xie, M. Chen, S. Zhou, W. Higgins, C. Zou, Q. Liu, Y. Chen, Y. Han, L. Cucurull, R.W. Reynolds, G. Rutledge and M. Goldberg (2010) The NCEP Climate Forecast System Reanalysis. *Bulletin of the American Meteorological Society*, **91**, pp 1015-1057. doi: 10.1175/2010BAMS3001.1

Taylor, K.E., R.J. Stouffer and G.A. Meehl (cited 2010) A Summary of the CMIP5 Experiment Design. Available online: http://cmip-pcmdi.llnl.gov/cmip5/docs/Taylor_CMIP5_dec18_marked.pdf

Wijffels, S.E. *et al.* (in prep) Detection and Anatomy of Linear Ocean Warming from 1960 to 2010

Examination

Response to Examiner Reports

Marine and Atmospheric Research
Hobart Laboratories: Castray Esplanade
GPO Box 1538 Hobart TAS 7001 Australia

Telephone +61 3 6232 5222 • Facsimile +61 3 6232 5000 • ABN 41 687 119 230

CSIRO

Professor Michael Coffin
Director
Institute of Marine and Antarctic Studies (IMAS)
University of Tasmania
Private Bag 129
Hobart, Tasmania 7001

7th June 2011

REF: Durack – Ocean Salinity: A Water Cycle Diagnostic?

Dear Professor Coffin,

Please find below responses to the examiners reviews of the thesis titled: "Ocean Salinity: A Water Cycle Diagnostic?"

I have responded to the examiner #1 and #2 remarks below [*italics*], and have addressed the key points raised.

Changes to the thesis as documented in responses (noted below) to examiner #1 have been undertaken. Examiner #2 has made many comments relating to chapter 2, however, as this chapter is published (noted in thesis text) I have responded to these queries below, with only a few minor changes (noted below) required in the thesis itself. I thank both reviewers for their suggestions. Additionally, some minor corrections, along with appropriate updates to cited references which are now published have also been included.

I hope that you now find this improved thesis suitable for acceptance.

Yours sincerely,

Paul J. Durack
Paul.Durack@csiro.au

*****Examiner #1*****

Examiners Recommendation: Overall, the thesis is an excellent piece of original research that addresses some key questions in climate science, including: (i) changes in the hydrological; and (ii) global and regional sea level rise. The observational analysis using both density and pressure coordinates is particularly useful since it allows us to make inferences about the underlying mechanisms behind the observed changes. I recommend the degree be awarded, subject to a number of minor corrections, which are detailed below.

Minor Revisions:

1) I would like to see the summary sections of each chapter expressed in short "bullet point" lists. I think this would greatly aid communicating the essence of the chapter findings to the reader.

[Many thanks for this feedback. The concise text presented in the "Summary and Future Directions" sections for Chapters 3 & 4, along with the brief abstracts in each chapter communicates the essence of the findings to the reader. While useful for quick-scan views (I have noted dot point summaries are now available on the American Geophysical Union (AGU) journal web pages) I do not feel that such information duplication is essential or of benefit to the style of the thesis. Consequently I have not included bullet point summaries for each unpublished chapter.]

2) The author should revise the thesis abstract to make it clearer and more concise. In particular please avoid using overly-long sentences – e.g.:

"Chapter 1 introduces the reader to ocean observations, observed changes over the 20th and early 21st century, and introduction to the global water cycle and the ocean's role in its operation and anticipated changes in response to climate change".

"Salinity increases at the surface are found in evaporation-dominated regions and freshening in precipitation-dominated regions, with the spatial pattern of change strongly resembling the climatological mean sea surface salinity field, consistent with an amplification of the hydrological cycle".

[Many thanks for this feedback. I have re-read the thesis, removed overly-long sentences and tightened text where possible. The two examples above now read: "..Chapter 1 introduces the reader to ocean observations and observed changes over the 20th and early 21st century. It provides an introduction to the global water cycle and the ocean's role in its operation and the anticipated future, as well as observed changes in response to climate change.." and "..Salinity increases at the surface are found in evaporation-dominated regions and freshening in precipitation-dominated regions. This spatial pattern of change strongly resembles the climatological mean sea surface salinity field, consistent with an amplification of the global water cycle.."]

3) Please insert a suitable figure in Chapter 1 to give the reader an idea of the spatial distribution of ocean observations over time.

[Many thanks for this feedback. Chapter 1 now includes a new figure (1.2) which expresses the spatial coverage of data used in the analysis over 5-year bins from 1950-2010.]

4) In Chapter 2, include a definition for "surface" salinity observation. What are the nearest surface observations you include and what are the deepest?

I note this point is partly addressed on p. 21 in reference to "30 dbar", but something explicit about what constitutes a "surface" observation would be useful (and any assumptions to do with mixed layer depths etc).

[This study assumes a well-mixed ocean from 30m to 0m. Following the MLD climatology of Montégut et al. (2004), calculated for density deviations > 0.03, less than 10.7% of the analysis grid points express annual mean MLD values shallower than 30m (~5% <25m; ~1.5% <20m; ~0.25% <15m). Additionally, the majority of Argo profiles (which provide the seasonal coverage) report values between 5-10m. As a result 28% of the 1.6 million profiles used in the analysis were extrapolated to the surface using values from 30m and above. When reviewing this, the largest reduction in profile coverage was found from 20m to the surface (Table R1.1). This suggests that interpolation from 20m or above to the surface is valid for more than ~98.5% of the global ocean by area. Consequently the effect on results obtained after interpolation has been undertaken is minimal.]

Table R1.1. Profile data coverage over varying depths

Percentage of profiles for each database which have no value for the stated depth (m)					
Data Source	***0m***	***5m***	***10m***	***20m***	***30m***
Argo	*99.03%*	*40.83%*	*5.72%*	*1.65%*	*1.24%*
SeHyD	*24.30%*	*7.04%*	*3.93%*	*1.61%*	*1.10%*
Hydrobase2	*30.56%*	*7.45%*	*4.92%*	*4.18%*	*6.63%*
SODB	*29.28%*	*10.57%*	*6.09%*	*1.92%*	*1.21%*

5) I have a scientific concern about a potential aliasing effect in the surface salinity analysis. Is there any evidence for systematic changes in the "surface" observation depths? I think this should be commented on by the author in the text somewhere – backed up by some suitable analysis, although I do not expect any additional figures will be necessary.

[Table R1.1 suggests that there are similar patterns of depth coverage below 5m in all observational databases (contrast 10m estimates - historical vs Argo). There is a clear reduction in the shallowest (<=5m) observations in the Argo database when compared to the historical archive. However, noting the Montégut et al. (2004) MLD climatology and conclusion in the text above, does not suggest an aliasing issue is apparent in the analysis.]

6) Similar to point 4), is there any evidence of systematic changes to the mixed layer depth? Under global warming, we expect near-surface stratification to increase and mixed layer depths reduce. This could lead to an amplification of the surface salinity field without any changes to E-P. The author should comment somewhere in the thesis on how important this effect could be for their results.

[In response to this comment, an analysis of changes to the MLD was undertaken – using the > 0.03 MLD definition as described in Montégut et al. (2004). These results are expressed in Figure R1.1. The key point the reviewer raises is that a consistent, broad-scale <u>reduction</u> in MLD occurs over the period of analysis. As expressed in panel C below (which shows the difference between a reconstructed 2000 MLD and a reconstructed 1950 MLD), there appears to be a broad-scale <u>deepening</u> of MLD over the period of analysis. This would then act to reduce salinity amplification, the inverse response suggested by the reviewer's comments above. It would be useful if the reviewer had provided a key citation (or two) that expresses why a shallower MLD is expected in response to climate change. I am presently unaware of such work.]

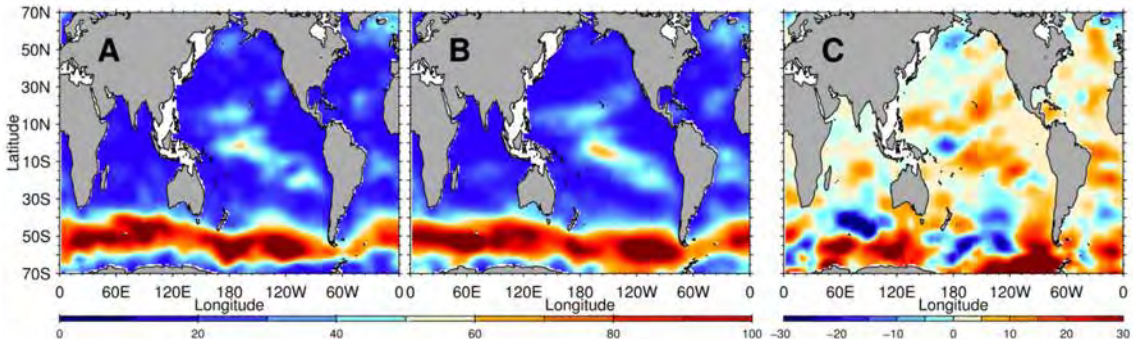

Figure R1.1. Reconstructed estimates of mixed layer depth (MLD) for A) 1950, B) 2000 and C) the difference between these reconstructed estimates. Units are metres (A, B) and change in metres 50 yr^{-1} (C).

7) Please revise Chapter 2 to include separate sections titled "Discussion" and "Summary and Future Directions", so that it is consistent with the later chapters.

[As noted on page 18 of the submitted thesis, Chapter 2 has been published in the Journal of Climate. As such, the published text and figures are presented verbatim as Chapter 2, aside from minor errors which have been corrected (noted below).]

8) On page 72 the author refers to "a simple linear model". The author needs to provide a reference for the model or include a more full description of the model and the results. Alternatively, this paragraph should be removed from the discussion.

[There is no reference for this "model". As suggested in the text, a simple linear model was created to investigate the magnitude and spatial pattern of salinity change in response to an enhancement of climatological E-P patterns. To attempt to further clarify this, the addition of the word "box" has been added to the model description.]

9) On page 111 the author provides a very cursory explanation of their Figure 4.6 with Figure 1 from Levitus et al (2005b). Please expand the text to highlight the key similarities and differences between the figures for each of the basins.

[This paragraph has been rewritten to read: "..The new results presented here (Figure 4.6) agree qualitatively with Levitus et al. (2005b; their Figure 1), with a strong thermosteric expansion associated with warming expressed for each independent ocean basin. Similarities in the halosteric responses are also apparent, the Levitus et al. (2005b) result suggesting; an expansion for the entire Pacific basin, and a strong tropical and subtropical contraction, counteracting a strong thermosteric expansion in the Atlantic basin. The Indian basin however shares less similarity with the Levitus (2005b) result, the mode water freshening centred around 50°S and expressed as a clear expansion is not apparent in their analysis. However even though there is broad spatial agreement between results, the magnitudes of change are consistently larger, likely associated with the bias in the optimal average technique they employed."]

Specific Minor Text Changes:

(i) Page 2, line 15: Remove "Obviously". *[Corrected, thank you.]*

(ii) Page 2, 9th line from bottom: Remove ".., a consequence of climate change, ..". *[Corrected, thank you.]*

(iii) Page 4, lines 8-9: Remove "once retrieved". *[Corrected, thank you.]*

(iv) Page 5, 7th line from bottom: replace "at" with "of". *[Corrected, thank you.]*

(v) Page 6, 13th line from bottom: Is the author referring to 70% of the total number of profiles? *[The word "profile" has been added to clarify what comprises this large global database.]*

(vi) Page 7, 5th line from bottom: The sentence beginning "The distribution of ocean salinity changes in response to E-P.." does not make sense to me. Please revise. *[The apparent text confusion has been further clarified and now reads: "The distribution of regional ocean salinity reflects changes to E-P and the associated atmospheric transports of freshwater from one part of the ocean to another".]*

(vii) Page 8, line 12: Remove "in response" before (Chen et al., 1994). *[Corrected, thank you.]*

(viii) Page 9, paragraph 3. I think Stott et al. (2008) used the analysis of Smith and Murphy (2007) in addition to Boyer et al. (2005). Please check and update citation if necessary. *[You are correct. The Smith & Murphy (2007) reference is now included.]*

(ix) Page 27, Table 2.2. <Gamma-a> is defined as neutral density but please check that <gamma> is defined somewhere as well (I assume this is some type of potential density?). *[To represent this analysis uses of gamma should have included a superscript a. All cases where this is missing have been corrected. Additionally, a number of studies used both γ^n and σ^ϑ as their reference density. These inconsistencies have now been corrected in Table 2.2.]*

(x) Page 31, 12th line from bottom: after "..in agreement with Boyer et al. (2005).." introduce a full stop and capital "H" in "however" to break up this sentence. *[Corrected, thank you.]*

(xi) Page 63, line 14. I do not agree with the sentence "..sharing no resemblance to the observed changes .." Once can clearly see areas where the patterns in panel F and panel D of Figure 3.5 are similar, e.g. the North Atlantic. Suggest revising the above sentence using a term such as "..shows much poorer agreement with the observed changes". *[Fair comment. The text has been updated to read "..sharing little broad-scale resemblance to the observed changes."]*

(xii) Page 71, 6th line from bottom. Replace "plagued by" with "subject to". *[Corrected, thank you.]*

(xiii) Page 73, 4th line from bottom. Suggest replacing that sentence with something like: "The new global salinity estimates support the idea of an enhanced water cycle over the 20th Century." *[Figure 3.10 expresses numerous independent estimates of water cycle amplification over the 20th and early 21st century. Figures 3.6 & 3.8 express the strong relationship between surface salinity and E-P changes in the CMIP3 model suite. For these reasons, I do believe that the statement beginning "..An enhanced water cycle has occurred over the 20th century.." is accurate, supported by the results presented in Chapter 3, and the previous estimates cited (and presented in Figure 3.10). For this reason the existing text remains unchanged.]*

(xiv) Page 96, line 8: The line beginning "The global halosteric average.." does not make sense to me – particularly the reference to "integrated errors". Please make this sentence (or sentences) clearer. *[This sentence has been rewritten to read "..The error is comprised of integrated errors which may be partly compensated by signals from unobserved regions (high latitude, marginal seas and the deep ocean) and eustatic sea-level rise from terrestrial ice melt. In a global sense, redistribution of salinity in the ocean and the integrated halosteric effect must sum to zero, as eustatic (mass addition) effects are too small over the observed record to be recorded accurately in a halosteric global average.."]*

(xv) Page 99, 2nd paragraph: Please remove repetition in this paragraph: "..need therefore to approach estimates of halosteric SLR cautiously.." followed by "..it is necessary to consider salinity-driven steric changes with caution..". *[This duplication has been removed, with the updated sentence included: "..For this reason, regional, rather than globally-integrated halosteric changes provide more quantitative information.."]*

(xvi) Page 100, 3rd paragraph: insert "associated purely with ocean density changes" after "This implies a 6mm yr^{-1} mean SLR for the period 1955-1995". I think this will help make it clear that the sea-ice melt does not constitute any mass addition. *[I agree that*

this text need clarification, the sentence has been rewritten: "..Using observed estimates of global freshening, and after accounting for their estimate of (Arctic and Antarctic) sea-ice contributions, Wadhams & Munk (2004) suggest that a eustatic contribution of 220 km^3 yr^{-1} has occurred from terrestrial runoff, which implies a 0.6 mm yr^{-1} mean eustatic SLR for the period 1955-1995.."]

(xvii) Page 103, 2nd paragraph: I disagree that "The broad-scale warming is more spatially widespread in this study". I would agree that the warming magnitude is greater in the present study than Levitus et al. (2009), and also the S. Ocean is more consistent with the other basins in the present study. You could check this point by looking at the % area of +ve and –ve points. *[Fair comment. The percentage of points with a positive temperature anomaly is 84% for this study and 88% for Levitus et al. (2009). The text has been updated to read: "..The broad-scale warming has a larger magnitude almost everywhere and is more spatially widespread in the Southern Ocean.."]*

(xviii) Page 103, 2nd paragraph: replace "..the prevalence of a.." with "..an area of.." in reference to the North Pacific. *[The sentence has been rewritten to read: "..It is interesting to note the cooling trend in the North Pacific subpolar gyre (40-50°N) apparent in both surface temperature estimates.."]*

I take "prevalent" to mean the most widespread or common, and I would say that the North Pacific as a whole is still dominated by surface warming.

*****Examiner #2*****

I. Overview

The scope of this thesis, the scale and breadth of analyses undertaken, and the interpretation of those results as meaningful indicators of global climate change collectively demonstrate mastery of scientific concepts, the ability to design and conduct topical research, and a level of scholarly achievement that are commensurate with the award of a Ph.D degree. The subject of a changing global water cycle and its response to natural and anthropogenic forcing is important from the scientific as well as societal perspective, and will become increasingly so in this century as a consequence of Earth's growing energy imbalance and expanding human populations. The work presented here is thus relevant and extensive in its consideration of large-scale ocean salinity distributions, observed patterns of change, comparisons to climate models and previous observational studies, and implications for climate system components such as the global water cycle and regional sea level rise.

I have limited my comments to the scientific, as opposed to the compositional, elements of the thesis, leaving judgement of what constitutes acceptable writing style to the members of the University Committee. In the following sections, I have outlined specific strengths of the research and thesis, followed by a short discussion of a few issues that merit some consideration. The research is clearly at a mature stage of development, and meets the criteria of advanced study and substantial original contribution set forth in the University's Rules and Procedures. Chapter 2 has already been published in the *Journal of Climate*! On the basis of my examination, I recommend the Ph.D. degree be awarded provided the questions posed in section III are given some consideration and minor revisions are undertaken.

II. Strengths

In exploring potential links between ocean salinity and climate change, Paul has sorted through two enormous bodies of information – the 58-year hydrographic observational record and the CMIP3 database of coupled climate model results. He has used these to produce estimates of change in ocean salinity distributions, to identify the underlying roots of these changes, to assess the potential uses of salinity as a quantitative indicator of water cycle changes and as a means to differentiate contributions of heat and freshwater to sea level rise. The process of data assembly, quality control, development and testing of analysis method is intensive, and a great deal of effort was clearly invested in this portion of the project. A novel multi-parameter regression model, including spatial and temporal terms, and a parameterization to dampen ENSO signals in the record, was adapted to deal with some of the imperfections of the instrumental dataset. The fitting technique has produced demonstrably smoother ocean anomaly fields compared to optimal interpolation methods employed by most previous studies (e.g. by the Levitus group), especially in data-sparse regions like the southern hemisphere. Some effort was made to provide estimates of the errors and statistical significance associated with the computed property distributions. (Whether enough attention was given depends on one's "religion".) Despite large limitations on accuracy imposed by spatial sampling, I do feel like the resulting fields have provided an improved basis for evaluating long-term changes in the ocean salinity record – at least qualitatively – and that this constitutes a significant contribution to the climate research field.

The analysis described in Chapter 2 documents a 50-year trend of pattern amplification in observed ocean salinity distributions that reinforces previous

perceptions of underlying intensification of global evaporation/precipitation rates. As in earlier studies, care was taken to differentiate the effects of vertical heave from T-S shifts through parallel analyses on pressure and isopycnal surfaces. The present investigation has gone a step further by identifying a third process – lateral migration of isopycnals in a warming ocean – as a significant contributor to subsurface salinity changes. These analyses, illustrated in figures 2.5 - 2.10, are substantial and their sum provides a comprehensive view of the anatomy of large-scale salinity changes in the 20th century that transcends prior descriptions. It represents a valid forward step in using ocean properties (temperature, salinity and density) to diagnose trends in the climate system and a basis for evaluating how well individual climate models reproduce the processes that govern these changes.

In Chapter 3, salinity trends were used to infer rates of global water cycle change in the observations and then compared to a subset of CMIP3 models. This revealed a tendency for those climate models to significantly underestimate the observed 20th century changes. While the model disparities themselves are not especially surprising, the compilation and comparisons of specific metrics presented in Chapter 3's Supplement are impressive in scope, and provide valuable insights regarding the nature and magnitude of the spread in those models. This effort to connect model outputs to observations is praiseworthy, and reflects an avenue that must be increasingly pursued by the research community.

As I had not seen pattern amplification (PA) previously used as an ocean metric, I found it innovative and quite useful as a means of connecting salinity, E-P and surface temperature changes, and for making quantitative comparisons between models and observations. Several intriguing results based on this metric emerged: 1) the relatively high rate of observed 20th century salinity PA per degree of warming (16±7 K^{-1}); 2) that this rate is not expressed in any of the 20C3M realizations (Figure 3.6A); and 3) that the 2-to-1 ratio in PA of salinity compared to E-P diagnosed in CMIP3 would translate the observed 20th century salinity PA to a figure closely approximating Clausius-Clapeyron (7% K^{-1}). If such a simple relationship (between salinity PA and E-P PA) can actually be determined within reasonable error bars, it would represent a key finding. Despite the large errors associated with the observed PA presented here, it is a reasonable first step in a positive direction. I am very curious to see how this bears out in future modelling and observational investigations.

The linear trends were also evaluated in the context of their contributions to steric sea level rise (Chapter 4). While a logical extension to the previous chapters, the analysis and presentation were less compelling and much of the discussion was rambling and repetitive. The 50-year linear trends of total steric changes diagnosed in this study were shown to be generally consistent with the best of previous and current estimates. The dominant signal, a nearly global steric rise, reflects broad-scale warming of the upper ocean. Halosteric effects were found to be significant on the basin scale – regionally enhancing (e.g. Pacific warm pool) or counteracting (e.g. tropical/subtropical Atlantic) there thermosteric rise. A comparison of steric changes in models and observations proved largely inconclusive, although parallels were found between the observed 20th century spatial patterns and models that run strong greenhouse gas forcing scenarios for the 21st century.
[*Many thanks for this feedback. Chapter 4 has been rewritten to remove duplication, and tidy text so to ensure a more concise and compelling narrative.*]

Chapter 5 provided a fitting summary of the thesis: its major findings, questions raised and future directions to pursue.

III. Issues

1. The text sometimes refers to the period of the analysis as 1950-2008 (e.g. Chapter 2 abstract , pg. 20, pg. 29, Fig 2.3, Fig 4.3), but in other places that the trends presented are for 1950-2000 (e.g. Chapter 2 figures, tables and title, Chapter 3 abstract, Figure 4.9, Chapter 5 Research Overview). I concluded that most of the analysis represents the shorter time period 1950-2000, but I am truly puzzled by the omissions of what is arguably the most significant portion of the observational record in terms of spatial and seasonal coverage (post 2000) from the trend analysis. Since Argo came up to speed around 2003 (Figure 1.1), it will not have made much contribution to the 50 year estimates presented here, despite claims to the contrary in the text. Perhaps the longer period was used to estimates the seasonal cycle of temperature and salinity for each grid point in the analysis-?

   [*The examiner is directed to pg. 29, lines 1-3:*
   "Linear salinity changes for the 1950 to 2008 period of analysis will now be described. To simplify future comparisons changes are reported for the 50-year period (nominally 1950-2000)."
   It is true that omission of the "Argo period" would indeed be counterproductive, as the spatial and seasonal coverage of the historical hydrographic database is very sparse in comparison. In fact the analysis requires this coverage to provide reasonable estimates of the seasonal cycle for the global ocean. For clarity, the analysis used all available historical hydrographic data (as described in Table 2.1) and additionally included the Argo data included in the April 2009 (pg. 20, line 40) version of the database. A linear trend was then obtained from this 1950-2008 data series. Scaling this 58-year linear trend to present 50-years was selected to simplify comparisons to previous studies (Table 2.2; pg. 29 lines 1-3). In isolation, it would be reasonable to present these linear trends in units of PSS-78 yr^{-1}; however, there are not many comparative studies which use this notation.]

   This restriction to the period 1950-2000 raises several questions which I think deserve some explanation:

   A. How do the distribution and amplitude of the linear trends over the longer time period (1950-2008) compare to those reported here? I expect that the longer term trends were computed – but not shown in the thesis. Why?
      [*This query is answered by the description and additional analysis below.*]
   B. Do the 50-year (1950-2000) salinity trends presented here represent secular, versus, cyclical, salinity changes? I would expect the 1950-2000 time period to strongly reflect biases from regional patterns such as the NAO and PDO – both of which exhibited a 50-year amplification from low to high phases over this period, following by subsequent declines in the years 2000-2010 (see figure). Discussion of these modes of variability was noticeably muted throughout the thesis (with one mention on page 104 to explain a cooling patch in the N. Pacific). Comparing these trends to another 50-year time period (1958-2008) might provide a reasonable indication of whether the global trends at the heart of this dissertation are indeed secular – or strongly influenced by cyclical changes reflecting the internal variability of the climate system.
      [Plot of NAO index 1870-2010 and PDO index 1900-2010 not reproduced here]
      This bears directly on whether applying the 50-year trend to scale the resolved trends from previous studies (Table 2.2) provides a meaningful basis for comparison. Because the author clearly invested some effort in doing so, I assume here has thought this through and can offer some justification
      [*There is no question that in order to truly quantify long-term changes, an accurate assessment of the true magnitude of cyclical climate variability, represented by in-situ salinity measurements is required. However, as spatial and temporal coverage of observations is sparse, and the Earth's climate system has already undergone significant warming, isolating variability from true changes is difficult.*

This study attempts to further our understanding of long-term changes by more effectively accounting for cyclical patterns in the observed record (mean climatological gradients, seasonal cycle and ENSO influence), and once aliasing is minimised, the long-term linear trend is obtained from the de-aliased time series. By no means is this method perfect, however, by accounting for the largest sources of variability, a cleaner, more interpretable pattern of change is the result (Figure 2.6, 4.2) – with this spatial pattern and magnitude largely supported by previous global and regional analyses of ocean salinity (Table 2.2) and temperature (Table 4.2) change.

Some consideration has been made to determine how "robust" this long-term trend actually is. Due to the dependence on the Argo data to resolve the spatial mean field and seasonal cycle, undertaking the trend fit using less historical data is a more appropriate way to test out the "robustness". Figure R2.1 expresses an updated analysis (including pressure-corrected Argo data through to 14th January 2011) which has been undertaken for numerous temporal periods to test out the "robustness" of the spatial pattern, and amplitude of change. Consequently, 6 additional temporal periods have been assessed: the updated analysis (directly comparable to 1950-2008; A1-A4) 1950-2010, 1960-2010 (C1-C4), 1970-2010 (D1-D4), 1980-2010 (E1-D4), 1990-2010 (F1-F4), 2000-2010 (G1-G4) and 2005-2010 (H1-H4). As the reviewer has noted the role of PDO and NAO in regional patterns in earlier comments, the effect of the PDO and NAO have been analysed in another comparative analysis over 1950-2010 (B1-B4). For this additional analysis, a 24 (rather than the 22) parameter multiple linear regression was undertaken, with the 23rd parameter resolving the response to a 36-month smoothed PDO index (Mantua et al., 1997) and the 24th parameter the response to a 36-month smoothed NAO index (Hurrell, 2003).

It is clear that the long-term analyses (A-D; >=40yrs) share more similarities than the shorter-term analyses. From these analyses, stronger basin-zonal mean correlations (R=0.7-0.4; A2-D2) are apparent, with the broad-scale spatial features of a freshening Western Pacific Warm Pool, enhanced salinity North and South Atlantic, and broad-scale freshening Southern Ocean all captured. Analyses <40yrs (E-H) do not show the same long-term, broad-scale patterns of change, with much lower spatial correlations between the basin-zonal mean surface salinity mean and change apparent. It would appear that as the temporal window reduces, the coherence of this pattern amplification reduces, with noise swamping the broad-scale pattern on analyses shorter than the 30-yr window over which WMO mean climatologies have historically been determined. This result is supported by Figures A2-E2, with a continuously decreasing spatial correlation, and associated decreasing pattern amplification the result. Conversely, Figures F2-H2 appear to be dominated by spatial noise, with corresponding low (or negative) pattern amplifications reported, and negative or near zero spatial correlations between the mean climatological surface salinity and its corresponding change.

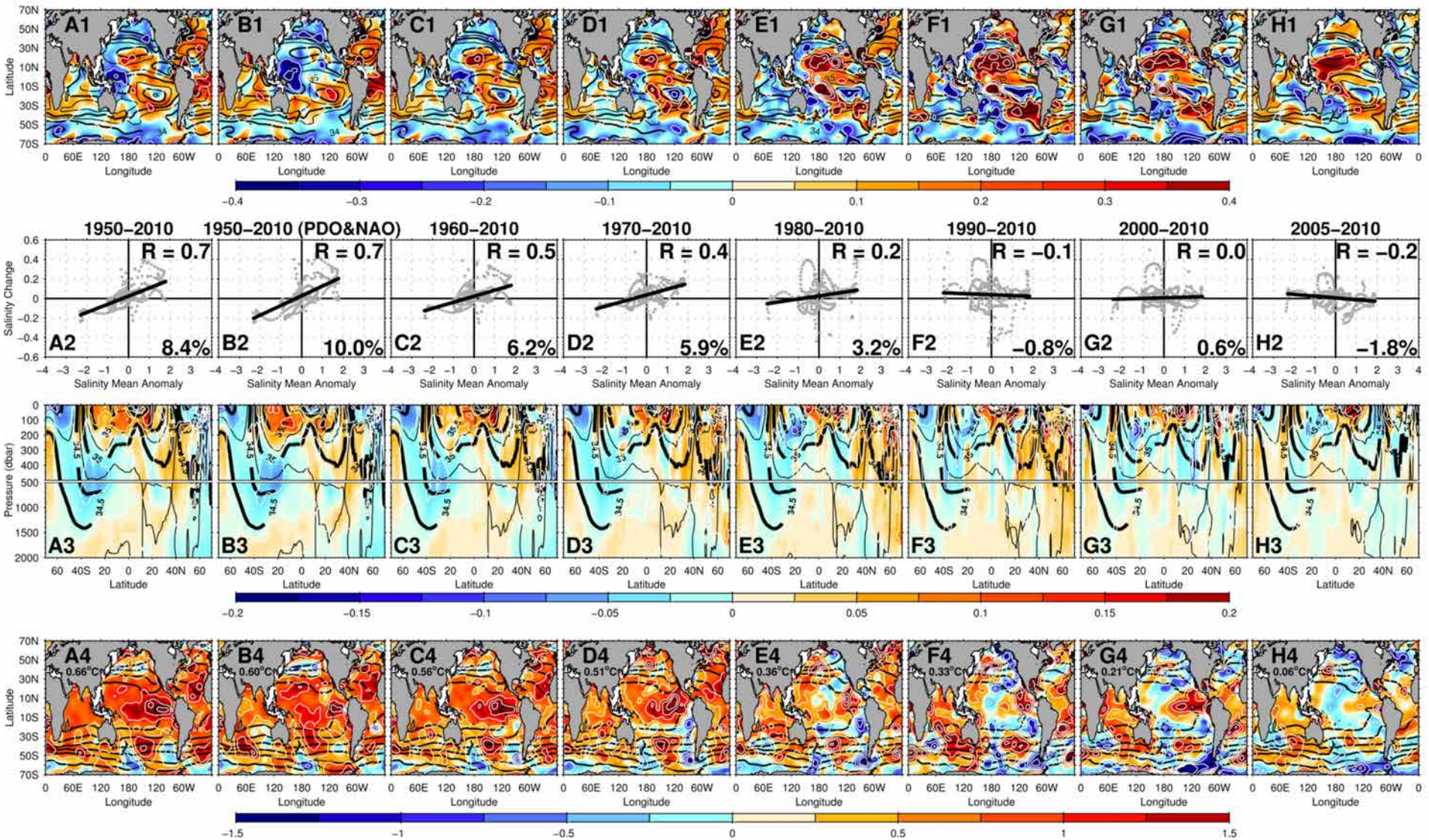

Figure R2.1. Temporally varying analyses expressing A1-H1) surface salinity change, A2-H2) surface salinity pattern amplification, A3-H3) subsurface global zonal mean salinity change and A4-H4) surface temperature change and the area-weighted global mean value. Columns left to right express changes over 1950-2010 (A), 1950-2010 with PDO & NAO variability removed (B), 1960-2010 (C), 1970-2010 (D), 1980-2010 (E), 1990-2010 (F), 2000-2010 (G) and 2005-2010 (H) respectively.

The addition of the supplementary analysis (Figure R2.1) above, along with the exhaustive comparisons included in Table 2.2 would support the idea that indeed the pattern and amplitude of change patterns is robust.]

2. While there is ample discussion of the strengths of the new estimates of salinity and temperature changes, it is also important to provide a candid assessment of the limitations of the dataset and multi-parameter regression applied to it.

A. The description of formal errors (pg. 24-26) is remarkably vague.

As I understand it, local standard errors produced by the parametric fit were found to underestimate the standard deviation of bootstrapped ensembles "by around 10%". Therefore reported errors were increased globally by a "representative factor" (the globally average difference between the bootstrapped result and standard error). If this constitutes a rigorous error analysis, it certainly is not reflected by the description in the text. This could be clarified to better convey the derivation of the errors.
[*Providing valid error estimates for change trends is truly a difficult task, as the examiner notes in their introduction. A key issue here is the variability which is associated with the varying global eddy field. For each independent ocean profile, large- and very local/small-scale variability is inherently included in the measurement, particularly in the upper layers of the ocean. The bootstrap technique undertook a random resampling of unfitted variance (essentially resampling the eddy noise) onto the selected observations at each grid point in the analysis, in an attempt to randomly introduce the variance associated with eddies onto the historical record. I feel that while this technique is simplistic, it is a reasonable attempt to quantify uncertainties associated with the sparse coverage provided by the analysis. Indeed I would be open to any further suggestions the reviewer might have on this issue.*]

B. A frank discussion of the spatial sampling errors that plague the historical data (in this study as well as previous studies) is never undertaken. The parametric fitting does not alter or improve these spatial sampling errors. Yet the first two paragraphs under Significance of Resolved Trend seem to imply that the new estimates do not suffer (or suffer less) from this problem:

"A number of recent studies …describe limitations imposed by poor historical data records … However, these studies analyse the ocean in small spatial bins, increasing the chase of noise swamping a broad-scale trend signal. The method employed here is tailored to resolve the linear trend of the large scale pattern of 50-year global salinity change. This method exploits all available regionally-representative data for 1950-2008 to achieve this aim."
[*The primary difference between these analyses is the new methodology which is optimised to extract the broad-scale, multidecadal linear trend from the de-aliased time series, and the use of the new Argo data. Argo provides a significant improvement to the spatial and temporal ocean coverage in the modern era (~2003-onwards). As noted above, this study attempts to further our understanding of long-term changes by more effectively accounting for cyclical patterns in the temporally and spatially sparse observed record (mean climatological gradients, seasonal cycle and ENSO influence). Once aliasing has been minimised, an extraction of the long-term linear trend is undertaken. By no means is this method perfect, however, by accounting for the largest sources of variability, a cleaner, more interpretable pattern of change is the result (Figure 2.6, 4.2) – with this spatial pattern and magnitude largely supported by previous global and regional analyses of ocean salinity change (Table 2.2).*

An attempt to describe some of the study limitations is found on pg. 23-24: "Two key assumptions underpin the model in (2.1). First, that the seasonal cycle (both phase and amplitude) are constant over the 58-years (1950-2008) of analysis. Second, that the response of the ocean variable to ENSO is also linear and constant in time. The large

number of parameters used to describe the mean and seasonal cycle are required as the spatial footprint of the data fitted can be large (Figure 2.2A, C). Note that this model will not account for ocean responses which involve a time lag, as can be expected due to ocean wave dynamics associated with ENSO. Thus an 18-month smoother has been applied to the ENSO index so that only the low frequency ENSO response is fitted..” and “..The key advantage of this novel approach was the reduction of seasonal and spatial sampling bias, achieved by fitting the mean climatology and trends concurrently, and removing bias due to sampling of strong ENSO cycles in the tropics. In the sparsely historically observed Southern Hemisphere oceans the analysis relies on Argo’s ability to highly resolve the mean, seasonal and ENSO responses. This reduces aliasing by these observed phenomena into the multi-decadal trend. The varied temporal global sampling also means that any “simple” average represents different eras in different parts of the ocean (Figure 2.2B, D), and by fitting the trend and mean climatology at the same time errors due to a biased climatology were avoided..”

In Figure R2.1, it does appear that accounting for variability associated with the cyclical modes captured by the PDO and NAO indices, does enhance the signal from the data somewhat (contrast Figure R2.1B vs R2.1A). However I would note that this does not significantly improve the spatial correlation (Figure R2.1B2 - R = 0.7 vs Figure R2.1A2 - R = 0.7).]

First, I'm not sure I understand the meaning of the last sentence – (the time period of the analysis arises here too.) Can the significance of sampling errors to this study be clarified in some way? On a related note, the stippling depicting regions of low significance was nearly indiscernible in the figures!

[*Many thanks for this feedback, stippling on figures have been enhanced to provide more clarity to the reader.*]

C. The multi-parameter model imposes its own set of characteristics on the dataset that may not necessarily be more accurate that other methods of objective mapping. The author may already have considered these, and wish to comment on the degree to which they influence the analysis and results:

[*The parametric model includes many terms which attempt to resolve the spatial structure of the ocean's mean, and seasonally varying field. In the analysis presented in the thesis, the parametric model was limited to 22 parameters (pg. 22-23). In subsequent analyses, a 24 parameter (Figure R2.1) and in a parallel analysis of ocean temperature (Wijffels et al., in prep) a 42 parametric model has been used to attempt to resolve the influence of numerous mean spatial structures, and additionally the effect of volcanic aerosols, solar irradiance, the Southern Annular Mode (SAM), and the PDO and NAO as accounted for in the Figure R2.1. The broad-scale spatial pattern and magnitude of the absolute changes does not change much with the addition of many more parameters. This would suggest to me that the largest modes of variability, and indeed the spatial structure, along with the linear trend are captured well by this analysis.*]

   a. The substantial search radius utilized ("until 1000 observations were found") assumes that salinity anomalies are coherent over very large spatial scales. This imposes a correlation structure that may not reflect the true spatial covariance function. How much has this contributed to the appearance of smoother anomaly fields in this analysis? I bring this up, because the smoothness is cited by the author as a reason for confidence in the present analysis – which seems to be a somewhat circular argument

   [*The primary issue is the sparseness of observations in the historical database. This is clearly presented in Figure 1.1 and the new Figure 1.2 (see response to reviewer #1 above). The analysis makes the assumption that there is no spatial bias in the location of historical observations. Most historical observations were obtained from research cruises, which criss-cross the ocean basins (Figure 1.2) and do not appear to be distributed in a pattern which would bias the analysis. Additionally, a criterion used in the analysis ensures that if enough spatially representative points are not available, the analysis is aborted for that grid point. This is noted on pg. 21 "..For each target location, data were collected within a spatial ellipse, with a latitude (zonal) radius twice that of longitude. The search radius was expanded until a minimum of 1000 observations were found and each decadal bin (from 1950 to 2008) contained a minimum of 10 data points. Consequently the spatial footprint of the data fit for each point was dependent on the availability of observations both spatially and historically. As a result, the resolved scales were small where historical data coverage was good (northern hemisphere basins, in particular the Atlantic) and large where historical coverage was poor (the central South Pacific and interior Indian Ocean). A maximum radius of 1100km was set, resulting in a small analysis "hole" of around 10° in longitude and latitude, centred at 35°S and 142°W in the central South Pacific where historical coverage is very sparse. Linear interpolation on pressure and density surfaces across this "hole" allowed a complete global analysis to be formed..". As such a long-term analysis is dependent upon the availability of such observations; I am unaware of a more appropriate way to deal with this issue. Clearly, dealing with the large eddy-noise which is apparent in both modern and historical profile data is a key problem here, and is the reason that the large (1000 observations) number of profiles to average across this noise was selected.*]

b. To some extent the temporal terms in the parametric model (C_1-C_3) impose a 50-year trend *a priori*. For the sake of argument, suppose it is imposing a trend that is not real – would this significantly affect/alter the results of this study?
[*There is no doubt in current literature that a clear warming signal is pervasive in both global terrestrial surface and ocean profile databases. For this reason I believe that it is a fair assumption to assume that associated changes to ocean properties have also occurred in concert with this observed warming. The additional analysis undertaken, and presented in Figure R2.1 tends to suggest that over short temporal periods (e.g. 1980-2010), where climate variability dominates over long-term trends, a much smaller, and less spatially coherent change is reported (Figure R2.1E; reduced spatial correlation (0.2) when compared to longer temporal analyses). Additionally, including additional terms to account for the modes of variability associated with PDO and NAO did not dramatically affect the broad-scale result.*]

D. Figure 2.3 shows two examples of linear fits to observations in the tropics. Given the decadal-multidecadal signals that permeate ocean fields outside the tropics, are there places where the linear model is not appropriate? When describing the CMIP3 models, for example, the best and worst cases were shown (Figure 3.5). It would be instructive to show this for the observational dataset as well.
[*Presenting near trends for each of the 16,873 ocean grid points where the analysis has been undertaken is an unrealistic expectation. However, while undertaking the analysis I visually inspected many of these resolved linear trend fits – and was satisfied that these were accurately reporting such long-term changes. Figure 2.3 was explicitly included to covey to the reader that a very large envelope of variability is inherent when attempting to ascertain long-term changes over time. The regions selected were representative of high-variability zones (Figure 2.4), and expressed again below in Figure R2.2 for the updated analysis presented in Figure R2.1A.*

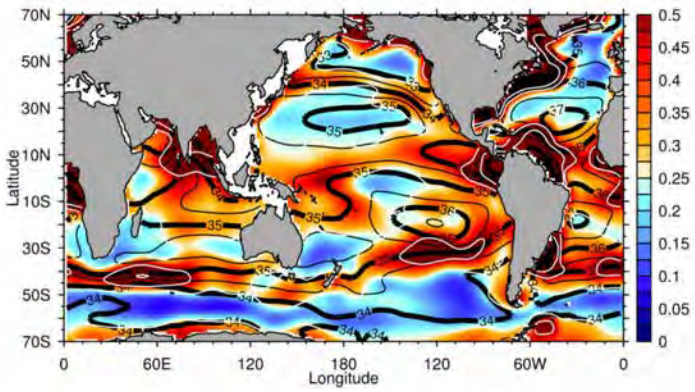

Figure R2.2. Resolved surface salinity standard deviation for the 1950-2010 analysis. Units are PSS-78.

Where a poor signal-to-noise ratio was ascertained for the local linear trend, an associated large error was reported. The additional bootstrap analysis allowed further investigation as to whether any clear spatial biases were apparent in the analysis – and resolved that a bias did not exist. As described in Chapter 2 in the section titled "Significance of Resolved Trends" this representative underestimation of the errors (associated with unresolved eddy noise) was then incorporated into the formal errors resolved during the linear trend estimation.]

E. The uncertainties for the basins-averaged estimates of salinity trends are quite large relative to the signal, but there is never any comment about this. How much caution should be exercised in using these results as a metric or diagnostic tool? The error bars (i.e. Atlantic +0.078 ± 0.095, Pacific -0.044±0.064, Indian -0.001±0.061) are large enough to actually invert the signal of the salinity trends. The signal-to-noise ratio in the data examples provided in Figure 2.3 underscores the fact that ocean salinity is a noisy (and undersampled) field. I bring this up because, in subsequent chapters, there are frequent references to how "robust" these estimates of salinity change are – and yet I would conclude that the statistics don't really bear this out. Comment?
[*The use of the term "robust" was selected as regardless of the analysis technique, coherent and broad-scale patterns of salinity changes over the long-term are the consensus result as presented in Table 2.2. While instructive for a broad-scale understanding, areal means, as expressed for each of the basins contains a complex spatial pattern. Even though repeating subsurface spatial patterns are independently replicated in each of the basins, integrated means of such large spatial regions (basin-wide) incorporate many errors, with these conservatively expressed in the large error estimates above.*]

*****End of Reviews*****

References:

De Boyer Montégut, C., G. Madec, A.S. Fischer, A. Lazar and D. Ludicone (2004) Mixed layer depth over the global ocean: An examination of profile data and a profile-based climatology. *Journal of Geophysical Research*, **109**, C12003. doi: 10.1029/2004JC002378

Mantua, N.J., S.R. Hare, Y. Zhang, J.M. Wallace and R.C. Francis (1997) A Pacific Interdecadal Climate Oscillation with Impacts on Salmon Production. *Bulletin of the American Meteorological Society*, **78**, pp 1069-1079. doi: 10.1175/1520-0477(1997)078<1069:APICOW>2.0.CO;2

Hurrell, J.W. (2003) Climate Variability: North Atlantic and Arctic Oscillation. *Encyclopedia of Atmospheric Sciences*, J.R. Holton (Ed) Academic Press, Oxford, U.K., pp 439-445. doi: 10.1016/b0-12-227090-8/00109-3

Wijffels S.E. *et al*. (in prep) Detection and Anatomy of Linear Ocean Warming from 1960 to 2010.